

THE DIFFUSION THERMOEFFECT IN BINARY
LIQUID MIXTURES

By

Richard L. Rowley

A DISSERTATION

Submitted to

Michigan State University

in partial fulfillment of the requirements

for the degree of

DOCTOR OF PHILOSOPHY

Department of Chemistry

1978

4113521

ABSTRACT

THE DIFFUSION THERMOEFFECT IN BINARY
LIQUID MIXTURES

By

Richard L. Rowley

The heat flow induced by a composition gradient is known as the diffusion thermoeffect or Dufour effect. It is characterized by the heat of transport, formally defined as the ratio of the heat flux to the mass flux under isothermal conditions. Although theoretical treatments allow calculation of heats of transport from thermal diffusion experiments on the basis of Onsager heat-mass and mass-heat reciprocity, no direct, quantitative, experimental determinations of the heat of transport in liquid mixtures have previously been reported. The direct experimental determination of the heat of transport for carbon tetrachloride-cyclohexane mixtures reported here has provided the first experimental verification of the Onsager heat-mass reciprocal relation. Also reported here are the first measurements of the behavior of the heat of transport in a mixture (isobutyric acid-water) near its consolute temperature.

The equations of nonequilibrium thermodynamics and the hydrodynamic conservation equations have been used to formulate coupled, nonlinear, nonhomogeneous partial differential equations which when solved subject to appropriate initial and boundary conditions yield time and space distributions for the barycentric velocity, composition, and temperature. These equations are solved with a Crank-Nicholson implicit numerical scheme which allows inclusion of the composition and temperature dependence of the thermodynamic and transport parameters.

The heat of transport for carbon tetrachloride-cyclohexane liquid mixtures has been determined directly by diffusion thermoeffect experiments. The technique employs a withdrawable "liquid gate" to create a nonturbulent, sharp, diffusional interface. The heat of transport is obtained from nonlinear least squares fitting of numerically predicted values to actual temperature differences measured about the interface. The agreement of these direct heat of transport measurements with values calculated from thermal diffusion experiments constitutes the first experimental verification of Onsager heat-mass and mass-heat reciprocity in binary liquid mixtures.

The temperature dependence of the heat of transport has also been measured, for isobutyric acid-water mixtures near the critical solution temperature. A microwave oven was used to jump the temperature of the initially two-phase

system from just below to just above the consolute temperature. Above the consolute temperature, a uniform, one-phase system is the equilibrium state. Consequently, as soon as the temperature of the two-phase system is raised above the consolute temperature, diffusion commences and induces a temperature gradient. Temperature differences about the interface obtained as a function of nearness to the consolute temperature yield the critical exponent for the heat of transport. The heat of transport vanishes with a $+2/3$ critical exponent as the critical solution temperature is approached. There thus exists a previously unsuspected critical anomaly in the heat of transport, which can be traced to a diverging Onsager coefficient. Because current kinetic theories are inconsistent with the critical behavior of the heat of transport, a new molecular interpretation of the heat of transport is proposed to explain the nature of coupling between molecular heat and mass transport as well as its critical behavior.

To Vickie

ACKNOWLEDGMENTS

I wish to thank the Department of Chemistry for the financial support I have received from teaching assistantships. I also wish to thank the Department of Chemistry and the General Electric Foundation for awarding me a 1978 summer fellowship.

I am indebted to Professor Larry Dawson of the Food Science Department for use of his microwave oven which enabled completion of some of the experimental work. I also appreciate the work of Mr. Andrew Seer, master glassblower, who was able to construct the assortment of glass apparatus used in this project. The time and photographic talents of Dr. Daniel and Kathleen Bradley are appreciated. The photographs contained in this thesis are the results of their help. Thanks are due to Professor Alexander Popov for use of his Karl Fischer Titrator.

My gratitude is extended to Professor Frederick H. Horne whose teachings of nonequilibrium thermodynamics, thermodynamics, and analytical thinking have been the foundation of this work. I sincerely appreciate his encouragement and his confidence in my capabilities.

Above all, I thank my wife Vickie for her support, encouragement, and optimism. Her unselfish support of this work has been a large driving force in its completion.

TABLE OF CONTENTS

Chapter	Page
LIST OF TABLES	vii
LIST OF FIGURES	x
1. INTRODUCTION	1
A. Phenomenology of the Diffusion Thermoeffect	1
B. Objectives	4
C. Plan of the Dissertation	6
2. MATHEMATICAL FORMULATION OF THE DIFFUSION THERMOEFFECT	8
A. Introduction	8
B. Hydrodynamic Equations	9
C. Nonequilibrium Thermodynamics Equations	13
D. Transport Parameters and Equations	15
E. Mole Fraction Equations for Carbon Tetrachloride-Cyclohexane Mixtures	23
3. NUMERICAL SOLUTION OF THE DIFFUSION THERMOEFFECT EQUATIONS	28
A. General Scheme	28
B. Solutions for the Carbon Tetrachloride- Cyclohexane System	41
4. DIFFUSION THERMOEFFECT EXPERIMENTS ON CARBON TETRACHLORIDE-CYCLOHEXANE MIXTURES	50
A. Experimental Design	50
B. Analysis of Technique	63

Chapter	Page
C. Literature Values for the Physico-chemical Properties of the Carbon Tetrachloride - Cyclohexane System.	76
D. Experimental Results for Thermal Conductivity.	80
E. Experimental Results for Heat of Transport	84
5. LIQUID-LIQUID CRITICAL PHENOMENA.	97
A. Classical Thermodynamics of Liquid-Liquid Critical Phenomena.	97
B. Critical Exponents.	102
1. Definitions	102
2. Universality.	111
3. Scaling	113
C. Transport Properties in the Critical Region	113
D. Predicted Liquid-Liquid Critical Exponents for Transport Phenomena	116
E. Experimental Liquid-Liquid Critical Exponents for Transport Parameters.	117
1. Techniques.	117
2. Thermal Conductivity.	120
3. Mutual Diffusivity.	122
4. Thermal Diffusion	127
5. Heat of Transport	131
6. THE HEAT OF TRANSPORT IN THE CRITICAL SOLUTION REGION OF ISOBUTYRIC ACID-WATER MIXTURES.	133
A. Transport Equations	133
B. Experimental.	138

Chapter	Page
1. Cell Considerations	138
2. Critical Temperature Measurements	143
3. Experimental Procedure.	148
4. Data Analysis	150
C. The Temperature Jump Technique.	155
D. Literature Parameters for IBW	167
E. Experimental Results.	173
7. CONCLUSIONS	191
A. Interpretations of the Heat of Transport.	191
B. A New Interpretation of the Heat of Transport	198
C. Summary and Future Work Needed.	206
APPENDIX A - TRANSFORMATION RELATIONS AND IDENTITIES.	210
APPENDIX B - DIFFUSION THERMOEFFECT DATA FOR THE CARBON TETRACHLORIDE-CYCLOHEXANE SYSTEM.	214
APPENDIX C - DIFFUSION THERMOEFFECT DATA FOR THE ISOBUTYRIC ACID-WATER SYSTEM IN THE CRITICAL REGION.	218
REFERENCES.	225

LIST OF TABLES

Table	Page
4.1 Literature values for the physico-chemical properties of the carbon tetrachloride - cyclohexane system at 1 atm. The properties are expressed in the general form $L = L_0[1 + L_x(x_1 - 0.5) + L_T(T - 298.15) + L_{xT}(x_1 - 0.5)(T - 298.15) + 1/2 L_{xx}(x_1 - 0.5)^2]$ to include the temperature and composition dependence . .	77
4.2 Thermal conductivity of CCl_4 - C_6H_{12} mixtures at 20°C and 1 atm	83
4.3 Values of the heat of transport and Onsager coefficients in carbon tetrachloride-cyclohexane mixtures at 25°C. . .	86
4.4 Heat-mass transport coefficients for carbon tetrachloride-cyclohexane mixtures at 25°C and 1 atm.	91
4.5 Values for the difference in thermal conductivity between the equilibrium and steady states in thermal diffusion experiments.	95
5.1 Critical exponents for some equilibrium thermodynamic properties. References are cited in Scott's [1972] review	98

Table	Page
5.2	The behavior of transport coefficients in the critical region 100
5.3	Theoretical predictions for critical exponents of transport properties. 118
5.4	Light scattering results for the mutual diffusion critical exponent 126
5.5	Literature transport parameters and their critical exponents 132
6.1	Expressions used for IBW transport and thermodynamic parameters in analysis of diffusion thermoeffect experiments in the critical region 168
6.2	Experimental conditions for the diffusion thermoeffect experiments performed on IBW in the critical region 174
6.3	Results of diffusion thermoeffect experiments in the IBW critical region 175
6.4	Transport parameters and their critical exponents 187
B.1	Initial Conditions 215
B.2	Temperature differences. 216
C.1	Initial conditions 220

Table	Page
C.2 Run I.	221
C.3 Run II	222
C.4 Run III.	222
C.5 Run IV	223
C.6 Run V.	223
C.7 Run VI	224
C.8 Run VII.	224

LIST OF FIGURES

Figure	Page
1.1	Schematic of the diffusion thermo- effect 2
3.1	Crank-Nicholson grid scheme for finite difference equations. Properties are evaluated at the i, n positions, \circ . Derivatives are evaluated at the $i, n +$ $1/2$ positions, \blacksquare 29
3.2	Graphical comparison of the first and second order correct analogs for the first derivative as illustrated by Rosengren [1969]. a. Actual derivative. b. Second order correct analog. c. First order forward difference. d. First order backward difference. 32
3.3	Flow diagram for simultaneous numeri- cal solution of the composition and temperature equations. 38
3.4	Barycentric velocity surface for the carbon tetrachloride-cyclohexane system 42
3.5	Composition surface for the carbon tetrachloride-cyclohexane system 43

Figure	Page
3.6	Temperature surface for the carbon tetrachloride-cyclohexane system. ΔT represents the local temperature minus the initial temperature. 45
3.7	Effect of excess enthalpy on the time dependence of temperature distribution. Plots are for $\tilde{H}^E = x_1 x_2 (A + Bx_1)$ with —, A=B=0. ---, A=670 J/mol; B=0. . . . , A=670 J/mol; B=67 J/mol. Upper curves are for (z/a)=0.6 and lower curves are for (z/a)=0.4 47
3.8	Effect of excess enthalpy on the time behavior of the temperature difference for the thermocouple pair (z/a)=0.4 and (z/a)=0.6. The curve is identical for $\tilde{H}^E = x_1 x_2 (A + Bx_1)$ and (1) A=B=0, (2) A=670 J/mol; B=0, (3) A=3350 J/mol; B=0, (4) A=670 J/mol; B=67 J/mol, and (5) A=670 J/mol; B=167 J/mol 48
4.1	Withdrawable "liquid gate" diffusion thermoeffect cell. 55
4.2	Schematic diagram of withdrawable "liquid gate" diffusion thermoeffect

	cell. A. Upper phase storage reservoir. B. Cell jacket for thermostating or adiabatically insulating. C. Diffusion thermo-effect chamber. D. Thermocouple banks. E. Equatorial water entrapment rim. F. "Liquid gate" withdrawal spout. G. Ground glass fittings for thermocouple leads and cell drainage. H. T-connector to vacuum line and thermostat. I. Filling tubes. J. Glass-syringe	57
4.3	Comparison of experimental ΔT data to predicted values for adiabatic walls (—) and diathermic walls (---)	69
4.4	Nonlinear, weighted, least squares fit of $(\tilde{Q}_1^*/\tilde{M})$ for run I. The solid line represents calculated \tilde{Q}_1^* values based upon the fit value of $(\tilde{Q}_1^*/\tilde{M})$ while the solid circles are experimental data.	73
4.5	Test of the stability of \tilde{Q}_1^* obtained as a function of the time range for which ΔT data were input. The dashed line indicates 1% deviation from the long-time value	74

Figure	Page
4.6	Thermal diffusion factor at 25°C as a function of composition. Method of measurement is in parentheses. ▲, this work (Dufour effect); ÷, Anderson and Horne [1971] (pure thermal diffusion); -I--, Stanford and Beyerlein [1973] (thermogravitation); o, Turner, <u>et al.</u> [1967] (flow cell); ■, Korchinsky and Emery [1967] (thermogravitation). (Rowley and Horne [1978]). 88
4.7	The Dufour coefficient β_T as calculated from the experimental \tilde{Q}_1^* values. ■, experimental data; —, least squares fit. 92
4.8	Heat of transport \tilde{Q}_1^* as a function of mole fraction x_1 . ■, experimental data; —, least squares fit 93
5.1	Free energy of mixing vs. mole fraction of component 1 as illustrated by Moore [1972]. A. Complete miscibility. B. Two phase system of compositions x_1' and x_1'' . C. Phase stability limit. 98

Figure	Page
5.2	Behavior of the chemical potential of component 1 vs. mole fraction of component 2 for a critical system as depicted by Prigogine and Defay [1954]. The dashed line indicates metastable regions. 100
5.3	Coexistence curve for the n-hexane - nitrobenzene system as depicted by Prigogine and Defay [1954] 101
5.4	Photographic sequence of liquid-liquid critical phenomena as the temperature is lowered to the consolute temperature of the isobutyric acid-water system. (a) $T \gg T_c$. (b) $T - T_c \sim 3^\circ\text{C}$, mixture becomes a hazy blue hue as opalescence begins. (c) $T - T_c \sim 1^\circ\text{C}$, blue hue becomes a white fog as T is lowered and opalescence increases. (d) $T - T_c \leq 0.01^\circ\text{C}$, critical opalescence intensifies as dense white cloud. (e) $T - T_c \geq -0.01$, onset of phase separation as marked by dense turbidity. (f) $T < T_c$, completion of phase separation 104
5.5	Deviation from the simple form $D = A\epsilon^\lambda$ for $T - T_c \geq 5^\circ\text{C}$ in the light

Figure	Page
	scattering results of Chu, Lee, and Tscharnuter [1973] 107
5.6	Behavior of properties as functions of ϵ for various values of the critical exponent λ 110
5.7	Thermal conductivity in the critical region as reported by Gerts and Filippov [1956]. A. 63 wt. % <u>n</u> - hexane + 37 wt. % nitrobenzene. B. system <u>n</u> -heptane-nitrobenzene with: 1. 62 wt. % nitrobenzene; 2. 52.3 wt. % nitrobenzene 121
5.8	Mutual diffusion in the critical region. (A) Results of Haase and Siry [1968] for the water-triethylamine system exhibiting a lower consolute temperature at 91.26 mol % water and 18.3°C. (B) Results of Claesson and Sundelöf [1957] for the <u>n</u> -hexane- nitrobenzene system at equal mole fractions. 124
5.9	Log-log plot of the thermal diffusion data of Thomaes [1956] for the n-hexane -nitrobenzene system and of Tichacek

Figure	Page
and Drickamer [1956] for the perfluoro- n-heptane + 2,2,4-trimethylpentane system	128
5.10 Thermal diffusion and mutual diffu- sion results of Giglio and Vendramini [1975] for the critical region of aniline-cyclohexane mixtures	130
6.1 Temperature jump cell for diffusion thermoeffect experiments in the critical region.	142
6.2 Critical solution temperature cell	146
6.3 Coexistence curve for IBW as determined by Woermann and Sarholz [1965]	152
6.4 The function $(T_c - T)^{1/3}$ vs. mole fraction of isobutyric acid. \square , data of Woermann and Sarholz [1965]; \bullet , data of Chu <u>et al.</u> [1968]; —, least squares fit.	154
6.5 Predicted decay of initial tempera- ture nonuniformities in a temperature jump diffusion thermoeffect experi- ment	158

Figure	Page
6.6	Predicted composition surface for IBW in a temperature jump diffusion thermoeffect experiment 4°C above T_c 161
6.7	Computer verification of steady state maintenance for diffusion thermoeffect as $T_{cell} \rightarrow T_c$. —, predicted ΔT in system 1; ---, ΔT in isothermal systems 2; ■, predicted ΔT in system 1 when T_{cell} is identical to that of system 2. 165
6.8	Run I. Experimental results for $\tilde{Q}_1^* = A\epsilon^{\lambda_4}$ with A and λ_4 as adjust- able parameters. 178
6.9	Run II. Experimental results for \tilde{Q}_1^* $= A\epsilon^{\lambda_4}$ with A and λ_4 as adjustable parameters 179
6.10	Run III. Experimental results for $\tilde{Q}_1^* = A\epsilon^{\lambda_4}$ with A and λ_4 as adjust- able parameters. 180
6.11	Run IV. Experimental results for $\tilde{Q}_1^* = A\epsilon^{\lambda_4}$ with A and λ_4 as adjust- able parameters. 181
6.12	Run V. Experimental results for $\tilde{Q}_1^* = A\epsilon^{\lambda_4}$ with A and λ_4 as adjustable parameters . . 182

Figure	Page
6.13 Run VI. Experimental results for $\tilde{Q}_1^* = A\epsilon^{\lambda_4}$ with A and λ_4 as adjustable parameters.	183
6.14 Run VII. Experimental results for $\tilde{Q}_1^* = A\epsilon^{\lambda_4}$ with A and λ_4 as adjustable parameters.	184
6.15 Simulated temperatures relative to the mean cell temperature in temperature jump diffusion thermo-effect experiments as T approaches T_c	189

CHAPTER 1

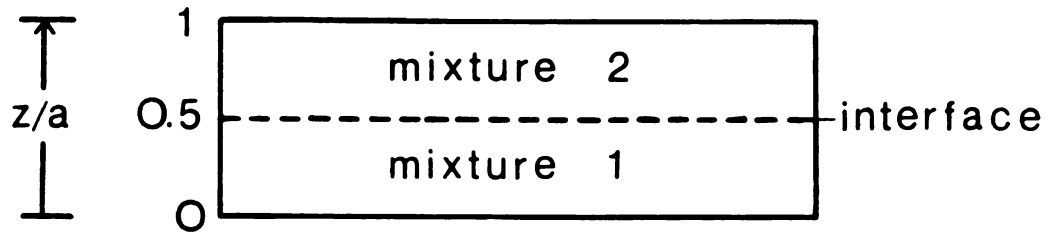
INTRODUCTION

A. Phenomenology of the Diffusion Thermoeffect

It is well-known that a gradient of composition induces a mass flow or diffusional flux. Similarly, a heat flux results from a thermal gradient. The phenomena of diffusion and thermal conduction represent empirical relationships between flows or fluxes and their respective driving forces. Less well-known are the relationships between flows and cross driving forces. Partial separation of the components occurs when a mixture is subject to a temperature gradient. Similarly, heat fluxes can be induced by composition gradients.

The diffusion thermoeffect is just such a cross phenomenon. The heat flux in a binary, field free liquid mixture can be written, according to Onsager, as a linear combination of the gradients of temperature and chemical potential - the former drives thermal conduction while the latter produces the diffusion thermoeffect. The mass flux is similarly a linear combination of the diffusion and thermal diffusion driving forces, which are chemical potential and temperature gradients, respectively.

Figure 1.1 illustrates the basic phenomenology of the



IC: $T = \text{constant}$
 $X_1 = X_1^l \quad (0 \leq z/a < 0.5)$
 $X_1 = X_1^u \quad (0.5 < z/a \leq 1)$

BC: $(\partial X_1 / \partial z)_{z/a=0 \& 1} = 0$
 $(\partial T / \partial z)_{z/a=0 \& 1} = 0$

Figure 1.1. Schematic of the diffusion thermoeffect.

diffusion thermoeffect. In Figure 1.1 z represents the coordinate axis perpendicular to the interface between two mixtures. Since "a" is cell height, (z/a) is the reduced coordinate. The initial conditions shown in Figure 1.1 are for isothermal mixtures ($T = \text{constant}$) and a step function in mole fraction x_1 of component 1; i.e., the mole fraction of component 1 in the upper layer x_1^u is different from that in the lower layer x_1^L . When two isothermal mixtures containing different compositions of the same two components are brought into contact such that an initially distinct interface is formed between the upper less dense phase and the more dense lower phase, mutual diffusion begins. As diffusion continues, the initially isothermal temperature distribution changes in time through three effects: (1) heat of mixing, (2) diffusion thermoeffect - heat transported by mutual diffusion, and (3) thermal conduction. If equations are available which describe these three phenomena, then temperature measurements with respect to time and position will yield information concerning the diffusion thermoeffect.

Though not essential, the initial conditions shown in Figure 1.1 best illustrate the effect. The boundary conditions listed apply to impermeable and adiabatically insulated walls. These conditions maximize the measurability of the phenomenon (Ingle and Horne [1973]).

Although the diffusion thermoeffect, also called the

Dufour effect after its discoverer (Dufour [1873]) has been suspected for over a century, interest in it was dormant until Waldmann [1939], [1943], [1947], and [1949] studied and described it in gaseous mixtures. The equations used by Waldmann are based on ideal gas assumptions and are not valid for liquid mixtures. Attempts to measure the diffusion thermoeffect in liquid mixtures by Rastogi et al. [1965], [1969], and [1970] were only qualitative and disagreed with the Onsager reciprocal relations. Their experimental apparatus was not suitable for studying the Dufour effect unambiguously. The theoretical prediction by Ingle and Horne [1973], that the diffusion thermoeffect was indeed measurable prompted initial consideration of the effect as a tool for this work's study of the behavior of transport properties near the critical point.

B. Objectives

Unlike gases and solids, liquids and liquid mixtures have not yet been fully treated theoretically, although great progress has recently occurred in both equilibrium and nonequilibrium theories. The liquid-liquid critical point (consolute point) in a binary mixture, where the system rapidly changes from a single-phase homogeneous mixture to a stable two-phase system, is characterized by increasing molecular correlation lengths. Transport properties in liquids are often dramatically affected by

this transition and therefore can serve as a probe in understanding liquid phenomena in this region. Transport experiments near the consolute point also aid the understanding of how molecular phenomena and interactions couple to yield macroscopic transport.

The goal of the research described in this treatise was to examine experimentally the diffusion thermoeffect first in mixtures away from the critical region (since it had never before been quantitatively measured in liquids) and second in mixtures near the critical solution temperature. Since the diffusion thermoeffect involves the coupling of heat and mass transport, any anomalous effects in the critical region may help elucidate the manner in which intermolecular correlations and interactions are involved in the coupling of fluxes to their various driving forces. The diffusion thermoeffect is particularly suitable for studying heat-mass interactions in the critical region since only small temperature effects are produced by moderate composition gradients. Thermal diffusion on the other hand requires a large temperature gradient as a driving force and therefore restricts the closeness of approach to the consolute temperature and introduces ambiguities in the difference $T_{\text{cell}} - T_c$ where T_{cell} is the mean cell temperature and T_c is the consolute temperature.

The particular objectives of this work, toward the overall goals described above, were fourfold: (1) to

measure quantitatively for the first time the diffusion thermoeffect in liquid mixtures, (2) to test experimentally the Onsager heat-mass reciprocal relation, (3) to measure the behavior of the diffusion thermoeffect in the consolute region of a binary mixture in order to understand how it may relate to microscopic phenomena; and (4) to examine experimentally and compare the behavior of the Onsager heat-mass and mass-heat coefficients in the consolute region. It is hoped that the result will provide direction for further theoretical and experimental studies, particularly of transport properties, in the liquid-liquid critical region.

C. Plan of the Dissertation

Chapter 2 describes the diffusion thermoeffect mathematically within the framework of the fundamental equations of hydrodynamics and nonequilibrium thermodynamics. Solutions of the equations developed therein have the capability of describing measured temperature distributions in terms of initial conditions, boundary conditions, and transport properties. These equations are solved numerically. Chapter 3 indicates special techniques used and the simulated solutions obtained.

Chapter 4 describes experimental investigation of the diffusion thermoeffect for the carbon tetrachloride-cyclohexane system. The results of these experiments, when

compared with thermal diffusion data, provide the first verification of the Onsager heat-mass reciprocal relation (ORR).

Background for critical mixtures and for transport properties in the critical region is presented in Chapter 5. Literature results clearly indicate the need for the further experiments described in Chapter 6 on the isobutyric acid-water system near its consolute temperature. Results obtained for the diffusion thermoeffect in this region show a strong dependence on the microscopic changes that prepare the system for phase separation. These results are discussed in terms of possible models in the final chapter.

CHAPTER 2

MATHEMATICAL FORMULATION OF THE DIFFUSION THERMOEFFECT

A. Introduction

As Figure 1.1 shows, the diffusion thermoeffect occurs as a result of diffusion across an initially distinct interface between two phases containing different compositions of the same two components. The response is a disruption of the initial temperature distribution. The time-dependent temperature distribution at a given position is related not only to the diffusion thermoeffect but also to thermal conduction and heat of mixing effects. In accord with the findings of Ingle and Horne [1973], measurements of temperature differences between points symmetric about the interface as a function of time are used throughout this thesis. The procedure is to fit predicted temperature differences to measured values from which the magnitude of the diffusion thermoeffect can be deduced. This requires equations which relate the temperature distribution to the heat of transport - the commonly used parameter in describing the diffusion thermoeffect. The equations of nonequilibrium thermodynamics and hydrodynamics yield partial differential equations for composition, barycentric velocity, and temperature as functions

of time and spatial position. The heat and mass fluxes in the hydrodynamic equations are identified from an entropy production equation. Substitution of the proper fluxes into the conservation equations, identification of the transport parameters involved in the fluxes, and derivation of appropriate boundary and initial conditions yield a system of partial differential equations which describe the temperature distribution of the fluid in terms of transport properties and experimental conditions. Nonlinear, weighted, least squares fitting of measured and calculated temperatures provides a method for obtaining the heat of transport.

The method used in setting up the partial differential equations is not new. Therefore, more consideration will be given to transformations, simplifications, and solutions rather than derivations of the appropriate equations. Details of the derivation and assumptions involved in obtaining the starting partial differential equations are readily available from Fitts [1962], de Groot and Mazur [1969], Haase [1969], Anderson and Horne [1970], and Horne [1966] as well as elsewhere. In particular, the notation of Horne and Anderson is used.

B. Hydrodynamic Equations

In displaying the conservation equations of hydrodynamics, limitation to continuous, isotropic, nonreacting

binary liquid systems is intended. The continuity equations of mass for the bulk liquid and for component 1 (only 2 of the 3 possible equations for a binary system are independent) are

$$(\rho/dt) + \rho \nabla \cdot \underline{v} = 0 \quad (2.1)$$

and

$$\rho(dw_1/dt) + \nabla \cdot \underline{j}_1 = 0 \quad (2.2)$$

where t is time, ρ is density, w_1 is mass fraction, and \underline{v} is the center of mass or barycentric velocity related to individual laboratory referenced component velocities by $\underline{v} = w_1 \underline{v}_1 + w_2 \underline{v}_2$. The diffusion flux \underline{j}_1 is defined by

$$\underline{j}_1 = \rho_1 (\underline{v}_1 - \underline{v})$$

where $\rho_1 = w_1 \rho$.

The Navier-Stokes equation derivable from the momentum conservation equation for a Newtonian fluid is

$$\begin{aligned} \rho(d\underline{v}/dt) + \nabla[(2/3\eta - \phi)(\nabla \cdot \underline{v})] - 2\nabla \cdot \eta \text{sym} \nabla \underline{v} \\ = \rho \sum_{i=1}^3 X_i - \nabla P \end{aligned} \quad (2.3)$$

where $\text{sym} \nabla \underline{v}$ is the symmetric part of the tensor $\nabla \underline{v}$, η is

shear viscosity, ϕ is bulk viscosity, X_i are external forces, and P is pressure.

The equation of energy transport with temperature and pressure as independent variables is

$$\rho \bar{C}_p \frac{dT}{dt} - T\beta \frac{dP}{dt} = \phi_1 - \nabla \cdot \underline{q} - j_1 \cdot \nabla (\bar{H}'_1 - \bar{H}'_2) \quad (2.4)$$

where \bar{C}_p is specific heat, T is temperature, β is thermal expansivity, ϕ_1 is the entropy source term for bulk flow, \underline{q} is the heat flux, and \bar{H}'_1 is partial specific enthalpy of component 1 (prime indicates inclusion of any necessary work terms due to external forces). The entropy source term ϕ_1 is

$$\phi_1 \equiv (\underline{g} + P\underline{1}) : \nabla \underline{v} \quad (2.5)$$

where \underline{g} is the stress tensor.

Equations (2.1) - (2.4) are formulated in general terms for pedagogical reasons. Considerable simplification occurs in the preceding equations for the experimental arrangements necessary to measure the diffusion thermo-effect. If the width/height ratio of the fluid slab in Figure 1.1 is large, wall effects can be excluded, and the above equations need only be written for the z -direction taken perpendicular to the interfacial plane. No external fields are present - gravity effects are extremely small since the cell height is only one or two centimeters.

Pressure terms are very small for this experimental arrangement (Anderson and Horne [1970]). Because liquid densities are usually quite similar, the barycentric velocity will be small enough that all terms of order $(\partial v/\partial z)^2$ can be safely neglected. These simplifications eliminate the Navier-Stokes equation - there is no convection in the cell unless temperature gradients cause density inversions. Likewise, the entropy source for bulk flow ϕ_1 is negligible due to its dependence on the square of the velocity gradient.

With the above restrictions and the relation between substantial and local time derivatives, $d/dt = (\partial/\partial t) + \underline{v} \cdot \underline{\nabla}$, Equations (2.1), (2.2), and (2.4) become

$$(\partial \rho / \partial t) + (\partial \rho v / \partial z) = 0, \quad (2.6)$$

$$\rho (\partial w_1 / \partial t) + (\partial j_1 / \partial z) + \rho v (\partial w_1 / \partial z) = 0, \quad (2.7)$$

and

$$\rho \bar{C}_p (\partial T / \partial t) = (\partial q / \partial z) - j_1 [\partial (\bar{H}_1 - \bar{H}_2) / \partial z] - \rho \bar{C}_p v (\partial T / \partial z) \quad (2.8)$$

respectively. Before these three equations can be solved for v , w_1 , and T ; expressions for the heat and mass fluxes must be introduced. These are deduced from the theories of nonequilibrium thermodynamics.

C. Nonequilibrium Thermodynamics Equations

The framework of nonequilibrium thermodynamics rests on the foundation of "local states". This simply requires that all thermodynamic functions of state exist for each microscopic volume element of the system. Furthermore, these thermodynamic quantities, in the case of nonequilibrium systems, are the same functions of the local state variables as the corresponding equilibrium thermodynamic quantities (Fitts [1962]). This permits the concepts of temperature and entropy in nonequilibrium systems even though their definitions evolved from thermostatic states. Likewise, the Gibbsian equations are valid and, therefore,

$$\rho \frac{d\bar{S}}{dt} = \frac{\rho}{T} \frac{d\bar{U}}{dt} - \frac{P}{T} \frac{d\ln\rho}{dt} - \frac{\rho}{T} \sum_{i=1}^2 \bar{\mu}_i \frac{dw_i}{dt}, \quad (2.9)$$

where \bar{S} is specific entropy, \bar{U} is specific internal energy, and $\bar{\mu}_i$ is the specific chemical potential of component i .

Entirely from balance techniques for the entropy of a local volume element (similar to the method by which the hydrodynamic equations are often derived), an entropy equation can be written in the form

$$\rho d\bar{S}/dt = \phi/T - \nabla \cdot \underline{j}_s \quad (2.10)$$

where \underline{j}_s is the entropy flux due to mass and heat flows and the semidefinite positive quantity ϕ/T is the rate

per unit volume of the internal entropy production. Substitution of the hydrodynamic equations for mass and energy balance into Equation (2.9) and subsequent comparison to Equation (2.10) allows identification of ϕ after considerable rearrangement. For the system at hand (a binary, field-free, isotropic, nonreacting, nonelectrolyte liquid mixture),

$$\phi = \phi_1 + \phi_2 \quad (2.11)$$

where

$$\phi_1 = (\underline{\underline{\sigma}} + P\underline{\underline{1}}) : \underline{\underline{\nabla}}\underline{\underline{v}}$$

and

$$\phi_2 = -\underline{\underline{q}} \cdot \underline{\underline{\nabla}} \ln T - \underline{\underline{j}}_1 \cdot \underline{\underline{\nabla}}_T (\bar{\mu}_1 - \bar{\mu}_2)$$

with $\underline{\underline{\nabla}}_T \bar{\mu}_1 \equiv \underline{\underline{\nabla}} \bar{\mu}_1 + \bar{S}_1 \underline{\underline{\nabla}} T$.

It is important to note that ϕ is of the form $\phi = \sum_1 \underline{\underline{J}}_1 X_1$ where the $\underline{\underline{J}}_1$ and X_1 represent fluxes and driving forces respectively. The fluxes and forces in ϕ_1 are tensors of rank 2 while those of ϕ_2 are vectors. Centuries of experimental work have shown linear coupling of fluxes and forces $\underline{\underline{J}}_1 = \sum_j \Omega_{1j} X_j$. For the isotropic liquids considered here, Curie's theorem, based on spacial symmetry

arguments, allows coupling only between those fluxes and forces which do not differ in tensorial character by an odd integer. In Equation (2.11), the fluxes and forces of ϕ_1 and ϕ_2 cannot interact. Therefore, heat and mass fluxes are

$$-\underline{q} = \Omega_{00} \nabla \ln T + \Omega_{01} \nabla_T (\bar{\mu}_1 - \bar{\mu}_2) \quad (2.12)$$

$$-\underline{j}_1 = \Omega_{01} \nabla \ln T + \Omega_{11} \nabla_T (\bar{\mu}_1 - \bar{\mu}_2) \quad (2.13)$$

where the Ω_{ij} are called Onsager coefficients. The utility and indeed the present reason for the nonequilibrium thermodynamic approach is the identification of correct fluxes and driving forces and their proper coupling as required by the entropy production equation. For many years, the driving force for diffusion was thought to be a composition gradient (Fick's original laws), but the equations of nonequilibrium thermodynamics readily identify it as a gradient of chemical potential.

D. Transport Parameters and Equations

The Onsager coefficients which appear in Equations (2.12) and (2.13) are related to experimentally observed transport coefficients. In fact, their identification is made by comparison with their phenomenological counterparts (Fick's law, Fourier's heat conduction law, etc.).

The Ω_{ij} for this binary nonelectrolyte mixture are

$$\Omega_{00} = \kappa T \quad (A)$$

$$\Omega_{01} = \rho D \bar{Q}_1^* w_2 / \bar{\mu}_{11} \quad (B)$$

$$\Omega_{10} = \rho D_T \quad (C)$$

$$\Omega_{11} = \rho D w_2 / \bar{\mu}_{11} \quad (D)$$

$$(2.14)$$

where κ is thermal conductivity, D is mutual diffusivity, \bar{Q}_1^* is specific heat of transport (the commonly used measure of heat transported by diffusion in a diffusion thermo-effect arrangement), $\bar{\mu}_{11} \equiv (\partial \bar{\mu}_1 / \partial w_1)_{T,P}$, and D_T is the thermal diffusion coefficient. Often experimental thermal diffusion results are expressed in terms of the thermal diffusion factor α_1 or the thermal diffusion ratio K_T rather than the thermal diffusion coefficient D_T . These three coefficients are related by

$$K_T \equiv D_T / D \quad (2.15)$$

and

$$-\alpha_1 \equiv K_T / w_1 w_2 \quad (2.16)$$

Likewise, it is sometimes desirable to retain the form of Equation (2.12) in which only a single transport coefficient appears but written in terms of mole fraction rather than chemical potential. If Equation (2.12) is written

$$-\underline{q} = \kappa \underline{\nabla} T + \beta_T \underline{\nabla} x_1 \quad , \quad (2.17)$$

a new coefficient β_T is defined known as the Dufour coefficient. From Equation (2.14B) and the relationship between mass fraction and mole fraction, β_T is related to \bar{Q}_1^* by

$$\beta_T = \rho D \bar{Q}_1^* M_1 M_2 / \tilde{M}^2 \quad (2.18)$$

where \tilde{M} is the mean molecular weight defined by $\tilde{M} = x_1 M_1 + x_2 M_2$.

From Equations (2.12), (2.13), (2.14B), and (2.14D), the defining equation for the heat of transport \bar{Q}_1^* is seen to be

$$\bar{Q}_1^* \equiv (\underline{q} / \underline{j}_1)_{\Delta T = 0} \quad . \quad (2.19)$$

The heat of transport can therefore be thought of as a heat flux produced by an isothermal mass flux. If the isothermal conditions of Equation (2.19) are relaxed, then

$$\underline{q} = \underline{j}_1 \bar{Q}_1^* - \kappa \underline{\nabla} T \quad (2.20)$$

(de Groot and Mazur [1969]). This relationship shows the two effects which determine the magnitude of the temperature

difference measured between two points in a diffusion thermoeffect cell. The heat transported via the mass flux builds up a temperature gradient while thermal conduction tends to diminish it. The relative magnitudes of \bar{Q}_1^* and κ , for a given diffusional flux, determine the magnitude of the ensuing temperature gradient. Note also that the transient nature of the diffusion thermoeffect is due to a nonconstant mass flux. When $\underline{q} = 0$ the heat flow transported by diffusion identically balances the conduction heat flow and

$$\underline{\nabla}T = \underline{j}_1 \bar{Q}_1^* / \kappa \quad . \quad (2.21)$$

If \underline{j}_1 remained constant throughout the experiment, a steady state $\underline{\nabla}T$ would be measured. However, as diffusion decreases the composition gradient, \underline{j}_1 decreases. This lowers $\underline{\nabla}T$ and a time dependent behavior is observed.

Not all of the set $\{\kappa, D, \bar{Q}_1^*, D_T\}$ are independent. Onsager [1931], applying microscopic reversibility concepts, showed that the matrix of coefficients involved in the flux-force relations must be symmetric. Though experimental evidence accrues constantly in support of the Onsager reciprocal relations (Miller [1960] and [1975]), the results reported herein constitute the first experimental evidence of the heat-mass ORR. For the system described by Equations (2.12) and (2.13), ORR implies

$$\Omega_{01} = \Omega_{10} \quad . \quad (2.22)$$

Substitution of Equations (2.14) for the Onsager coefficients in Equations (2.12) and (2.13) yields for the applicable one dimensional flux equations

$$-q = \kappa(\partial T/\partial z) + \rho D \bar{Q}_1^* (\partial w_1/\partial z) \quad (2.23)$$

$$-j_1 = \rho D (\partial w_1/\partial z) - \rho D \alpha_1 w_1 w_2 T^{-1} (\partial T/\partial z) \quad (2.24)$$

where the Gibbs-Duhem equation has been invoked to help transform chemical potential gradients to single mass fraction gradients.

Ingle and Horne [1973] argue on the basis of numerical values for common liquid systems that $|\alpha_1 w_1 w_2 T^{-1}|$ is of the order 10^{-3} deg^{-1} and that therefore thermal diffusion is at most 0.01% of diffusion, assuming that composition gradients are an order of magnitude larger than temperature gradients for diffusion thermoeffect experiments. Neglect of the thermal diffusion term in Equation (2.24) and substitution of Equations (2.23) and (2.24) into Equations (2.7) and (2.8), yields partial differential equations which completely (with appropriate initial and boundary conditions) define v , w_1 , and T as functions of t and z :

$$(\partial\rho/\partial t) + (\partial\rho v/\partial z) = 0 \quad (2.25)$$

$$\rho(\partial w_1/\partial t) = \{\partial[\rho D(\partial w_1/\partial z)]/\partial z\} - \rho v(\partial w_1/\partial z) \quad (2.26)$$

$$\begin{aligned} \rho\bar{C}_p(\partial T/\partial t) = & \rho D[\partial(\bar{H}_1 - \bar{H}_2)/\partial z](\partial w_1/\partial z) \\ & + \{\partial[\rho D\bar{Q}_1^*(\partial w_1/\partial z)]/\partial z\} \\ & - \rho\bar{C}_p v(\partial T/\partial z) + \{\partial[\kappa(\partial T/\partial z)]/\partial z\}. \quad (2.27) \end{aligned}$$

These equations are identical to the starting equations used by Ingle and Horne [1973] in their analytical double perturbation solution of the diffusion thermoeffect problem. Their perturbation scheme, while allowing solution even with composition and temperature dependent parameters, results in solutions which are extremely bulky and complex. The number of terms required and the rapidly increasing complexity of successively higher order terms limit the practical application of this technique to those liquid systems whose properties are only slightly temperature and composition dependent. This unfortunately is not the case for the systems of interest here. To avoid these difficulties the numerical scheme discussed in Chapter 3 is used.

The initial condition for the composition equation is a step function

$$w_1(z/a > 0.5, 0) = w_1^u \quad (2.28)$$

$$w_1(z/a < 0.5, 0) = w_1^L$$

where w_1^u and w_1^L are the mass fractions of component 1 at which the upper and lower phases respectively are prepared. Exactly at the interface w_1 is an arithmetic average of the two phases but it need not be defined unless a grid point of the numerical scheme is located at that position. The measured temperature distribution just prior to interface formation becomes the initial condition for the temperature equation. It should roughly correspond to isothermal conditions so that thermal diffusion can be neglected. Thus, the initial condition is

$$T(z/a, 0) = T(z/a) \quad (2.29)$$

where $T(z/a)$ is a constant for isothermal conditions.

Boundary conditions can be imposed from the physical aspects of the experimental design. Because the walls are impermeable to matter,

$$v(0,t) = 0 = v(1,t) \quad (2.30)$$

for the barycentric velocity and $j_1 = 0$ at $(z/a) = 0$ & 1 for the mass flux. Fick's law restates the vanishing

mass flux boundary condition as

$$(\partial w_1 / \partial z)_{0,t} = 0 = (\partial w_1 / \partial z)_{1,t} \quad (2.31)$$

since D never vanishes. The boundary conditions for the temperature equation depend on the experimental arrangement desired. If the walls are adiabatically insulated the heat flux vanishes at the walls and, from Fourier's heat conduction law,

$$(\partial T / \partial z)_{0,t} = 0 = (\partial T / \partial z)_{1,t} \quad (2.32)$$

Although Equation (2.32) is the boundary condition used in these experiments (the cell was adiabatically insulated to maximize induced temperature inequalities), it is not the only boundary condition which can be used.

Before limiting discussion to the carbon tetrachloride-cyclohexane system (which provides a convenient system for study of the diffusion thermoeffect away from critical regions), it is appropriate to list the assumptions involved in the derivation of Equations (2.25) - (2.27) for they will also serve as the starting point in the analysis of systems exhibiting critical mixing. The assumptions employed are:

- (1) The linear hydrodynamic equations for conservation of mass and energy are valid.

- (2) The binary system is isotropic, nonreacting, and field free.
- (3) Local states are assumed, i.e., the equations of thermostatics apply for local regions.
- (4) Fluxes are linear combinations of these forces which appear in the entropy production equation and which have the same tensorial rank.
- (5) Pressure terms are negligible.
- (6) The bulk flow entropy source term is small.
- (7) The thermal diffusion portion of the mass flux is small relative to the diffusional contribution.
- (8) The phenomenon takes place entirely in one dimension, so that wall effects are unimportant.

E. Mole Fraction Equations for Carbon Tetrachloride-Cyclohexane Mixtures

The properties of the carbon tetrachloride-cyclohexane system are much more nearly constant in molal rather than in specific quantities. A transformation is therefore useful, with respect to numerical step sizes and to possible simplifications, from mass fractions and specific properties to mole fractions and molal properties. Transformation of Equations (2.25) - (2.27) with the aid of the transformation identities in Appendix A results in

$$(\partial v / \partial z) = (M_2 \tilde{V}_1 - M_1 \tilde{V}_2) \{ \partial [(D / \tilde{M}) (\partial x_1 / \partial z)] / \partial z \}, \quad (2.33)$$

$$(\partial x_1 / \partial t) = \tilde{V}\tilde{M}\{\partial[(D/\tilde{V}\tilde{M})(\partial x_1 / \partial z)] / \partial z\} - v(\partial x_1 / \partial z), \quad (2.34)$$

and

$$\begin{aligned} (\partial T / \partial t) = & (\tilde{V} / \tilde{C}_p) \{\partial[\kappa(\partial T / \partial z)] / \partial z\} \\ & + (M_2 \tilde{V} / \tilde{C}_p) \{\partial[(D\tilde{Q}_1^* / \tilde{V}\tilde{M})(\partial x_1 / \partial z)] / \partial z\} \\ & + (D / \tilde{C}_p) (\partial^2 \tilde{H}^E / \partial x_1^2)_{T,P} (\partial x_1 / \partial z)^2 - v(\partial T / \partial z) \quad (2.35) \end{aligned}$$

where x_1 is mole fraction of component 1, \tilde{V} is molar volume, \tilde{C}_p is molar constant pressure heat capacity, \tilde{Q}_1^* is the molar heat of transport, and \tilde{H}^E is the molar excess enthalpy. Equations (2.33) - (2.35) are the mole fraction-molar property versions of the mass fraction-specific property Equations (2.25) - (2.27) which Ingle and Horne [1973] used. The excess molar enthalpy \tilde{H}^E is related to the difference in partial specific enthalpies by

$$[\partial(\bar{H}_1 - \bar{H}_2) / \partial z] = (\tilde{M} / M_1 M_2) (\partial^2 \tilde{H}^E / \partial x_1^2)_{T,P} (\partial x_1 / \partial z) \quad (2.36)$$

as derived in Appendix A.

For carbon tetrachloride-cyclohexane mixtures, the excess volume of mixing is very small (Wilhelm and Sackmann [1974] indicate it to be everywhere less than 0.2% of the total molar volume) and $\tilde{V}_1 = \tilde{V}_1^0$ where \tilde{V}_1^0 is the

pure component molar volume. Integration of Equation (2.33) subject to the boundary conditions

$$v(0,t) = 0 = v(1,t) \quad (2.37)$$

and

$$(\partial x_1 / \partial z)_{0,t} = 0 = (\partial x_1 / \partial z)_{1,t} , \quad (2.38)$$

yields for the barycentric velocity

$$v = (M_2 \tilde{V}_1^0 - M_1 \tilde{V}_2^0) (D / \tilde{V} \tilde{M}) (\partial x_1 / \partial z) . \quad (2.39)$$

Substitution of this expression into Equation (2.34) produces upon rearrangement

$$\begin{aligned} (\partial x_1 / \partial t) = & D (\partial^2 x_1 / \partial z^2) + [(\partial D / \partial x_1)_{T,P} \\ & - 2(D / \tilde{V}) (\partial \tilde{V} / \partial x_1)_{T,P}] (\partial x_1 / \partial z)^2. \end{aligned} \quad (2.40)$$

For the experiments reported in this dissertation, the composition and temperature dependencies of D and \tilde{V} in Equation (2.40) do not measurably contribute to the observed temperature difference produced by the diffusion thermoeffect. Numerical verification of this statement was made by determination of the heat of transport (from

experimental temperature differences) both with and without the composition and temperature dependencies of D and \tilde{V} . No detectable effect was found. There were of course small differences in the composition as a function of time and position because of the dependence of the parameters D and \tilde{V} on composition. Nevertheless, small errors in the composition profile due to relatively good assumptions in the diffusion equation had a negligible effect on the solution of the temperature equation. It suffices therefore to use

$$(\partial x_1 / \partial t) = D_0 (\partial^2 x_1 / \partial z^2) \quad (2.41)$$

instead of Equation (2.40) to describe composition in time and space where the subscript 0 is used to denote evaluation of the parameter D at $x_1 = 0.5$ and $T = 298.15$ °K. Explicit formulas for calculating directly the effect of the composition and temperature dependence of D and \tilde{V} on the experimentally observed temperature differences may be found in the paper by Ingle and Horne [1973]. As emphasized there, these dependencies do not contribute to the temperature difference measured symmetrically about the interface because they involve terms of only even symmetry about the center.

The solution of Equation (2.41), subject to the experimental boundary conditions, is

$$x_1 = \langle x_1 \rangle + 2(\Delta x_1/\pi) \sum_{\ell=0}^{\infty} (-1)^\ell (2\ell+1)^{-1} \\ \times \{\exp[-(2\ell+1)^2(t/\theta)]\} \cos[(2\ell+1)\pi z/a] \quad (2.42)$$

where $\langle x_1 \rangle$ is the initial arithmetic mean x_1 , Δx_1 is the difference in x_1 between the initial two phases, and $\theta \equiv a^2/\pi^2 D_0$. It is important to note that the numerical technique described in the next chapter allows solution of Equation (2.40) in its entirety when Equation (2.41) is not satisfactory for the desired system. In actual practice, numerical solutions for both the composition and temperature equations were used in the determination of the heat of transport. This allowed development of a computer program using the more general equation which could then be quickly simplified to Equation (2.41) for appropriate systems such as carbon tetrachloride-cyclohexane.

CHAPTER 3

NUMERICAL SOLUTION OF THE DIFFUSION THERMOEFFECT EQUATIONS

A. General Scheme

Equations (2.40) and (2.35) or Equations (2.41) and (2.35) with the initial and boundary conditions of Equations (2.28), (2.29), (2.32), and (2.38) completely describe the diffusion thermoeffect for the conditions of experimental interest. Explicit solution of these equations is not easy because they are not only nonhomogeneous but are also coupled and nonlinear with nonconstant coefficients. This type of problem is, in general, unsolvable without recourse to numerical techniques. The general presentation discussed here is due to Rosenberg [1969].

To obtain a numerical solution, continuous variables are replaced by their discrete counterparts. Partial derivatives are represented by finite differences so that the partial differential equations become finite difference equations - algebraic rather than differential. To obtain discrete variables, the continuous time-space domain of the problem is subdivided as shown in Figure 3.1. The time domain is divided into rows labeled with the

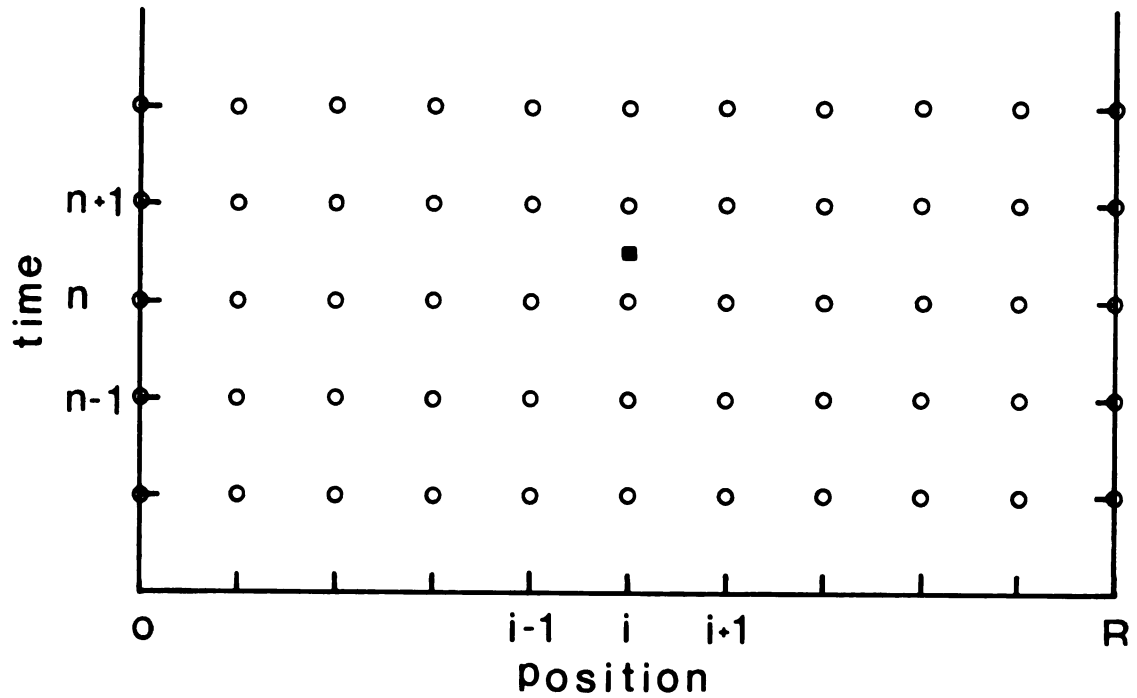


Figure 3.1. Crank-Nicholson grid scheme for finite difference equations. Properties are evaluated at the i,n positions, \circ . Derivatives are evaluated at the $i,n+1/2$ positions, \blacksquare .

index n . The spatial domain is divided into R columns each labeled with an index denoted by i . Any dependent variable U can be specified in time and space with its appropriate indices $U_{i,n}$.

If $U_{i+1,n}$ is expanded in a Taylor's series about the point $U_{i,n}$ (at constant n),

$$U_{i+1,n} = U_{i,n} + (\partial U / \partial z)_{i,n} \Delta z + (\partial^2 U / \partial z^2)_{i,n} (\Delta z)^2 / 2! + (\partial^3 U / \partial z^3)_{i,n} (\Delta z)^3 / 3! + \dots, \quad (3.1)$$

finite difference representations for spatial derivatives can be obtained in terms of the distance between two consecutive spatial grid points Δz . This is done by writing the Taylor's expansion for $U_{i-1,n}$ about $U_{i,n}$,

$$U_{i-1,n} = U_{i,n} - (\partial U / \partial z)_{i,n} \Delta z + (\partial^2 U / \partial z^2)_{i,n} (\Delta z)^2 / 2! - (\partial^3 U / \partial z^3)_{i,n} (\Delta z)^3 / 3! + \dots, \quad (3.2)$$

and then by comparing Equations (3.1) and (3.2). For instance, the forward and backward difference equations for the first derivative are obtained by rearranging Equations (3.1) and (3.2) respectively and then truncating them to obtain

$$(\partial U / \partial z)_{i,n} = (U_{i+1,n} - U_{i,n}) / \Delta z, \quad (3.3)$$

and

$$(\partial U / \partial z)_{i,n} = (U_{i,n} - U_{i-1,n}) / \Delta z \quad . \quad (3.4)$$

Notice that the first term omitted in the truncation is $(\partial^2 U / \partial z^2)_{i,n} \Delta z / 2!$. The truncation error is first order in Δz , and the finite difference expressions are therefore first order correct analogs. A better approximation for the first derivative is obtained by subtracting Equation (3.2) from Equation (3.1),

$$\begin{aligned} (\partial U / \partial z)_{i,n} &= (U_{i+1,n} - U_{i-1,n}) / 2\Delta z \\ &- (\partial^3 U / \partial z^3)_{i,n} (\Delta z)^2 / 3! - \dots, \end{aligned}$$

and then truncating terms of order $(\Delta z)^2$ and higher, with the result

$$(\partial U / \partial z)_{i,n} = (U_{i+1,n} - U_{i-1,n}) / 2\Delta z \quad . \quad (3.5)$$

Equation (3.5) is a second order correct representation of the first spatial derivative. A graphical comparison of first and second order correct finite difference analogs is reproduced in Figure 3.2 (Rosenberg [1969]) where line "a" represents the true slope of the curve at a point. Line "b" is the second order correct analog and approximates

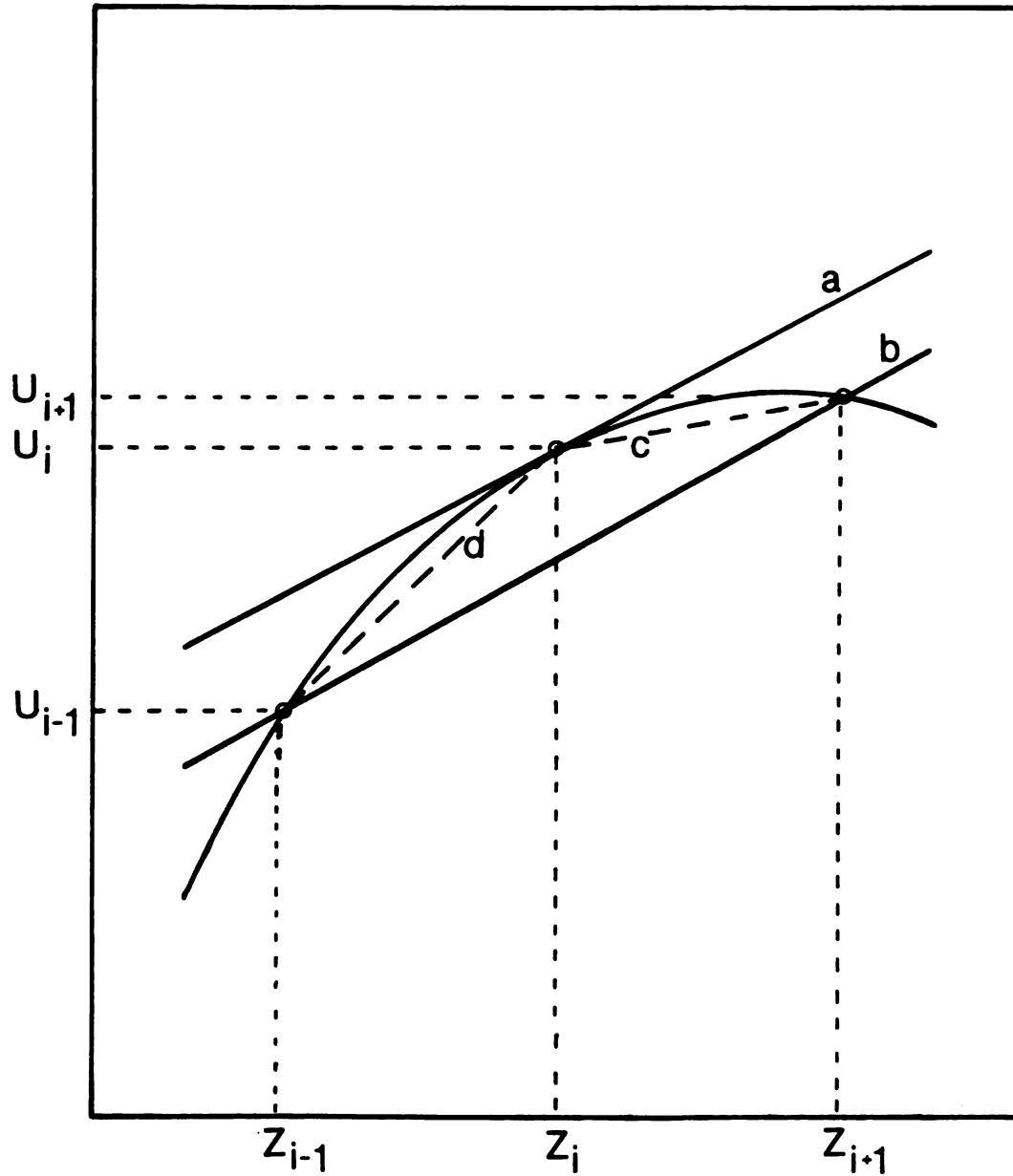


Figure 3.2. Graphical comparison of first and second order correct analogs for the first derivative as illustrated by Rosengren [1969]. a. Actual derivative. b. Second order correct analog. c. First order forward difference. d. First order backward difference.

the slope much more closely than the forward and backward first order correct analogs shown as lines "c" and "d", respectively.

A second order correct approximation for the second derivative can be obtained by adding equations (3.1) and (3.2) and truncating terms of order $(\partial^4 U / \partial z^4)_{i,n} (\Delta z)^2 / 4!$ and higher,

$$(\partial^2 U / \partial z^2)_{i,n} = (U_{i+1,n} - 2U_{i,n} + U_{i-1,n}) / (\Delta z)^2. \quad (3.6)$$

The finite difference expression for the first time derivative can also be made second order correct by using the Crank-Nicholson method. Finite difference expressions are centered about the points $z_i, t_{n+1/2}$ which are half-way between the known and unknown time levels. Dependent variables U are evaluated at grid points, represented by open circles in Figure 3.1, while derivatives are calculated at center points such as the one designated with the black square. The time derivative is

$$(\partial U / \partial t)_{i,n+1/2} = (U_{i,n+1} - U_{i,n}) / \Delta t \quad (3.7)$$

which is second order correct. The spatial derivatives in this scheme become

$$\begin{aligned}
 (\partial U / \partial z)_{i,n+1/2} &= 1/4[(U_{i+1,n+1} - U_{i-1,n+1})/\Delta z \\
 &+ (U_{i+1,n} - U_{i-1,n})/\Delta z] , \quad (3.8)
 \end{aligned}$$

and

$$\begin{aligned}
 (\partial^2 U / \partial z^2)_{i,n+1/2} &= 1/2[(U_{i+1,n} - 2U_{i,n} + U_{i-1,n})/(\Delta z)^2 \\
 &+ (U_{i+1,n+1} - 2U_{i,n+1} + U_{i-1,n+1})/(\Delta z)^2] . \quad (3.9)
 \end{aligned}$$

The Crank-Nicholson method is particularly effective for the diffusion thermoeffect problem because there is no stability restriction on $\Delta t/(\Delta z)^2$.

Equations (2.40) and (2.35) are of the same general form¹,

$$a(\partial U / \partial t) - (\partial^2 U / \partial z^2) + b(\partial U / \partial z) = d \quad (3.10)$$

where a, b, and d are combinations of various transport and thermodynamic properties and are, in general, functions

¹Although for the carbon tetrachloride-cyclohexane system Equation (2.41) was used in place of Equation (2.40), the solution procedure outlined here uses the more general Equation (2.40). Both equations yield the same temperature difference result for carbon tetrachloride-cyclohexane mixtures.

of temperature and composition. Substitution of Equations (3.7) - (3.9) into Equation (3.10) followed by a regrouping of terms yields the algebraic expressions

$$\begin{aligned}
 & A_{i,n+1/2}U_{i-1,n+1} + B_{i,n+1/2}U_{i,n+1} \\
 & + C_{i,n+1/2}U_{i+1,n+1} = D_{i,n+1/2}
 \end{aligned} \tag{3.11}$$

where

$$A_{i,n+1/2} = 1 + (\Delta z)b_{i,n+1/2}/2 \quad , \tag{3.12A}$$

$$B_{i,n+1/2} = -2-2(\Delta z)^2a_{i,n+1/2}/\Delta t \quad , \tag{3.12B}$$

$$C_{i,n+1/2} = 1-(\Delta z)b_{i,n+1/2}/2 \quad , \tag{3.12C}$$

and

$$\begin{aligned}
 D_{i,n+1/2} = & -A_{i,n+1/2}U_{i-1,n} + [2-2(\Delta z)^2a_{i,n+1/2}/\Delta t]U_{i,n} \\
 & - C_{i,n+1/2}U_{i+1,n} - 2(\Delta z)^2d_{i,n+1/2} \quad . \tag{3.12D}
 \end{aligned}$$

The equations are grouped in this fashion to display their recursive nature. Values of U on the right hand side of Equation (3.11) depend only on the nth time row while those on the left hand side depend only on the n+1st row. A

complete time row must be solved simultaneously from the previously calculated row since $U_{i,n+1}$ appears in Equation (3.11) with both adjacent neighbors $U_{i-1,n+1}$ and $U_{i+1,n+1}$.

Although the coefficients A, B, C and d are to be evaluated between the time rows, an iterative procedure can be avoided if $A_{i,n+1/2} \approx A_{i,n}$; $B_{i,n+1/2} \approx B_{i,n}$; $C_{i,n+1/2} \approx C_{i,n}$; and $d_{i,n+1/2} \approx d_{i,n}$. In this case, properties of the system need be evaluated only at the n^{th} time row where temperature and composition have already been calculated. Because the composition equation is solved prior to the temperature equation along the $n+1^{\text{st}}$ row, the temperatures and compositions of the n^{th} row grid points are used to evaluate the parameters at the respective $n+1/2$ locations. The temporal spacing of the grid points is based on a thermal conduction time scale which is much faster than a diffusion time scale. Hence, the change in composition between n and $n+1/2$ is negligible. Similarly, as long as the row spacing Δt is not too large, the temperature dependence of the parameters evaluated at t_n will be essentially identical to the values at $t_{n+1/2}$. For the temperature equation, the parameters are directly evaluated at $n+1/2$ with respect to composition by averaging the composition at t_n and t_{n+1} . The temperature dependence of the parameters, however, is again evaluated at t_n rather than $t_{n+1/2}$. Little or no error results for Δt small compared to that required for significant changes in the

temperature. Although time step sizes were increased as the experiment progressed, care was taken to ensure that they remained small enough that essentially no error was introduced by evaluating the parameters with respect to temperature at t_n rather than $t_{n+1/2}$. This procedure is summarized in the flow diagram of Figure 3.3.

To solve Equations (3.11) for $U_{i,n+1}$, the values of $U_{i,n}$ must be known. The values for $U_{i,0}$ are obtained from the initial conditions and are therefore completely specified. For any given row of R spatial increments, the values of $U_{0,n}$ and $U_{R,n}$ must also be specified - these are the boundary conditions. Putting Equations (2.32) and (2.38) into finite difference notation yields with the aid of Equation (3.5)

$$U_{0,n} = U_{2,n} \text{ \& } U_{R,n} = U_{R-2,n} \quad (3.13)$$

where the grid points are aligned such that $i=1$ and $i=R-1$ correspond to cell walls. This reflective boundary condition assigns imaginary grid points $i=0$ and $i=R$ outside the cell walls, but U_0 and U_R are never evaluated.

With the previous comments concerning the evaluation of A , B , C , and d ; Equations (3.11) and (3.13) can be combined to yield a $(R-1) \times (R-1)$ tridiagonal matrix for each row in time

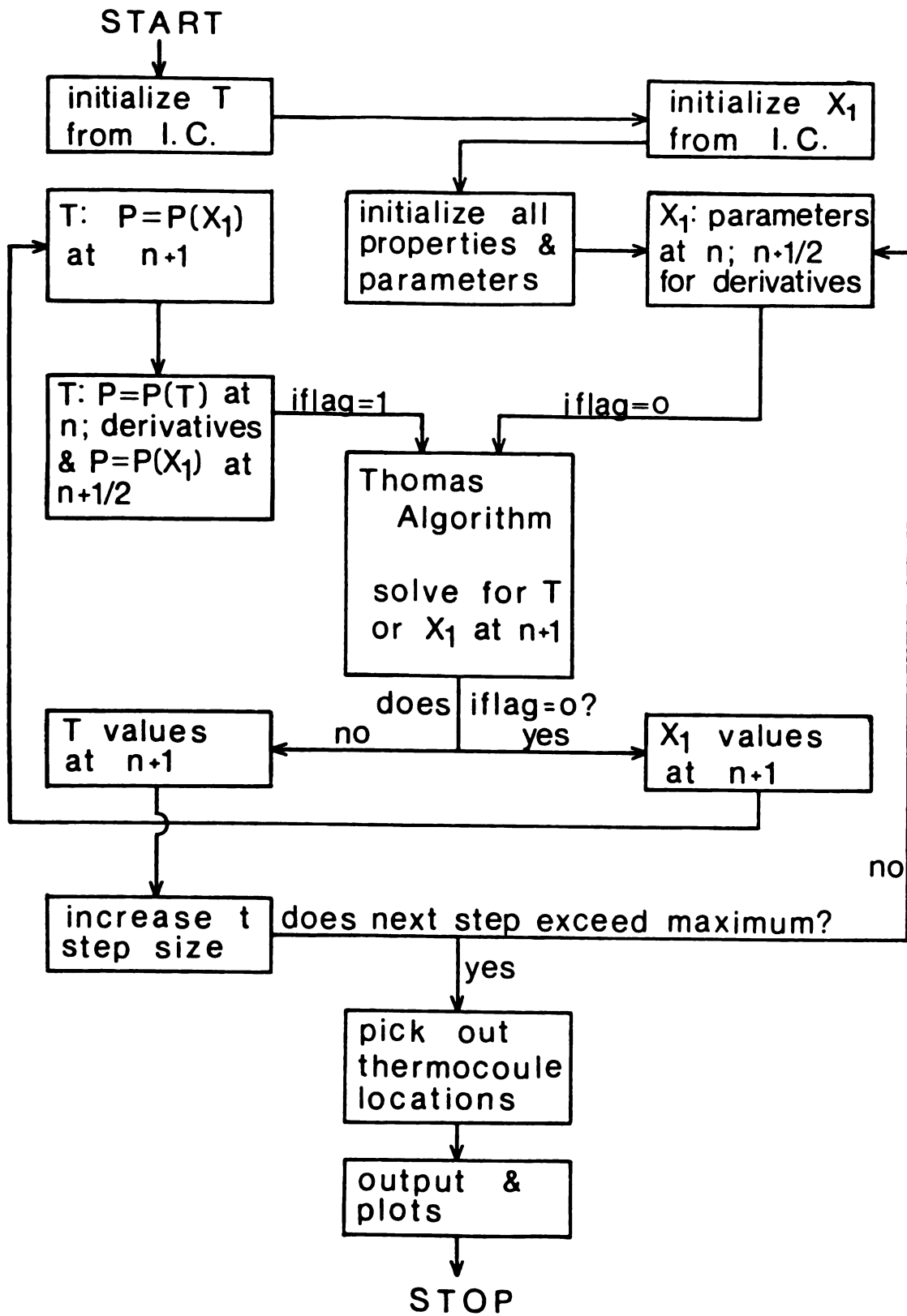


Figure 3.3. Flow diagram for simultaneous numerical solution of the composition and temperature equations.

$$\begin{bmatrix}
 B_1 U_1 & 2C_1 U_2 & 0 & 0 & 0 & \dots \\
 A_2 U_1 & B_2 U_2 & C_2 U_3 & 0 & 0 & \dots \\
 0 & A_3 U_2 & B_3 U_3 & C_3 U_4 & 0 & \dots \\
 0 & 0 & A_4 U_3 & B_4 U_4 & C_4 U_5 & \dots \\
 0 & 0 & 0 & A_5 U_4 & B_5 U_5 & \dots \\
 \cdot & \cdot & \cdot & \cdot & \cdot & \\
 \cdot & \cdot & \cdot & \cdot & \cdot & \\
 \cdot & \cdot & \cdot & \cdot & \cdot &
 \end{bmatrix}
 =
 \begin{bmatrix}
 D_1 \\
 D_2 \\
 D_3 \\
 D_4 \\
 D_5 \\
 \cdot \\
 \cdot \\
 \cdot
 \end{bmatrix}
 \quad (3.14)$$

where the displayed indices are i values. Each tridiagonal matrix system (one for each row in time) is solved via the Thomas Algorithm (Rosengren [1969]) as illustrated in Figure 3.3.

The numerical solution of the diffusion thermoeffect has certain advantages over the lengthy perturbation equations of Ingle and Horne [1973]. The composition and temperature dependence of the parameters are fully included without involving numerous infinite summations. Ingle and Horne's solutions work well for systems whose pure component properties are similar and whose mixture properties are only slightly composition dependent. Otherwise, too many higher order terms are needed in the perturbation scheme for it to succeed.

The main advantage of the numerical technique is that the boundary conditions and initial conditions can be slightly altered without necessitating an entirely new

analytical solution. Different solving techniques are usually required for different boundary conditions in the case of analytical solutions. The initial experimental conditions need not be isothermal to observe the diffusion thermoeffect as long as the initial temperature distribution (it must be small enough to avoid thermal diffusion terms) is known in order to assign values to the first row of grid points. The adiabatic or reflective boundary condition can be changed relatively easily. For diathermal walls, the grid points located at either cell wall can be assigned a value of constant temperature equal to the outside bath temperature.

Once the computer program has been set up to evaluate numerically Equations (3.10), many other transport phenomena are readily simulated by a simple change of variables. Thus, essentially the same program models diffusion, thermal conduction, thermal diffusion, and pressure diffusion (most thermodynamic transport equations are parabolic partial differential equations), as well as the diffusion thermo-effect.

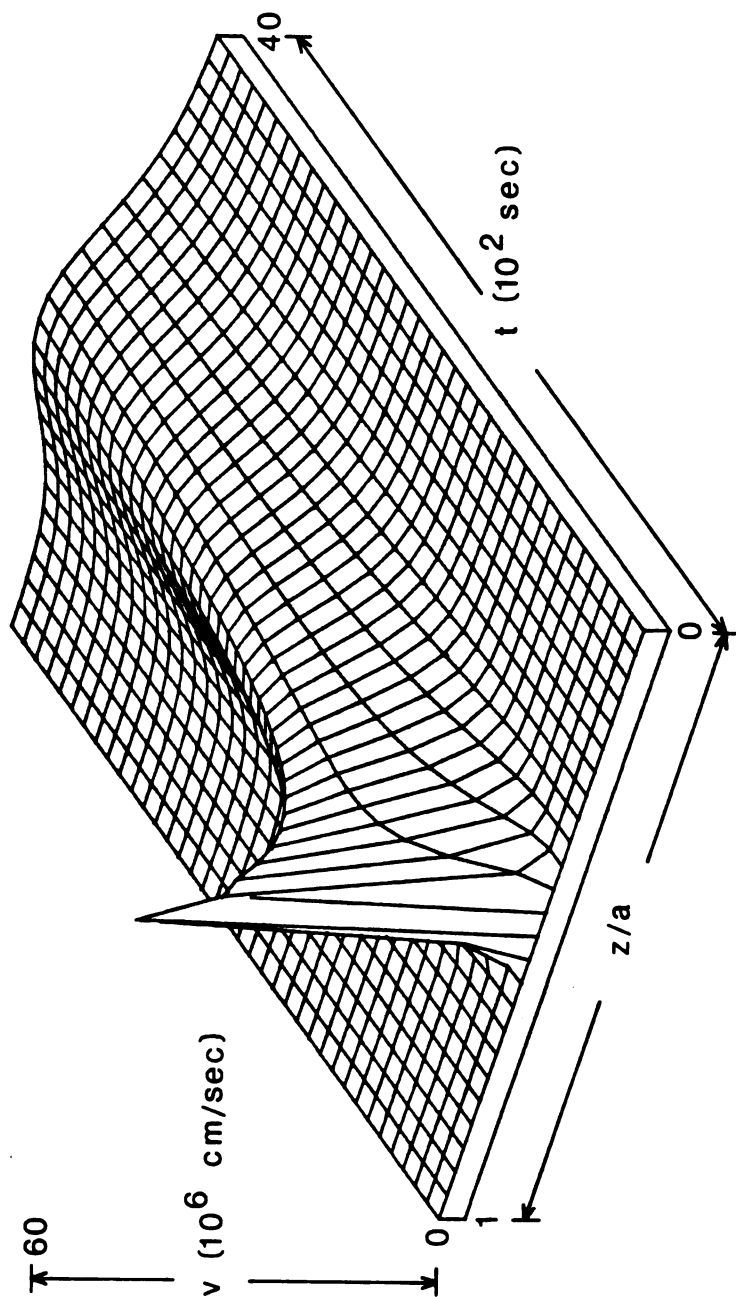
The solutions, obtained as outlined above, were checked for stability by comparison of results obtained using different step sizes. The number of spatial and temporal grid divisions were both varied by more than an order of magnitude without change in the dependent variables except at very short times. Programming was checked by comparison

to the solutions obtained by Ingle and Horne [1973] for a case in which their first order equations adequately described the system.

B. Solutions for the Carbon Tetrachloride-Cyclohexane System

Using parameter values for the $\text{CCl}_4 - \text{C}_6\text{H}_{12}$ system, numerical solutions were generated. Because solution of the corresponding system of tridiagonal matrices yields $U = U(z,t)$, U was generated as a three dimensional surface. The velocity surface obtained indirectly from $x_1(z,t)$ is shown in Figure 3.4. Note that the barycentric velocity v is essentially negligible except for very short times right at the interface. This results from the initial condition where composition (hence density) is a step function. If a simple algebraic solution for the Dufour effect is desired, a good approximation would be to neglect v .

The composition surface shown in Figure 3.5 is indicative of why the diffusion thermoeffect is a transient phenomenon in mixtures away from their critical solution temperatures. Note that as the experimental time proceeds, the gradient of composition flattens out. Heat and mass fluxes are related through the heat of transport by Equation (2.20). As j_1 decreases in time, the measured



VELOCITY SURFACE

Figure 3.4. Barycentric velocity surface for the carbon tetrachloride-cyclohexane system.

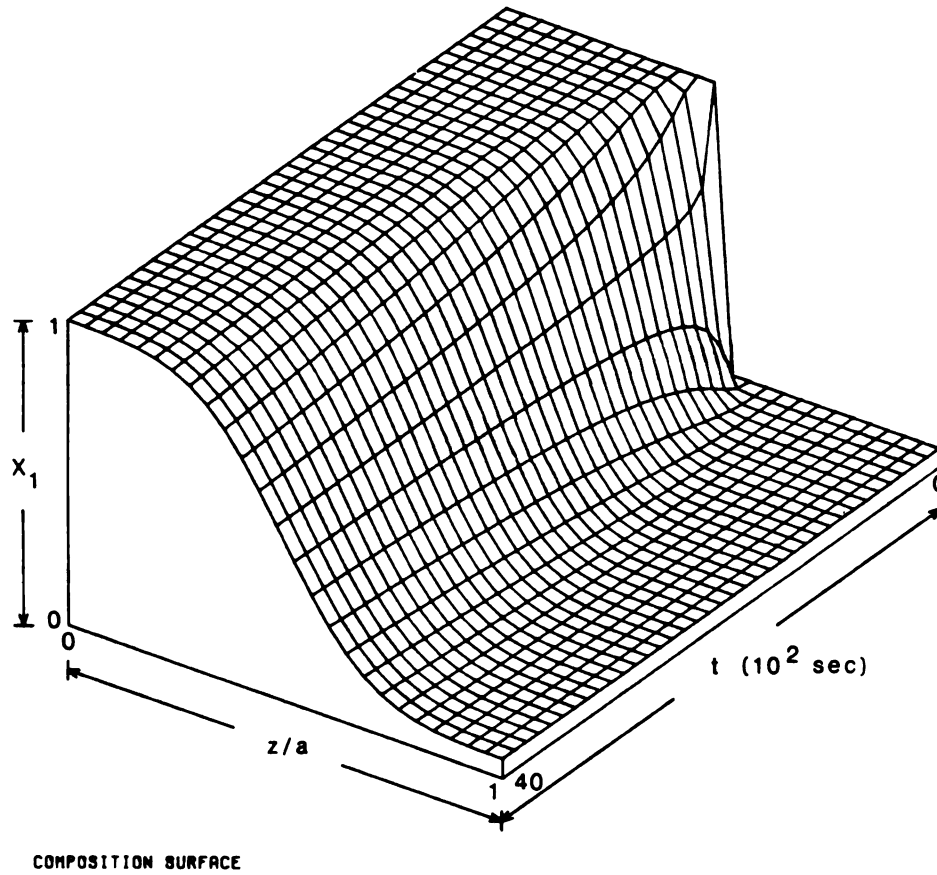
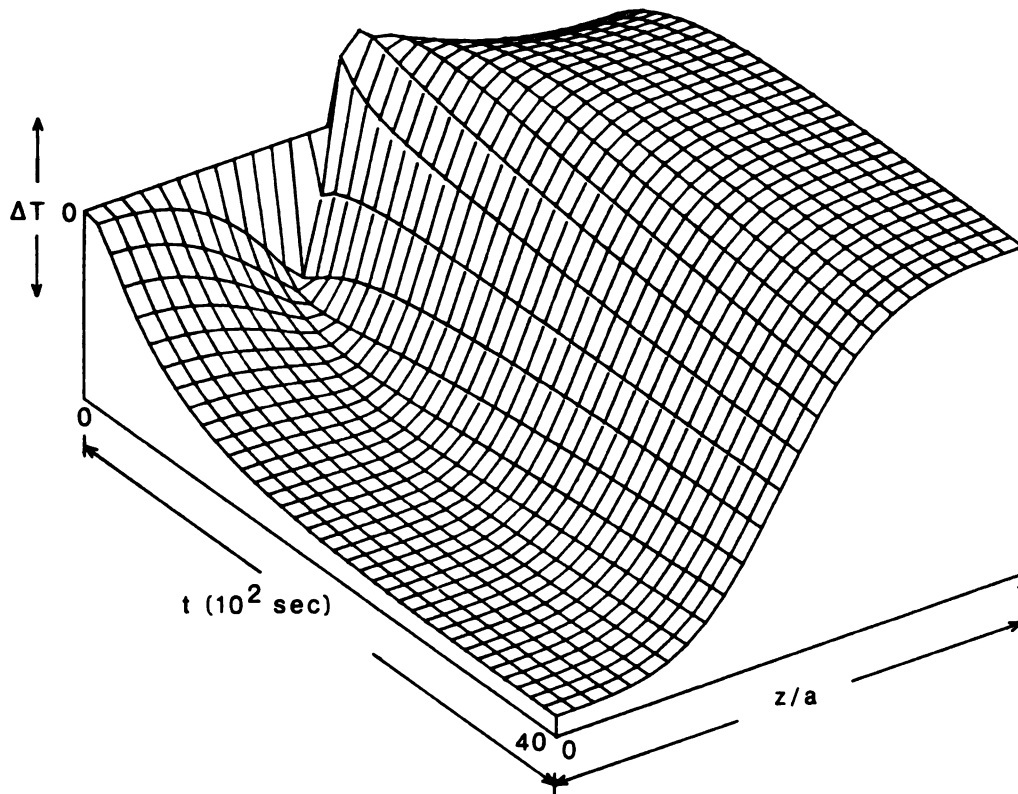


Figure 3.5. Composition surface for the carbon tetrachloride-cyclohexane system.

transient temperature gradient also decreases since thermal conduction down the temperature gradient balances the heat of transport term. The transient nature of the temperature distribution can be seen from Figure 3.6.¹ Note that the upper or less dense phase rapidly increases in temperature after initial boundary formation while the lower phase decreases. This conveniently eliminates density inversion possibilities. It also reflects a positive Q_1^* because the phase rich in component 1 induces the colder temperature. The maximum ΔT between the top and bottom phases shown in Figure 3.6 is about 0.28°C . Rapid establishment of the maximum is due to the large initial composition gradient which then slowly decays.

In confirmation of the results of Ingle and Horne [1973], numerical simulation shows that the heat of mixing contribution to the local temperature distribution is symmetric about the interface. While an endothermic (or exothermic) heat of mixing lowers (or raises) the overall temperature of the cell, the difference in temperature between two points symmetric about the interface is not affected by the heat of mixing term. This is dramatically illustrated in Figures 3.7 and 3.8. Even solutions in which

¹This plot was made for $\tilde{H}^E = 0$ with Q_1^* values evaluated from thermal diffusion factors using ORR.



TEMPERATURE SURFACE

Figure 3.6. Temperature surface for the carbon tetrachloride-cyclohexane system. ΔT represents the local temperature minus the initial temperature.

Figure 3.7. Effect of excess enthalpy on the time dependence of temperature distributions. Plots are for $H^E = x_2(A+Bx_1)$ with $\frac{z}{a}$, $A=B=0$. ---, $A=670$ J/mol; $B=0$, $A=670$ J/mol; $B=67$ J/mol. Upper curves are for $(z/a) = 0.6$ and lower curves are for $(z/a)=0.4$.

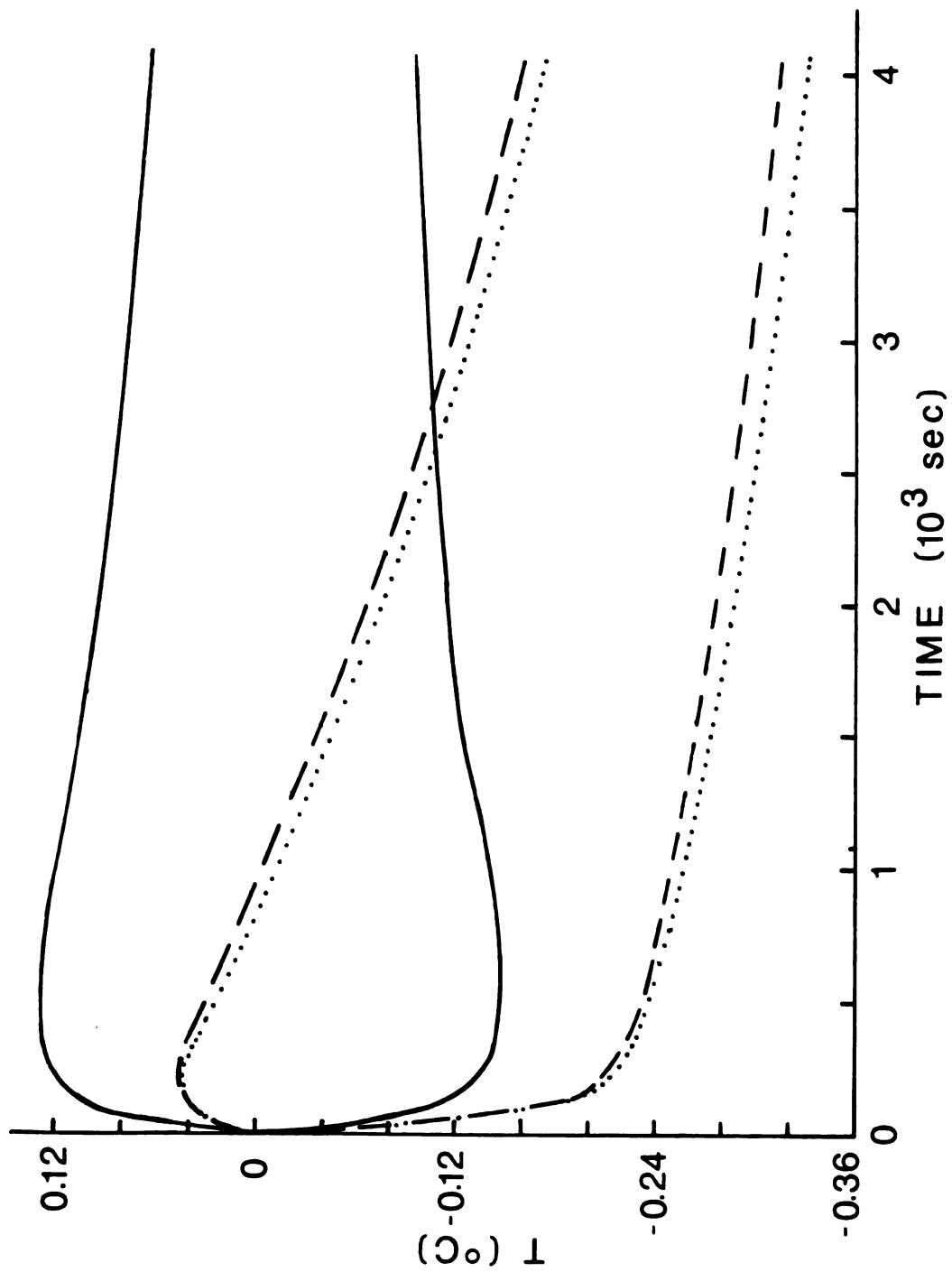


Figure 3.7

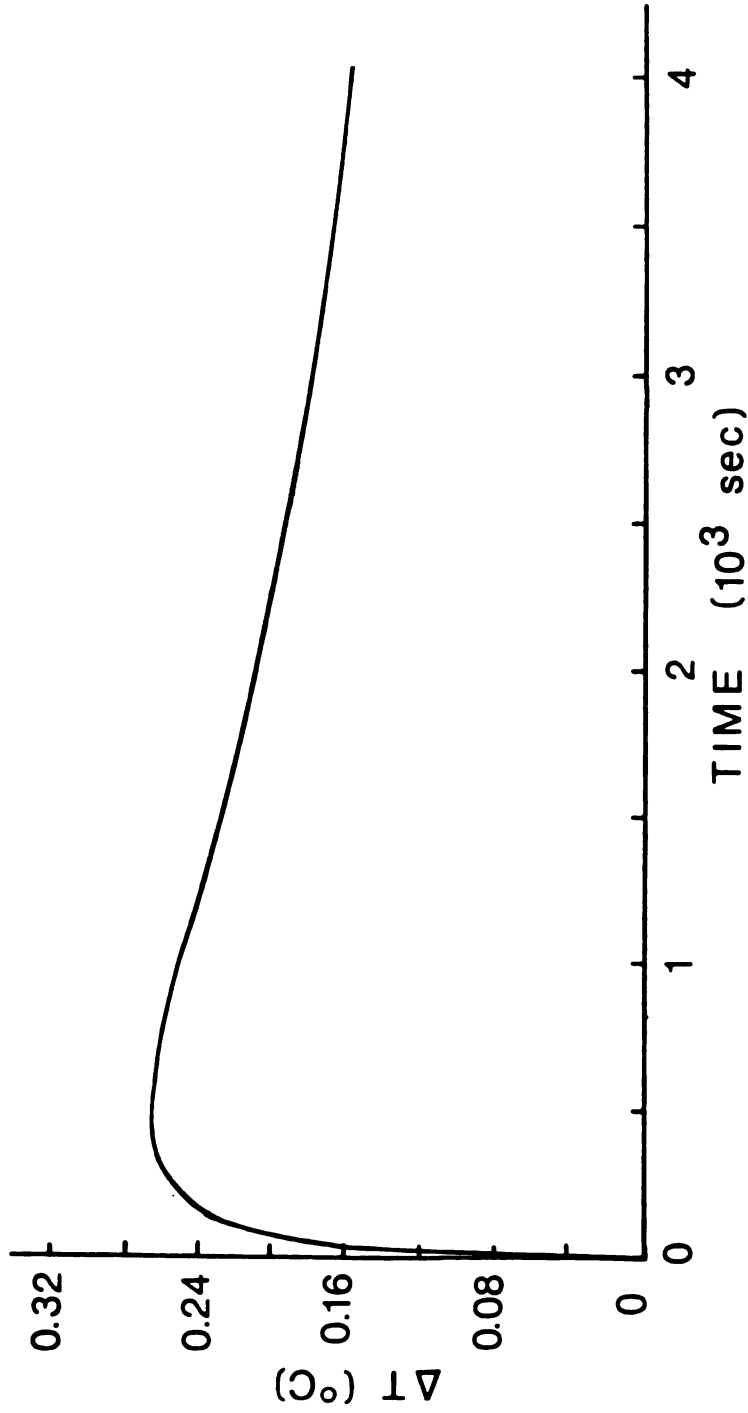


Figure 3.8. Effect of excess enthalpy on the time behavior of the temperature difference for the thermocouple pair (z/a)=0.4 and (z/a)=0.6. The curve is identical for $\bar{H}^E = x_1 x_2 (A + Bx_1)$ and (1) $A=B=0$, (2) $A=670$ J/mol; $B=0$, (3) $A=3350$ J/mol; $B=0$, (4) $A=670$ J/mol; $B=67$ J/mol, and (5) $A=670$ J/mol; $B=167$ J/mol.

\tilde{H}^E differs greatly from regular solution theory allow determination of ΔT between points symmetric about the interface without interference from the heat of mixing. This fact led to the experimental design and data analysis used in the next chapter. Although heat of mixing data are fully included in the equations, only temperature differences measured equidistant from the interface are necessary for the determination and evaluation of \tilde{Q}_1^* .

CHAPTER 4

DIFFUSION THERMOEFFECT EXPERIMENTS ON CARBON TETRACHLORIDE-CYCLOHEXANE MIXTURES

A. Experimental Design

For a meaningful analysis of diffusion thermoeffect data using the mathematical methods developed in the preceding chapters, the cell in which the measurements are made must be of a design consistent with the conditions of Figure 1.1 and the assumptions outlined in Chapters 2 and 3. Although Rastogi et al. [1965], [1969], and [1970] reported the first attempted measurements of the diffusion thermoeffect in liquid mixtures, their experimental design was not amenable to theoretical analysis as Ingle and Horne [1973] and Rowley and Horne [1978] point out. Most of the diffusion thermoeffect induced temperature gradient was in fact eliminated by their cell design. The cell used by Rastogi et al. had two vacuum-jacketed half cells into which the initial phases were introduced. These half cells were separated by a constricted region which was not insulated with a vacuum jacket. The interface was formed in the constricted region by opening a stopcock. With an interfacial diameter only half that of the bulk cell, radial diffusion and

radial heat conduction must have occurred in the two half cells, thereby vitiating the one dimensional transport equations. The temperature directly above the interfacial area was subject to change not only by the diffusion thermoeffect but also by thermal conduction into the concentric ring of diathermal fluid outside the interfacial area. Understandably, no quantitative analysis or verification of the Onsager reciprocal relations were obtainable from these results. The design and use of a diffusion thermoeffect cell consistent with the conditions required in the preceding chapters therefore constitutes the first direct measurement of heats of transport in binary non-electrolyte liquid mixtures as well as the first test of Onsager reciprocity between Ω_{01} and Ω_{10} in such systems.

Traditional diffusion cells use mechanical methods of interface creation often followed by siphon boundary sharpening. Although diffusion thermoeffect experiments require a distinct, sharp interface like that of diffusion experiments, the creation technique is more important in the former case since the response monitored is temperature rather than composition. Characteristic times are much shorter for thermal diffusivity than for diffusion, and boundary sharpening techniques are too slow to prevent heat conduction. Mechanical interfacial formation such as slide withdrawal or cell rotation can introduce turbulence as well as obscure the initial time of the experiment (Bryngdahl

[1958]). Initial times in cells employing these techniques are obscured by the finite time required for slide withdrawal or cell rotation during which only part of the interface has been formed. Turbulence and initial time problems are coupled. If the mechanical motion is accelerated to reduce time errors, interfacial turbulence is enhanced (Bryngdahl [1958]).

To allay these problems, the diffusion thermoeffect cell used here creates a sharp interface by the slow withdrawal of a third component from between the upper and lower layers. No ambiguity of the initial time is introduced since the third component is immiscible in the other two layers. Thus, diffusion is prevented until the middle layer has been completely withdrawn allowing contact between the two layers of interest. Interfacial turbulence is minimized since there are no moving surfaces. Furthermore, there are no seals or possible leakages in the interfacial region. Unfortunately, the binary systems amenable to investigation with this cell are those for which a third component can be found possessing the necessary properties: (1) a density intermediate to the densities of the upper and lower mixtures, and (2) insignificant solubility in either of the other two components. Distilled water satisfies these requirements for the carbon tetrachloride-cyclohexane system and therefore served as the withdrawable "liquid gate" for the experiments reported

in this chapter.

The glass cell shown in Figure 4.1 has two sections internally separated by an 8.5 cm length of glass tubing approximately 35 mm I.D. containing a stopcock. The upper and lower sections are jacketed for either thermostating or vacuum insulating the containers. A stopcock in the tube connecting these jackets allows a vacuum to be created around only the lower cell. The bottom container in Figure 4.1 (or in the schematic diagram of Figure 4.2) is the actual diffusion thermoeffect cell. The upper container serves only as a reservoir for the less dense phase during displacement of the withdrawable "liquid gate".

Inside dimensions are

height: 2.0 cm

diameter: 6.0 cm

rim opening: ~1 mm

rim depth: ~1 mm

where the rim is the bulge shown encircling the cell at half-height in Figure 4.1.

In preparation for each experimental run, the carbon tetrachloride-cyclohexane mixtures were gravimetrically prepared in two stoppered weighing erlenmeyer flasks of 50 mL capacity. Both components were "Baker analyzed" spectrophotocemical reagent grade of 99.0% guaranteed purity and were used without further purification. Horne

Figure 4.1. Withdrawable "liquid gate" diffusion thermo-effect cell.

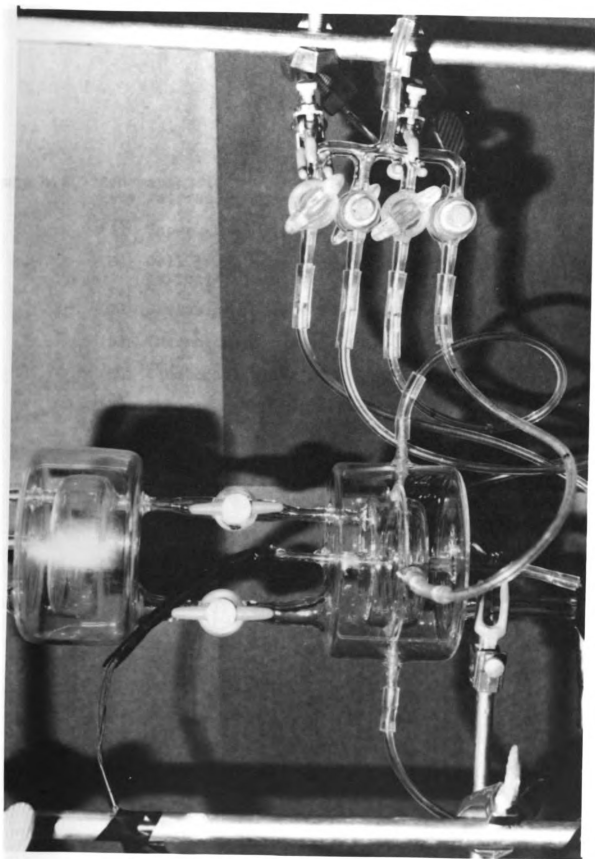


Figure 4.2. Schematic diagram of withdrawable "liquid gate" diffusion thermoeffect cell.

- (A) Upper phase storage reservoir.
- (B) Cell jacket for thermostating or adiabatically insulating.
- (C) Diffusion thermoeffect chamber.
- (D) Thermocouple banks.
- (E) Equatorial water entrapment rim.
- (F) "Liquid gate" withdrawal spout.
- (G) Ground glass fittings for thermocouple leads and cell drainage.
- (H) T-connector to vacuum line and thermostat.
- (I) Filling tubes.
- (J) Glass syringe.

[1962] has reported an in-depth error analysis for different techniques of gravimetrically preparing carbon tetrachloride-cyclohexane mixtures. The more volatile cyclohexane was added to the already weighed carbon tetrachloride and the flask was immediately sealed with a ground glass stopper lubricated with Fisher "Nonaq" grease, which is inert to both carbon tetrachloride and cyclohexane. Horne's [1962] discussion indicates carbon tetrachloride weight decrease via vapor loss during the addition of the cyclohexane to be less than 0.02%. No change of weight in time was detected for the filled flask once stoppered as described above.

The lower or diffusion thermoeffect chamber was filled in a two step process. First, distilled water was introduced from the bottom until it half filled the cell. Second, the more dense carbon tetrachloride-cyclohexane mixture was layered beneath the water layer by injection from below with a syringe pump purchased from the Harvard Apparatus Company. This technique prevented evaporational changes in composition during cell infusion. Introduction of the carbon tetrachloride rich layer raised the water level into the storage cell. Care was taken to remove any trapped air bubbles from the lower cell after which the stopcock between it and the reservoir was closed. The cyclohexane rich or less dense layer was then quickly introduced into the storage reservoir with a 100 mL syringe.

The syringe was left connected to the storage reservoir during withdrawal of the "liquid gate". It served as an enclosed piston for volume displacement as the distilled water was withdrawn.

After filling, the cell and storage reservoir were thermally equilibrated with the thermostating jacket surrounding them. To maintain the initial and boundary conditions used in the mathematical description of the effect, the initial nearly isothermal conditions (complete temperature uniformity is not required if the initial temperature distribution is known) must be quickly changed to adiabatic conditions upon interface formation. Adiabatic walls were imposed by evacuating the jacket with a vacuum pump. It was found that the above conditions could not be met if a liquid was circulated in the circumambient jacket as the thermostating fluid. Wetting of the cell walls by a thermostating liquid left residual droplets when the jacket was drained. Adiabaticity could not then be imposed due to vaporization (and associated heat effects) of the droplets as the jacket was evacuated. Consequently, room temperature air served as the thermostating fluid. No temperature effects were noticed when the jacket was evacuated for a trial run in which the cell contained only pure water. Nevertheless, some runs were performed by evacuating the jacket immediately after filling the cell and allowing internal thermal equilibrium to

take place before starting the experiment. No discrepancy was noted between the results obtained via the two different procedures. In all cases, temperatures at each thermocouple location were continuously monitored to obtain the temperature distribution at the time of interface formation. This measured initial temperature distribution served as the mathematical initial condition.

The "liquid gate" (distilled water) was withdrawn via the syringe pump at a rate of 0.764 mL/min until only a small phase separated the two carbon tetrachloride-cyclohexane layers. From this point until contact of the two layers, withdrawal rates were slowed to 0.0206 mL/min or 0.0382 mL/min to eliminate possible convection currents. Faster withdrawal rates slightly altered the initial temperature distribution in time even though the mixture displacing the water had been co-thermostatted in the reservoir with the cell itself. Smooth interface creation occurred uniformly and isochronously throughout the cell except within the equatorial rim where the menisci were curved by preferential wetting. However, due to this wetting, any residual water at the time of contact between the upper and lower layers was contained within the rim. Preliminary experiments indicated that constriction of interfacial diameter relative to cell bulk diameter reduced the ensuing temperature gradient. This is due to radial thermal conduction as mentioned earlier with respect to

the cell used by Rastogi et al. Therefore, care was taken to ensure that any residual water at the time of interface formation was contained within the equatorial rim from which the withdrawal spouts extended.

Immediately upon interface formation, a Precision Scientific Co. "time it" digital timer (0.1 second read-out) was activated, the syringe pump was disengaged, the stopcock between the reservoir and the cell was closed, and the vacuum jacket was evacuated. Temperature changes were monitored with 40 gage copper-constantan thermocouples placed equidistant above and below the interface as shown in Figure 4.2. Each thermocouple comb contained four thermocouples spaced 2.0 mm from each other, the outside walls, and the interface. Welded junctions (0.2 mm in diameter) were spaced 2.0 mm from the surface of the 1.5 mm thick Delrin[®] ($\kappa = 0.23 \text{ J}\cdot\text{m}^{-1}\text{K}^{-1}$) comb. Thermocouple potentials were monitored with a Leeds and Northrup Co. K-3 potentiometer facility provided with 16 thermocouple stations. Temperatures at the eight thermocouple locations were made at approximately 12 second intervals. Readings were taken alternately about the interface such that differences in temperature ΔT between symmetrically located thermocouples had uncertainties in time of about ± 6 seconds. For these experiments, differences in temperature were obtained by subtraction of two absolute temperatures because it was felt important to observe actual temperatures

everywhere during these pioneering measurements. In the experiments performed later on critical mixtures, enhanced precision was obtained by monitoring temperature differences directly rather than referencing each thermocouple to the ice bath. Exact thermocouple locations were measured in situ with a Beck Vernier Measuring Microscope. Accuracy in exact thermocouple location was limited by the finite size of the welded thermocouple junction (usually 0.2 mm in diameter).

Monolayers of water were assumed not to be present immediately following interface formation due to the hydrophobic character of both layers. Furthermore, since the sharp interface initially formed becomes indistinct as diffusion occurs, a monolayer cannot exist more than instantaneously. The system becomes continuous as soon as the initial step function in composition has vanished due to diffusion, and any interfacially adsorbed water must have previously been removed.

The maximum temperature difference between symmetric thermocouples was obtained after 500 - 800 seconds. The maximum temperature difference was found to be dependent upon the difference in initial compositions in accord with theory (Ingle and Horne [1973]). The starting mole fraction differences varied between 0.59 and 0.82 with corresponding temperature difference maxima from 0.21 °K to 0.30 °K respectively. Pure components were not used

for two reasons: (1) Preliminary experiments revealed an onset of turbulence at the newly formed interface when pure components were used, presumably due to large surface tension shock between two different pure components. (2) Heat of mixing effects are dependent upon the square of the initial composition difference and are thus lowered relative to the diffusion thermoeffect for smaller initial composition differences (Ingle and Horne [1973]). The second reason above is not very important for the experimental design used here because heat of mixing effects do not contribute to temperature differences taken at points symmetric to the interface.

B. Analysis of Technique

As alluded to in the previous section, the initial condition for the temperature equation was obtained from measurements of cell temperature prior to contact of the two layers. Temperatures at all eight thermocouple locations were continuously monitored as a function of time. The exact time of contact was recorded, and an extrapolation from the previous temperature readings to the contact time yielded temperatures for each thermocouple at $t = 0$. No extrapolation between a previous reading and $t = 0$ extended over 180 seconds, and no extrapolated temperature change exceeded 0.010 °K. The initial condition data are recorded in Table B.1 of Appendix B. For the five runs

performed, three were isothermal and two had essentially linear temperature distributions. Neither of these distributions included differences larger than 0.068 °K between the top and bottom surfaces of the cell. Presumably, the nonisothermal distribution in these two runs was due to faster withdrawal rates and hence to faster intake rates of reservoir thermostatted liquid. It should be emphasized again that isothermal initial conditions are not required as long as the actual temperature distribution is known, and the initial gradient in temperature is small enough that thermal diffusion terms are still negligible. Moreover, computer simulation using the equations developed in Chapters 2 and 3 indicates that small initial temperature distributions do not markedly affect the difference in temperatures between two symmetric points for times measured after the maximum temperature difference has been reached. This is because the magnitude of ΔT is fixed by a balance between the opposing effects of thermal conduction and the heat of transport and not by the previous temperature history of the mixture.

Care was taken to ensure that no vapor or air bubbles remained in the cell. Until they were removed, air bubbles aided in leveling the cell. Residual air pockets were removed with a filling needle connected to a syringe. Entrance to the filled cell could be made by dislodging the ground glass fitting (through which the upper

thermocouple leads entered) with the stopcock to the reservoir closed. By carefully opening the stopcock, hydrostatic pressure allowed displacement of the last air bubbles. The ground glass fitting, coated with a thin layer of Fisher "Nonaq" grease, was then firmly reinstated. A preliminary experiment with only \underline{c} -C₆H₁₂ showed that no vapor loss occurred around this fitting if coated with the inert lubricant. However, with a dry glass fitting, the upper portion of the cell persisted to be 0.05 °K colder than the lower region due to the endothermic vaporization of \underline{c} -C₆H₁₂ around the joint. A fresh seal of the "Nonaq" grease was applied before each experimental run.

Although temperature differences were monitored for all four thermocouple pairs, only data from the pair closest to the interface [(z/a) = 0.40 and (z/a) = 0.60] are reported in Appendix B Table B.2. Only data from this pair were used in the calculation of \tilde{Q}_1^* because the innermost thermocouple pair is least prone to the possible errors discussed below. Deviations from the mathematically predicted temperature differences can arise from: (1) Perturbations due to the presence and finite size of the thermocouple holder and the other thermocouples. (2) Thermal conduction through the thermocouple holders. (3) Side wall effects. (4) Heat losses through the cell ends; i.e., nonconformity to the prescribed adiabatic boundary

conditions. The first problem was minimized by allowing the thermocouple junctions to protrude 1.5 mm from the holders. In addition, the innermost thermocouple of each group (closest to the interface) extended 1.0 mm below the holders. Any effects due to the presence of other thermocouples and/or the thermocouple holders, would not be felt by this pair of thermocouples. For similar reasons, the difference in thermal conductivity between Delrin[®] holders and the system would not affect the temperature differences of the innermost pair. Side wall effects were probably negligible because of the relatively large diameter/height ratio. Furthermore, the main region of diffusion is the interfacial region and wall effects would be less important for those thermocouples closest to the interface.

The fourth problem warrants more concern. Obviously, it is impossible to have perfectly adiabatic walls, yet the mathematical boundary condition used implies perfect adiabaticity. Computer simulation shows that a change in boundary conditions from adiabatic to diathermal affects the innermost thermocouples the least. That is, small deviations from temperatures described by adiabatic boundary conditions due to imperfect adiabaticity of the walls are absorbed by the bulk fluid before they are felt near the interface. Therefore, any heat conduction through the cell ends where the thermocouple holder is connected

or where other tubes enter the cell may affect the outer thermocouple pairs. The innermost pair appears to be the most accurate and reliable set with respect to each of the above four sources of error. Therefore, only data from this pair were used in computing \tilde{Q}_1^* .

In view of the above discussion, computer simulation was used to check the validity of the adiabatic boundary conditions. Figure 4.3 compares the time dependent shapes of ΔT values, expected for adiabatic and diathermic boundary conditions for a given value of \tilde{Q}_1^* , to the experimental values obtained from the innermost thermocouples. As can be seen, the boundary conditions change the time dependent behavior of the predicted ΔT values considerably. Note that the actual ΔT time dependence clearly corresponds to that predicted on the basis of adiabatic walls. Data from thermocouple pairs further from the interface also agreed with the behavior predicted by the adiabatic model at shorter times but deviated at intermediate times. The length of time during which the ΔT behavior was consistent with the adiabatic model was inversely proportional to the distance from the interface at which the particular thermocouple pair was located.

Figure 4.3 is obvious verification that the innermost thermocouples provide accurate readings for the experimental time scale (~ 4000 seconds) when adiabatic boundary conditions are used. A comparison run was also made in

Figure 4.3. Comparison of experimental ΔT data to predicted values for adiabatic walls (—) and diathermic walls (----).

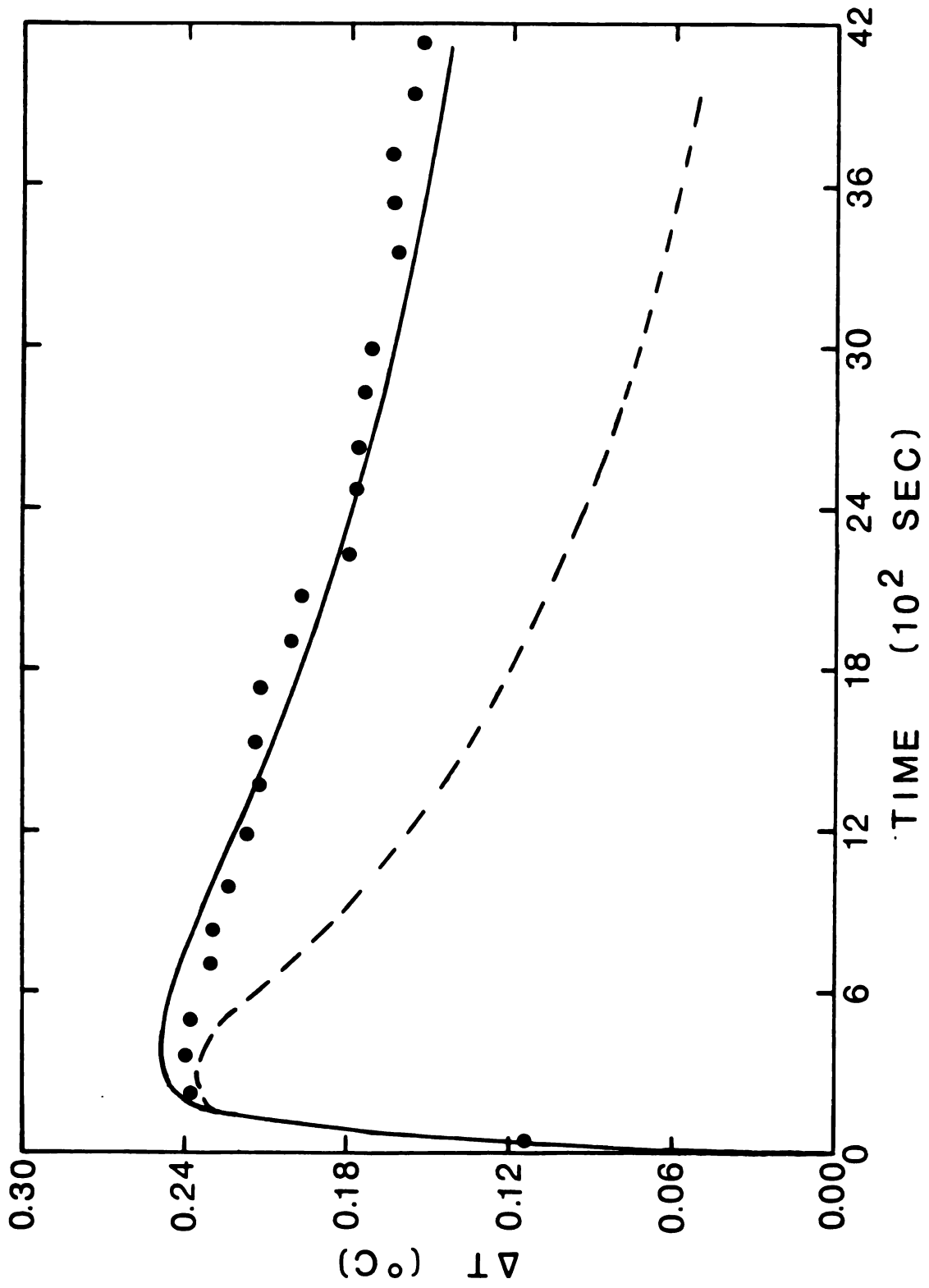


Figure 4.3

which the innermost thermocouples were each moved 10% further from the interface. The \tilde{Q}_1^* obtained was unchanged.

As previously mentioned, only temperature differences between thermocouples positioned equidistant from the interface were used in the parameter estimation procedure. More sensitivity is obtained in computing the heat of transport by this technique because the large background heat of mixing with accompanying uncertainties is eliminated. As Ingle and Horne [1973] have shown, the principal heat of mixing contribution is symmetric about the interface. Computer simulation using the previously described numerical routine substantiates their conclusions. In fact, the symmetry of the heat of mixing term, even for mixtures which deviate substantially from regular solution theory, allows calculation of the antisymmetric heat of transport term without including the excess enthalpy provided symmetric temperature differences are used as input data. The sacrifice made in using only ΔT data rather than individual T values is that only one rather than two parameters can be accurately determined for a given run.

Because only one parameter was to be obtained from the nonlinear, weighted, least squares fit of theoretical to measured ΔT values, the most composition independent form of the heat of transport was desired. As shown in Appendix A, the relationship between \tilde{Q}_1^* and α_1 , assuming Onsager reciprocity, involves various factors of which

\tilde{Q}_1^* and \tilde{M} are the only strongly composition dependent terms. In fact, α_1 is used for reporting thermal diffusion results because of its relative constancy with respect to composition. Consequently, $(\tilde{Q}_1^*/\tilde{M})$ is fairly composition independent and was used as the adjustable parameter in the fitting procedure. Program "KINFIT4" (the 1977 version of "KINFIT" as published by Dye and Nicely [1971]), a generalized, weighted, nonlinear, least squares fitting routine extensively used in fitting chemical kinetics data at Michigan State University, was used as the parameter estimating routine into which the previously described numerical partial differential equation solver was introduced. An example of the fit obtained using this procedure is shown in Figure 4.4.

To test the stability of parameter estimates obtained for $(\tilde{Q}_1^*/\tilde{M})$ as a function of the time range over which data were input, numerous fits of the first run (depicted in Figure 4.4) were made as a function of data truncation. Thus, only data out to $t = 1500$ seconds were included for obtaining a value of $(\tilde{Q}_1^*/\tilde{M})$, then data out to $t = 1700$ seconds were included and the value of $(\tilde{Q}_1^*/\tilde{M})$ was again computed; etc. The results of this data truncation test are shown in Figure 4.5. Note that the parameter estimate remains unchanged within 1% for inclusion of data past 2800 seconds. When data past 3400 seconds are included, essentially no change in \tilde{Q}_1^* occurs as more data

Figure 4.4. Nonlinear, weighted, least squares fit of $(\tilde{Q}_1^*/\tilde{M})$ for Run I. The solid line represents calculated Q_1^* values based upon the fit value of (Q_1^*/\tilde{M}) while the solid circles are experimental data.

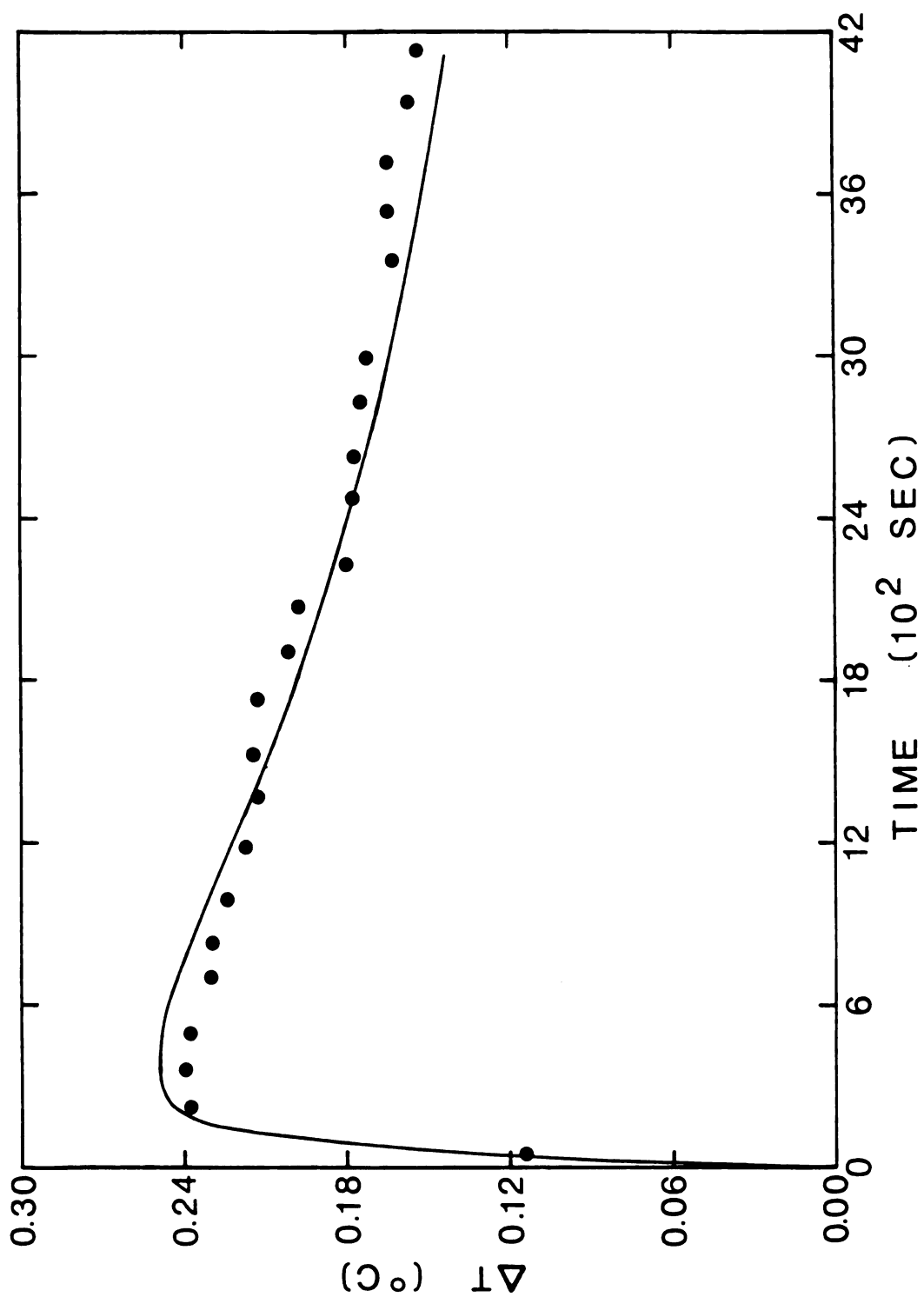


Figure 4.4

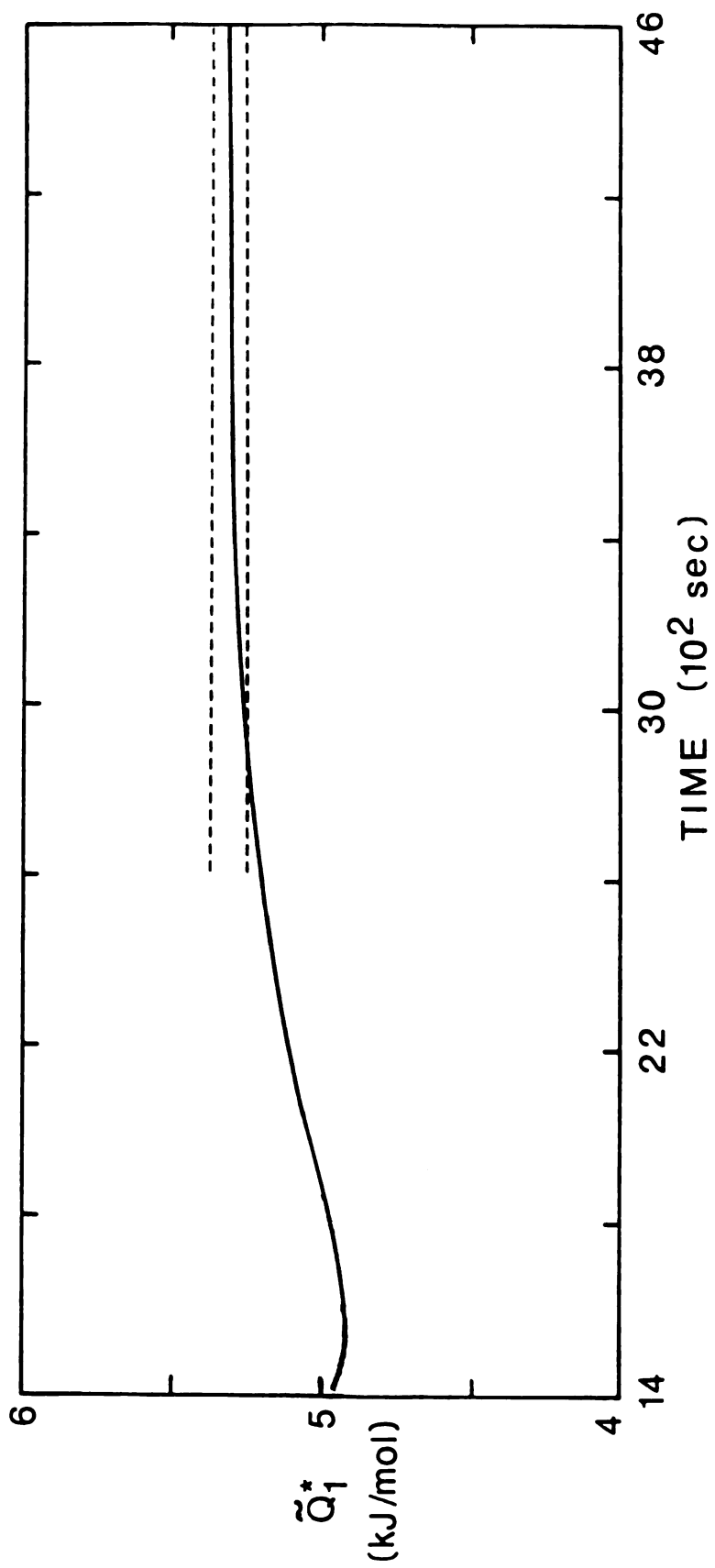


Figure 4.5. Test of the stability of \tilde{Q}_1^* obtained as a function of the time range for which ΔT data were input. The dashed line indicates 1% deviation from the long-time value.

points are included. The effect shown in Figure 4.5 has essentially two causes: (1) The value of the fit parameter becomes increasingly stable and (presumably) more accurate as statistically more points are included. (2) Although the parameter value for the perfect model would oscillate randomly about a mean value as more points are added, the assumed model, that $(\tilde{Q}_1^*/\tilde{M})$ is a constant independent of composition and temperature, is not strictly true. Therefore, inclusion of data taken at the relatively longer times is important in finding the appropriate $(\tilde{Q}_1^*/\tilde{M})$ for the mean composition reported for each run because at short times two very different compositions are located on either side of the interface. As diffusion levels the initially sharp composition gradient at $(z/a) = 0.5$, the compositions in the regions near the interface become more nearly the mean value, and the fit $(\tilde{Q}_1^*/\tilde{M})$ becomes the value for that composition.

All experimental runs were analyzed with respect to $(\tilde{Q}_1^*/\tilde{M})$ by inclusion of data up to 4200 seconds. This not only provided enough points for a statistically "good" estimate of $(\tilde{Q}_1^*/\tilde{M})$ but also eliminated the problems discussed in the previous paragraph. Analysis of the diffusion thermoeffect in gaseous mixtures has often relied entirely on the maximum temperature difference measured (Bousheri and Afrashtehfar [1975]). Inclusion of points spaced in time and use of the integrated equations provides a

statistically better estimate of the heat of transport, particularly since the maximum ΔT occurs so early that very few data points can be obtained up to that time. For thermocouples 2 mm from the interface, ΔT reaches its maximum value in 500 - 800 seconds.

C. Literature Values for the Physicochemical Properties of the Carbon Tetrachloride-Cyclohexane System

Before Equation (2.35) can be used in conjunction with experimental data to obtain values for \tilde{Q}_1^* , all other parameters appearing in (2.35) must be available. Table 4.1 contains a synopsis of the values used for the system carbon tetrachloride-cyclohexane. The parameters of Table 4.1 are based on the expansion

$$L = L_0[1 + L_x(x_1 - 0.5) + L_T(T - 298.15) + L_{xT}(x_1 - 0.5)(T - 298.15) + 1/2L_{xx}(x_1 - 0.5)^2] \quad (4.1)$$

where L is the property in question, L_0 is the value of L for an equimolar mixture at 298.15 °K, and L_x , L_T , L_{xT} ; L_{xx} are corresponding composition and temperature coefficients. The parameters are viewed as expansions about $x_1 = 0.5$ rather than about pure component values (L_1^0 and L_2^0) because the mean composition of each run was nearly 50 mole percent. In the sections below, further discussion

Table 4.1. Literature values for the physicochemical properties of the carbon tetrachloride - cyclohexane system at 1 atm. The properties are expressed in the general form
 $L = L_0[1+L_x(x_1-0.5) + L_T(T-298.15) + L_{xT}(x_1-0.5)(T-298.15) + 1/2L_{xx}(x_1-0.5)^2]$
 to include their temperature and composition dependence.

A. Properties of the pure components and of equimolar mixtures at 298.15°K.

L	$\frac{L_1^0}{L_2^0}$	$\frac{L_0}{L_2^0}$	$\frac{L_0}{L_1^0}$	Units	Reference
\bar{M}	0.15384	0.08418	0.11901	kg·mol ⁻¹	Weast [1970]
D	1.295x10 ⁻⁹	1.482x10 ⁻⁹	1.388x10 ⁻⁹	m ² s ⁻¹	Anderson [1970]
$(\partial^2\bar{H}^E/\partial x_1^2)_{T,P}$	-----	-----	-1.535	kJ·mol ⁻¹	Ewing [1970]
\bar{C}_{-p}	131.82	156.76	144.14	J·mol ⁻¹ K ⁻¹	Wilhelm [1974]
\bar{V}	0.9708x10 ⁻⁴	1.0867x10 ⁻⁴	1.0287x10 ⁻⁴	m ³ mol ⁻¹	Wood [1952] and Wilhelm [1974]
κ	0.103	0.119	-----	J·m ⁻¹ s ⁻¹ K ⁻¹	Jamieson [1975]

B. Composition and temperature coefficients.

L	$\frac{L_x}{L_T/^\circ K}$	$\frac{L_T/^\circ K}{L_{xT}/^\circ K}$	$\frac{L_{xx}}{L_{xx}}$	Reference
\bar{M}	0.585	-----	-----	Weast [1970]
D	-0.135	0.0185	0.0017	Anderson [1970]
$(\partial^2\bar{H}^E/\partial x_1^2)_{T,P}$	-0.675	-0.0032	-0.0012	Ewing [1970]
\bar{C}_{-p}	-0.173	0.0015	-0.0025	Wilhelm [1974]
\bar{V}	-0.113	0.0012	-0.0001	Wood [1952] and Wilhelm [1974]
κ	-----	-0.0019	-----	Jamieson [1975]

of the literature values is given.

(1) Diffusion coefficient - The diffusion coefficient as reported by Anderson and Horne [1970] agrees well with other literature values cited therein. The composition and temperature dependencies are included in their report and were used in the numerical fitting routine.

(2) Excess enthalpy - Ewing and Marsh [1970] report the composition dependence of the excess molar enthalpy at three different temperatures. The temperature dependence was obtained by a fit of their three temperature independent equations for \tilde{H}^E using program "MULTREG" (Anderson [1968]).

(3) Constant pressure heat capacity - Values for molar heat capacities were obtained from Wilhelm and Sackmann [1974]. They find that $(\tilde{C}_P/J \cdot K^{-1} \text{mol}^{-1}) = \Delta\tilde{C}_P + x_1\tilde{C}_{P,1}^0 + x_2\tilde{C}_{P,2}^0$ where $\Delta\tilde{C}_P = -0.6x_1x_2$, adequately describes the composition behavior of \tilde{C}_P . As must be the case for thermodynamic consistency, the constant pressure temperature derivative of the excess enthalpy agrees well with the excess heat capacity. Due to the smallness of the excess heat capacity, the temperature dependent behavior of \tilde{C}_P is contained entirely in the temperature dependencies of the pure component heat capacities. Upon rearrangement, the temperature dependence with respect to the mixture becomes that shown in Table 4.1.

(4) Molar volumes - Molar volumes were calculated

from the density data of Wood and Gray [1952]. The form $(\tilde{V}/\text{cm}^3\text{mol}^{-1}) = x_1\tilde{V}_1^0 + x_2\tilde{V}_2^0 + \tilde{V}^E$ yields excellent agreement with their results when $\tilde{V}^E = 0$ and \tilde{V}_1^0 and \tilde{V}_2^0 contain the pure component temperature dependencies. Program "MULTREG" provided best fits of their temperature dependent data which were then rearranged into the form required for Table 4.1. The values obtained by Wilhelm and Sackmann [1974] also agree well with these equations.

(5) Thermal conductivity - Thermal conductivity data for liquid mixtures are scarce due to experimental convection problems. For the same reason, the uncertainty in good experimental data is between 3% and 7% depending on techniques and equipment used. The only experimental data reported in the literature for carbon tetrachloride-cyclohexane mixtures are those of Venart [1968]. His results show a most peculiar cusp at $x_1 \approx 0.5$ when κ is plotted against x_1 . No other nonelectrolyte mixture displays this behavior. Furthermore, the scatter in data for this system relative to that of analogous systems studied by Venart indicates a peculiarity and/or difficulty in obtaining accurate thermal conductivity data for carbon tetrachloride-cyclohexane mixtures.

Jamieson, et al. [1975] and Jamieson and Hastings [1969] have recommended the NEL (National Engineering Laboratories) equation,

$$\kappa = w_1\kappa_1^0 + w_2\kappa_2^0 - C(\kappa_2^0 - \kappa_1^0)(1 - \sqrt{w_2})w_2, \quad (4.2)$$

for predictive estimates of the thermal conductivity of binary liquid mixtures, where κ_1^0 is the thermal conductivity of pure component 1 and C is an adjustable parameter. Component 2 is assumed to have the largest thermal conductivity in using Equation 4.2. Thermal conductivity predictions based on this equation have been shown by Jamieson et al. to agree with experimental values over the entire composition range to within 5% if a fit value obtained at a single composition is used for C and to within 7% if C is defined by $C \equiv 1.0$ (most nonelectrolyte mixtures are best represented by this value).

Rather than from Venart's data or from the NEL equation, the composition dependence of the thermal conductivity was obtained from the diffusion thermoeffect experiments themselves by an iterative technique. The method and the results obtained for the thermal conductivity are presented in the next section.

D. Experimental Results for Thermal Conductivity

The composition dependence of κ was obtained from the diffusion thermoeffect experiments. An iterative procedure was followed in which the composition dependence of $(\tilde{Q}_1^*/\tilde{M})$ was first neglected and then its experimental value was included in order to determine the composition dependence of the thermal conductivity. To illustrate the approach,

consider the temperature equation without the very small term due to the barycentric velocity [obtained from Equation (2.35) for D/\tilde{V} independent of x_1],

$$\begin{aligned} \tilde{C}_P(\partial T/\partial t) &= \tilde{V}\kappa(\partial^2 T/\partial z^2) + \tilde{V}(\partial\kappa/\partial x_1)_T(\partial x_1/\partial z)(\partial T/\partial z) \\ &+ DM_2(\tilde{Q}_1^*/\tilde{M})(\partial^2 x_1/\partial z^2) + D(\partial^2 \tilde{H}^E/\partial x_1^2)_T(\partial x_1/\partial z)^2 \\ &+ DM_2[\partial(\tilde{Q}_1^*/\tilde{M})/\partial x_1]_T(\partial x_1/\partial z)^2. \end{aligned} \quad (4.3)$$

In fitting the experimental data by the numerical scheme described in Chapter 2, the last term on the right-hand side of Equation (4.3) was first omitted. The calculations then gave \tilde{Q}_1^* and a first approximation for $(\partial\kappa/\partial x_1)_T$. Once \tilde{Q}_1^* was obtained for all the experimental runs, its observed composition dependence was included and Equation (4.3) was then used, in full, to obtain an improved estimate of $(\partial\kappa/\partial x_1)_T$.

Initial analysis of the 5 diffusion thermoeffect experiments reported herein was done using the NEL equation for the thermal conductivity with the adjustable parameter $C = 0.6$. This value was obtained by fitting both $(\tilde{Q}_1^*/\tilde{M})$ and C simultaneously to the data of Run I. However, because \tilde{Q}_1^* and κ at the mean mole fraction primarily determine ΔT , C and $(\tilde{Q}_1^*/\tilde{M})$ were largely coupled. Sensitivity coefficients for these parameters indicate coupling.

Nevertheless, the thermocouple pair was sufficiently removed from the interface that the magnitudes of κ at these thermocouple locations (hence compositions) sufficiently decoupled C and $(\tilde{Q}_1^*/\tilde{M})$ to obtain a unique but shallow minimum in the residual search. Once the parameter C had been identified ($C = 0.6$), Runs I through V were analyzed with the fixed value for C leaving only $(\tilde{Q}_1^*/\tilde{M})$ as an adjustable parameter. Since $(\tilde{Q}_1^*/\tilde{M})$ is not a constant as assumed in this fitting procedure, the composition dependence of $(\tilde{Q}_1^*/\tilde{M})$ was absorbed in the fit value of the NEL parameter C . The composition dependence of $(\tilde{Q}_1^*/\tilde{M})$ obtained from the five runs at different compositions was then introduced into the fitting routine in an iterative fashion to yield the improved value of $C = 1.05$. The value $C = 0.6$ is seen to be an "effective" value into which the residual composition dependence of $(\tilde{Q}_1^*/\tilde{M})$ was absorbed. Note that the improved value obtained for C in the NEL equation from diffusion thermoeffect data is in excellent agreement with the recommended value of $C = 1.0$ for nonelectrolyte mixtures.

Absolute values of the thermal conductivity, as predicted by the NEL equation with $C = 1.05$, are tabulated in Table 4.2. Also shown in Table 4.2 are values obtained from Venart's data by interpolation to the appropriate mole fraction. Note that the values obtained from this iterative treatment of the diffusion thermoeffect agree within

Table 4.2. Thermal conductivity of $\text{CCl}_4\text{-c-C}_6\text{H}_{12}$ mixtures
at 20°C and 1 atm.

$\langle x_1 \rangle$	$\kappa^D/W \cdot S^{-1}K^{-1}(a)$	$\kappa^V/W \cdot S^{-1}K^{-1}(b)$	$(\kappa^D - \kappa^V)/\kappa^V \times 100\%$
0.3469	0.1089	0.107	1.8
0.4112	0.1078	0.104	3.6
0.4295	0.1074	0.104	3.3
0.4843	0.1066	0.104	2.5
0.5514	0.1056	0.103	2.6

(a) Values obtained from diffusion thermoeffect experiments.

(b) Values interpolated from the data of Venart [1968].

experimental error (ca. 3%) with Venart's data in the composition range applicable to the measurements reported here. This range of compositions involved the previously noted cusp in Venart's data; i.e., actual data in this region were higher than expected on the basis of smooth composition behavior with no inflection points for the entire mole fraction range. Thermal conductivities predicted for compositions outside the experimental range of interest deviated more than 3% but are irrelevant to the analysis of data.

Although using ΔT data rather than values for T itself did not allow accurate simultaneous determination of two parameters, inclusion of multiple run information in the above described iterative fashion decoupled the two parameters allowing accurate determination of both the heat of transport and the thermal conductivity. The thermal conductivity values obtained agree, within the experimental uncertainties involved in measuring liquid mixture thermal conductivities, with those measured by Venart [1968]. The values obtained for the heat of transport are discussed in the following section.

E. Experimental Results for Heat of Transport

As previously indicated, the experimental data consisted of numerous temperature differences between thermocouples located at $(z/a) = 0.4$ and $(z/a) = 0.6$. Appendix

B contains the raw data obtained for the 5 experimental runs and the initial run conditions associated with each. Table 4.3 shows the results obtained for \tilde{Q}_1^* using the previously described fitting procedure. Initial compositions and temperatures are also included in this table. From the resultant \tilde{Q}_1^* values, the Onsager coefficient Ω_{01} is calculated on the basis of Equation (2.14B). Literature data for the thermal diffusion coefficient α_1 (Anderson and Horne [1971], Stanford and Beyerlein [1973]; and Turner, et al. [1967]) provide values for Ω_{10} after averaging, adjusting to the given temperature via the equation reported by Anderson and Horne, and using Equations (2.14C), (2.15), and (2.16). A comparison of these two Onsager coefficients, obtained independently of each other, is shown in Table 4.3 along with the actual values of Ω_{01} and Ω_{10} . As required by the Onsager heat-mass reciprocal relation, $\Omega_{01} = \Omega_{10}$ to within 3%. This constitutes the first experimental verification of the Onsager heat-mass and mass-heat reciprocal relation in liquid systems (Rowley and Horne [1978]).

The verification of the heat-mass reciprocal relation now allows transformation of experimental heats of transport to thermal diffusion factors by way of Equation (2.22) with the definitions of Equations (2.14) - (2.16). Thermal diffusion factors obtained in this manner are adjusted to 25 °C using the temperature dependence $-\alpha_1 = -1.827 + 0.181x_1 + 0.0104 (T-298.15) - 0.0008x_1 (T-298.15)$ reported by

Table 4.3. Values of the heat of transport and Onsager coefficients in carbon tetrachloride-cyclohexane mixtures at 25°C.

$\langle x_1 \rangle^a$	Δx_1^b	T°C	$\tilde{Q}_1^*/\text{kJmol}^{-1}$ ($\sigma = 0.12$) kJmol ⁻¹	$\Omega_{01}^c/10^{-7}$ kgm ⁻¹ sec ⁻¹ ($\sigma = 0.14 \times 10^{-7}$) kgm ⁻¹ sec ⁻¹	$\Omega_{10}^d/10^{-7}$ kgm ⁻¹ sec ⁻¹ ($\sigma = 0.11 \times 10^{-7}$) kgm ⁻¹ sec ⁻¹	$(\Omega_{01} - \Omega_{10})/10^{-7}$ kgm ⁻¹ sec ⁻¹
0.3469	0.5933	22.21	5.47	6.35	6.26	0.09
0.4112	0.7865	23.01	5.59	6.48	6.43	0.05
0.4295	0.6687	21.98	5.43	6.14	6.34	-0.20
0.4843	0.8185	22.87	5.84	6.38	6.28	0.10
0.5514	0.7160	23.28	6.13	6.16	5.96	0.20

- (a) Mean mole fraction of CCl₄.
- (b) Initial difference in mole fraction of CCl₄.
- (c) Calculated from Equation (2.14B).
- (d) Calculated from Equation (2.14C) using literature values for α_1 .

Anderson and Horne [1970]. A comparison of these thermal diffusion factors (obtained from diffusion thermoeffect experiments) to those obtained from various thermal diffusion experiments is shown in Figure 4.6. In particular, the solid triangles are the results of these diffusion thermoeffect experiments, the solid line and solid circles represent the pure thermal diffusion results of Anderson and Horne [1971], the dashed line represents the thermogravitational results of Stanford and Beyerlein [1973], the open circles are the flow cell data of Turner, Butler, and Story [1967]; and the solid squares represent thermogravitational results obtained by Korchinsky and Emery [1967]. The various techniques for obtaining thermal diffusion factors all yield consistent results within the experimental uncertainties. This comparison confirms the diffusion thermoeffect as a valid and accurate method for obtaining heats of transport and thermal diffusion factors. The advantages of performing diffusion thermoeffect measurements are perhaps manifest most strongly in the liquid-liquid critical region as will be shown in Chapters 5 and 6.

As shown in Appendix A, the relationship between \tilde{Q}_1^* and α_1 is

$$\tilde{Q}_1^* = -\alpha_1 \tilde{M}RT(1+\Gamma)/M_1M_2. \quad (4.4)$$

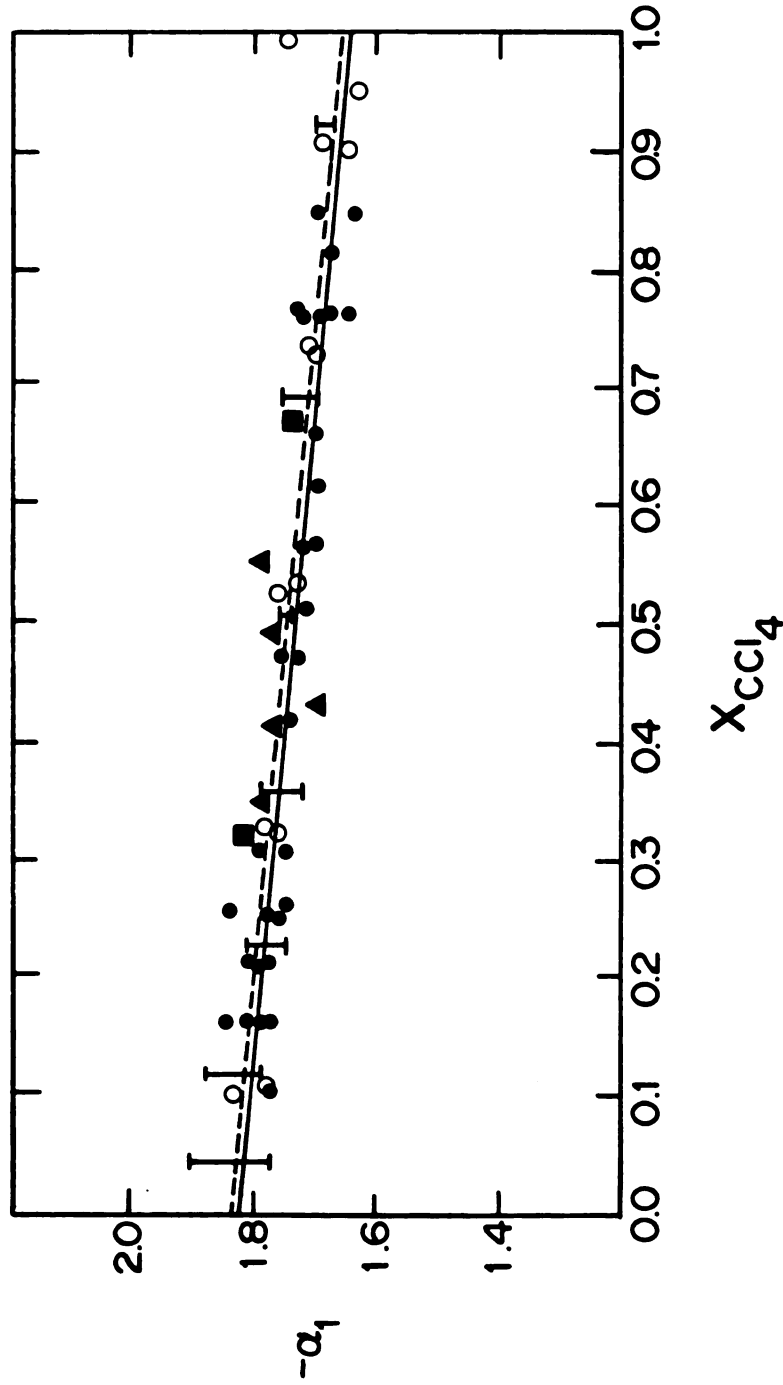


Figure 4.6. Thermal diffusion factor at 25 °C as a function of composition. Method of measurement is in parentheses. ▲, this work (Dufour effect); ✕, Anderson and Horne [1971] (pure thermal diffusion); -I-, Stanford and Beyerlein [1973] (thermogravitation); ○, Turner et al. [1967] (flow cell); ■, Korchinsky and Emery [1967] (thermogravitation). (Rowley and Horne [1978]).

The transformation from heats of transport to thermal diffusion factors therefore involves the "thermodynamic factor" $(1+\Gamma)$ defined by

$$(1+\Gamma) \equiv (1+\partial \ln \gamma_1 / \partial \ln x_1)_{T,P} \quad (4.5)$$

where γ_1 is the activity coefficient of component 1 (usually based on the pure component standard state for nonelectrolyte mixtures). Although $(1+\Gamma)$ is close to unity for this system at all mole fractions, a least squares fit of the activity coefficient data reported by Turner et al. [1967] was used to calculate α_1 values from corresponding \tilde{Q}_1^* values. It is straightforward (but tedious) to show from the excess enthalpy of Table 4.1 that the temperature dependence of $(1+\Gamma)$ is negligible over the experimental range. Nevertheless, in critical mixtures, the "thermodynamic factor" plays an important role in the behavior of properties very near the consolute temperature. Because the "thermodynamic factor" is often close to unity for nearly ideal mixtures, early formulations of diffusion assigned composition gradients as mass flux driving forces. Systems and regions (such as the critical region) where activity corrections are important have been invaluable in clearly identifying chemical potential gradients as the correct diffusional driving forces.

From the experimentally obtained heats of transport and the fundamental relationships between the heat-mass

cross coefficients, the other commonly used transport coefficients can be evaluated. From Equation (2.18), the Dufour coefficient β_T can be directly calculated. Similarly the thermal diffusion coefficient D_T can be obtained from Equation (2.14C) by using the now proven Onsager relation $\Omega_{10} = \Omega_{01}$. These dependent coefficients along with \tilde{Q}_1^* and α_1 are tabulated in Table 4.4. A comparison of Figures 4.7 and 4.8 reveal the main reason for the multiplicity of coefficients. Note that the Dufour coefficient β_T appears to be nearly independent of composition for this system at 25 °C. On the other hand, \tilde{Q}_1^* is quite dependent upon composition. A similar relationship holds between α_1 and D_T , α_1 being more composition independent.

The diffusion thermoeffect results allow calculation of another interesting quantity. There is some ambiguity in the thermal conductivity which appears in thermal diffusion equations. Before the temperature gradient is applied in a thermal diffusion experiment, the isothermal equilibrium mixture has a definite thermal conductivity κ_0 . After the temperature gradient has been applied, a steady state is reached when the temperature gradient-induced mass flux identically balances the mass flux caused by the propensity for diffusion down a chemical potential gradient. This steady state mixture also has a definite but different thermal conductivity κ_∞ . As Horne and Bearman [1967] show, these two properties are

Table 4.4. Heat-mass transport coefficients for carbon tetrachloride-cyclohexane mixtures at 25 °C and 1 atm.

$\langle x_1 \rangle$	$\tilde{Q}_1^*/\text{kJ}\cdot\text{mol}^{-1}$	$\beta_T/10^{-2}\text{J}\cdot\text{m}^{-1}\text{s}^{-1}$	$-\alpha_1$	$D_T/10^{-10}\text{m}^2\text{s}^{-1}$
0.3469	5.42	5.71	1.79	6.34
0.4112	5.56	5.60	1.77	6.12
0.4295	5.40	5.39	1.70	5.80
0.4843	5.80	5.59	1.77	5.74
0.5514	6.10	5.64	1.79	5.69

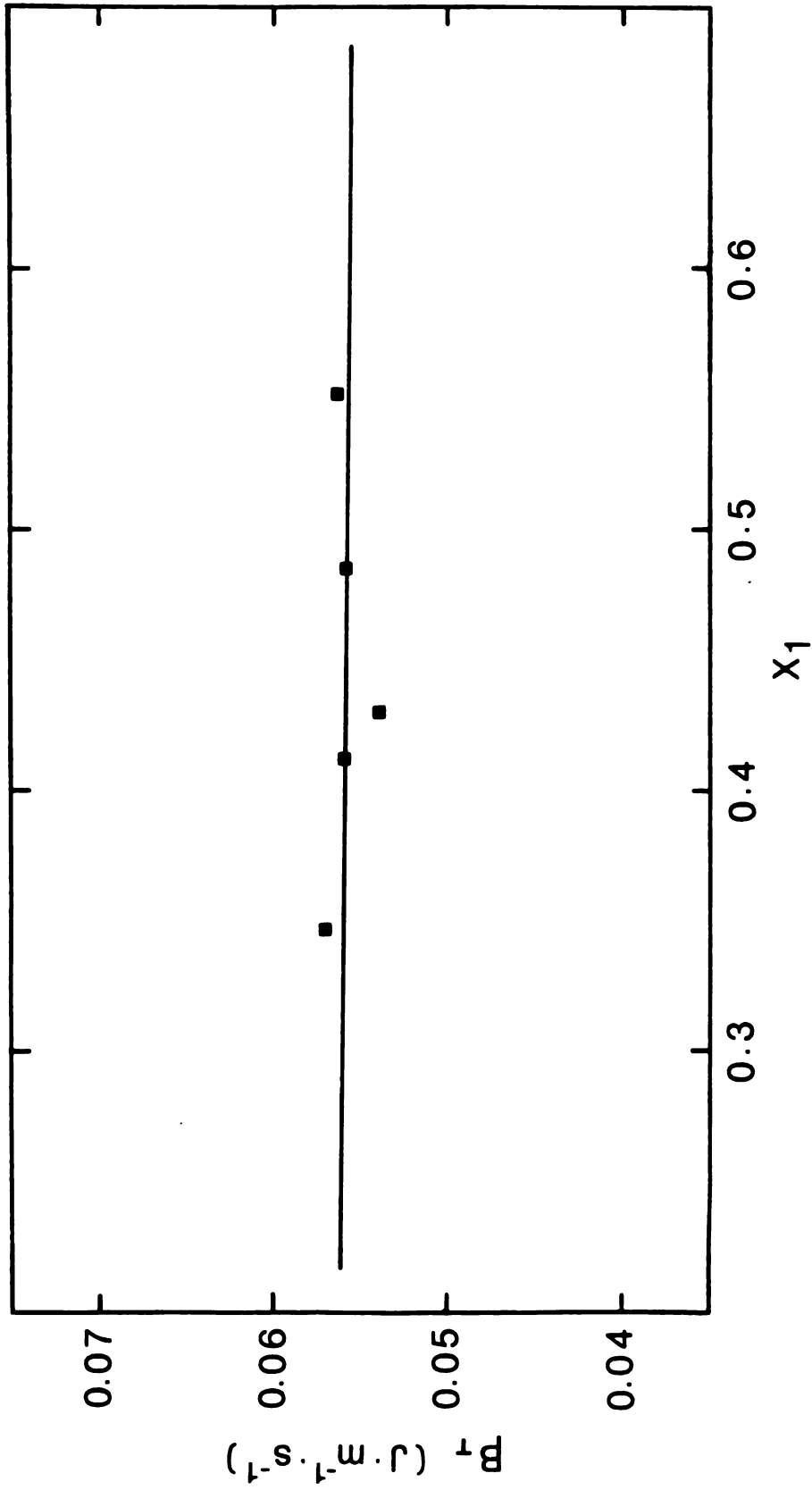


Figure 4.7. The Dufour coefficient β_T as calculated from the experimental \tilde{Q}_1^* values. ■, experimental data; —, least squares fit.

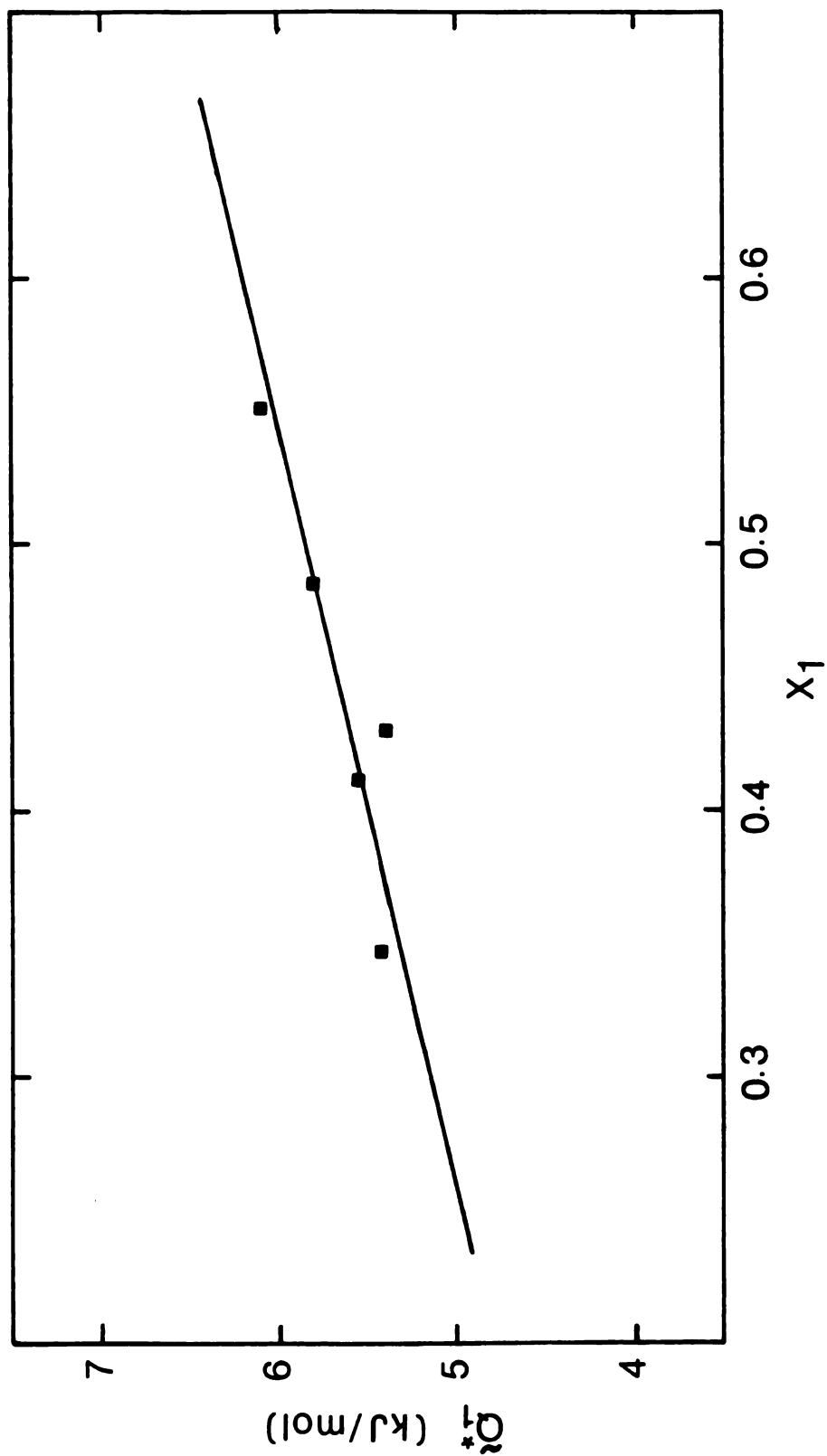


Figure 4.8. Heat of transport \bar{Q}_1^* as a function of mole fraction x_1 . ■, experimental data; —, least squares fit.

related by

$$\kappa_0 - \kappa_\infty = -\rho D \bar{Q}_1^* \alpha_1 w_1 w_2 / T = \Omega_{01} \bar{Q}_1^* / T \quad (4.6)$$

where \bar{Q}_1^* is the specific heat of transport of component 1. The relation $\Omega_{01} = \Omega_{10}$ has been used to obtain the second equality shown in Equation (4.6). From diffusion thermo-effect experiments, \bar{Q}_1^* and Ω_{01} are directly obtained. Therefore, the difference between the two thermal conductivities $\kappa_0 - \kappa_\infty$ is readily calculable from diffusion thermo-effect experiments. Table 4.5 shows the difference as obtained from the experimental results reported in this chapter. Note that current uncertainties in experimentally determined thermal conductivities are much larger than the difference between κ_0 and κ_∞ . The two may therefore be used interchangeably without sacrifice of numerical accuracy until very much improved thermal conductivity measurements can be made.

Unlike the ΔT versus time profiles, measured T versus time profiles were quite asymmetric about $(z/a) = 0.5$. In all cases, the increase from the uniform initial temperature was much less for the thermocouple located above the interface than was the decrease in temperature for the lower thermocouple. This asymmetric effect is analogous to that observed by Mason, Miller, and Spurling [1967], by Waldmann [1947], and by Miller [1949] for gaseous diffusion

Table 4.5. Values for the difference in thermal conductivity between the equilibrium and steady states in thermal diffusion experiments.

$\langle x_1 \rangle$	T/°K	$\kappa_0/\text{W}\cdot\text{s}^{-1}\text{K}^{-1}$ (a)	$(\kappa_0 - \kappa_\infty)/$ $10^{-5} \text{W}\cdot\text{s}^{-1}\text{K}^{-1}$ (b)	% Difference
0.3469	295.36	0.1084	7.64	0.07
0.4112	296.16	0.1072	7.95	0.07
0.4295	295.13	0.1070	7.34	0.07
0.4843	296.02	0.1060	8.18	0.08
0.5514	296.43	0.1049	8.28	0.08

(a) Taken from Table 4.2 and adjusted to proper temperature using Table 4.1.

(b) Calculated from Equation (4.6).

thermoeffect experiments. These investigators all noted that the temperature effect was greater below the diffusion interface than above it. Our computer simulation concurs with the hypothesis for this effect advanced by Mason, Miller, and Spurling - the asymmetry in the temperature effect is primarily due to composition dependencies of the transport parameters, particularly the thermal conductivity. Individual thermocouples were not used to fit the composition dependence of the thermal conductivity, however, because the theoretical T vs. t behavior at a given location, predicted with the inclusion of the large heat of mixing term, does not agree very well with observed behavior at long times. Reasons for this are not known, but may be due to wall effects or thermocouple effects.

In addition to its intrinsic importance for liquid mixture transport theory and behavior, the diffusion thermo-effect can also be useful for exploring the critical solution region. Anomalous behavior is often noted for transport properties near the consolute temperature. Attempts to measure thermal diffusion factors very near the critical temperature have been hampered by the large temperature gradients required to observe the effect. The diffusion thermoeffect should provide a valuable tool in this region since only very small temperature gradients are induced by the moderate composition gradients associated with critical coexistence curves.

CHAPTER 5

LIQUID-LIQUID CRITICAL PHENOMENA

A. Classical Thermodynamics of Liquid-Liquid Critical Phenomena

At uniform temperature and pressure, the tendency of a liquid mixture to separate into two phases is governed by the requirement that the Gibbs free energy be a minimum at equilibrium. That is, the criterion for phase stability in a binary liquid system is a downward convexity of the free energy G (or the free energy of mixing G_M) as a function of mole fraction at a given T and P (see for example Prigogine and Defay [1954] and Moore [1972]). Curve "A" of Figure 5.1 (Moore [1972]) depicts a system for which $(\partial^2 G_M / \partial x_1^2)_{T,P} > 0$ (G_M is convex downward) over the entire composition range. This corresponds to complete miscibility of both components at all concentrations. If, however, the free energy of mixing for a binary mixture is similar to curve "B" of Figure 5.1, G_M can be minimized (for those overall compositions between x_1' and x_1'') by a separation into two distinct liquid phases of compositions x_1' and x_1'' . Curve "C" represents a system at the stability limit (critical solution temperature or consolute temperature) where the two inflections of curve "B" have merged.

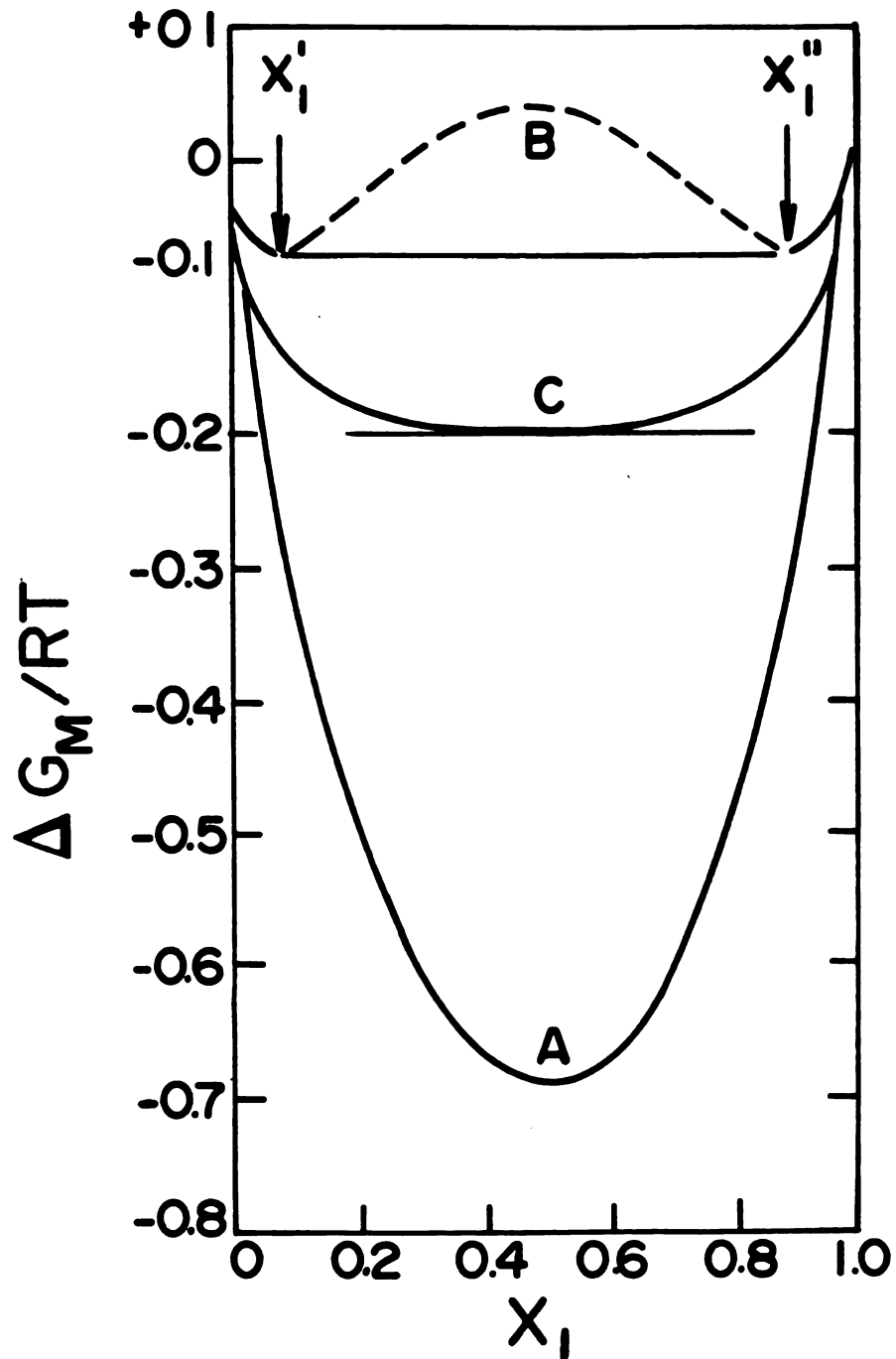


Figure 5.1. Free energy of mixing vs. mole fraction of component 1 as illustrated by Moore [1972]. A. Complete miscibility. B. Two phase system of compositions x_1' and x_1'' . C. Phase stability limit.

The stability criteria at this point are

$$(\partial^2 G_M / \partial x_1^2)_{T,P} = 0 = (\partial^3 G_M / \partial x_1^3). \quad (5.1)$$

Liquid-liquid phase coexistence criteria could be written equally well as

$$(\partial \mu_1 / \partial x_2)_{T,P} = 0 = (\partial^2 \mu_1 / \partial x_2^2)_{T,P} \quad (5.2)$$

with the additional restriction

$$(\partial^3 \mu_1 / \partial x_2^3) < 0 \quad (5.3)$$

at the critical point (Prigogine and Defay [1954]). The two-phase region corresponds to a horizontal line in a μ_1 vs x_2 plot (Figure 5.2, Prigogine and Defay [1954]); i.e., a region of two coexisting phases of compositions x_1' and x_1'' with $\mu_1' = \mu_1''$.

A coexistence curve (at constant P) for the system n-hexane-nitrobenzene (Figure 5.3, Prigogine and Defay [1954]) illustrates that the critical solution temperature (CST) is the maximum temperature at which two phases can coexist at a given pressure. The critical composition (x_{1c}) is the composition locus at which the CST occurs. Above the critical temperature T_c a mixture prepared at any composition forms a homogeneous fluid phase. However, at 10 °C and 0.5 overall mole fraction, for the system shown in Figure 5.3,

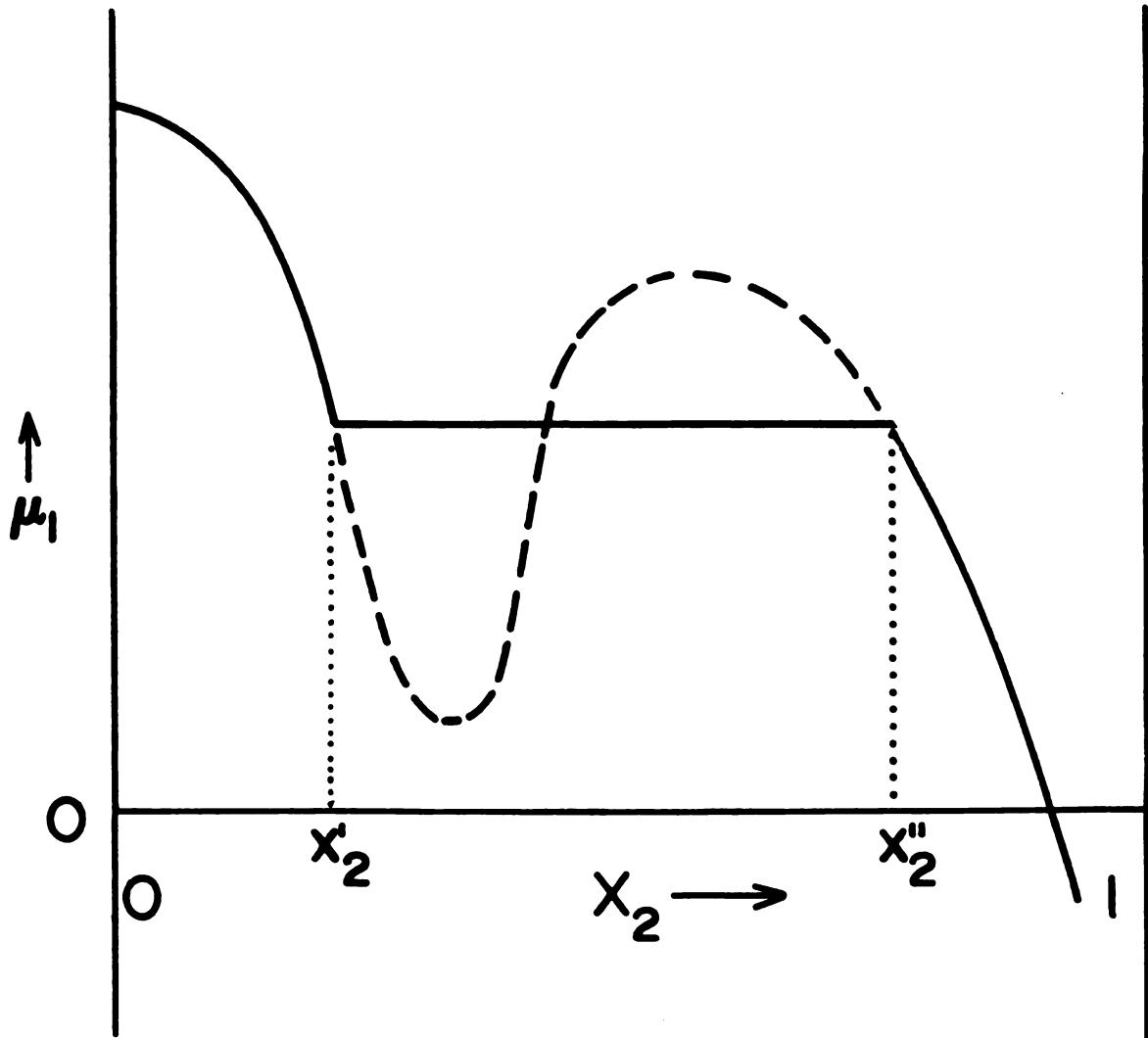


Figure 5.2. Behavior of the chemical potential of component 1 vs. mole fraction of component 2 for a critical system as depicted by Prigogine and Defay [1954]. The dashed line indicates metastable regions.

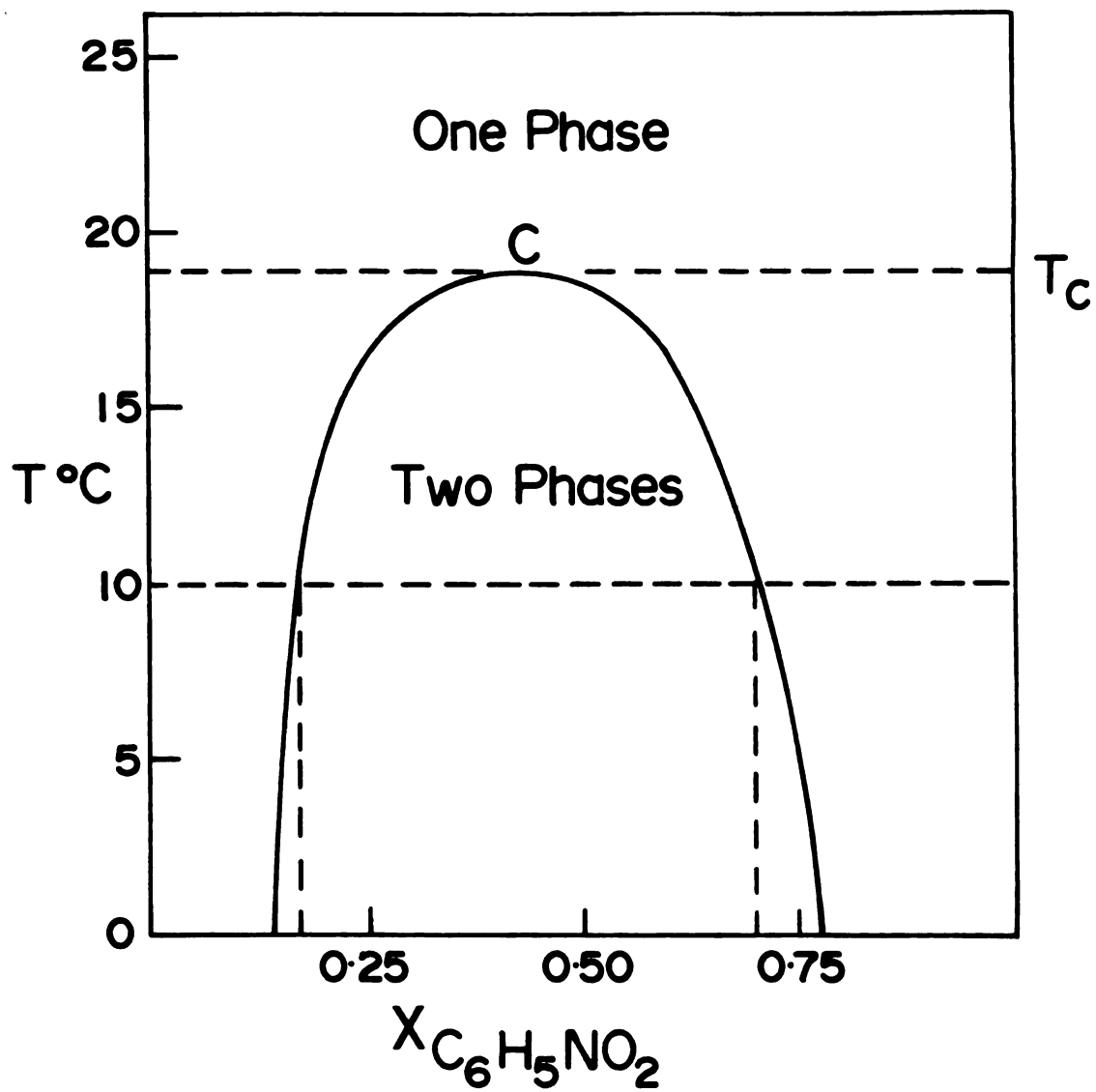


Figure 5.3. Coexistence curve for the *n*-hexane-nitrobenzene system as depicted by Prigogine and Defay [1954].

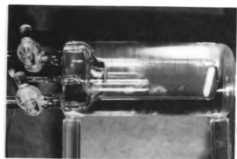
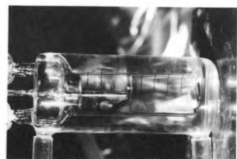
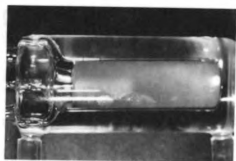
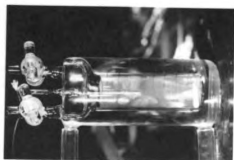
two phases of compositions $x_{\text{C}_6\text{H}_5\text{NO}_2} = 0.18$ and $x_{\text{C}_6\text{H}_5\text{NO}_2} = 0.82$ coexist.

B. Critical Exponents

1. Definitions - Figure 5.4 captures a time sequence of the physicochemical response of the isobutyric acid (IBA)-water system to a slow decrease in temperature from $T > T_c$ to $T < T_c$ along an isobar at the critical IBA mole fraction. Notice that even several degrees above the CST a change begins to occur. On a molecular level, A-A interactions relative to A-B interactions adjust rapidly. Local concentration fluctuations of dimension ξ increase dramatically, giving rise to a Tyndall-like light scattering effect known as critical opalescence. This occurs when ξ acquires lateral dimensions on the order of the wavelength of light. Figure 5.4 (b), (c), (d), and (e) show the light scattering associated with an increasing ξ . An understanding of how macroscopic transport properties are affected by this molecular commencement of phase separation promises to yield valuable information about the relationship between molecular and macroscopic phenomena.

Since the properties of the system obviously begin to adjust several degrees above phase separation (Figure 5.4), a set of indices known as critical exponents (CE) are used to correlate the temperature dependent behavior of properties as the CST is approached (Stanley [1971]). The

Figure 5.4. Photographic sequence of liquid-liquid critical phenomena as the temperature is lowered to the consolute temperature of the isobutyric acid-water critical mixture. (a) $T \gg T_c$. (b) $T - T_c \sim 3^\circ\text{C}$, mixture becomes a hazy blue hue as opalescence begins. (c) $T - T_c \sim 1^\circ\text{C}$, blue hue becomes a white fog as T is lowered and opalescence increases. (d) $T - T_c \lesssim 0.01^\circ\text{C}$, critical opalescence intensifies as dense white cloud. (e) $T - T_c \gtrsim -0.01$, onset of phase separation as marked by dense turbidity. (f) $T < T_c$, completion of phase separation.

**c****f****b****e****a****d**

limiting behavior of a property $f(\epsilon)$ in the critical region is denoted

$$f(\epsilon) \sim \epsilon^\lambda \quad (5.4)$$

where

$$\epsilon \equiv \frac{T - T_c}{T_c} \quad (5.5)$$

and

$$\lambda \equiv \lim_{\epsilon \rightarrow 0} \frac{\ln f(\epsilon)}{\ln \epsilon} . \quad (5.6)$$

It is important to realize that Equation (5.4) does not imply $f(\epsilon) = A\epsilon^\lambda$. In general, there will be correction terms which vanish as $T \rightarrow T_c$; i.e.,

$$f(\epsilon) = A\epsilon^\lambda(1 + B\epsilon^y + \dots) \quad (5.7)$$

where $y > 0$. Figure 5.5 shows the results of a light scattering determination of the mutual diffusion coefficient D by Chu, Lee, and Tscharnuter [1973]. They plot $\log D$ vs. $\log \epsilon$ to obtain the CE as the slope of the resultant line. Note the contribution of the higher order terms of Equation (5.7) as illustrated by the deviation from linearity when $T - T_c \geq 5$ °C.

Figure 5.5. Deviation from the simple form $D = Ae^{\lambda}$ for $T - T_c \geq 5$ °C in the light scattering determination of the mutual diffusion coefficient as measured by Chu, Lee, and Tscharrnutter [1973].

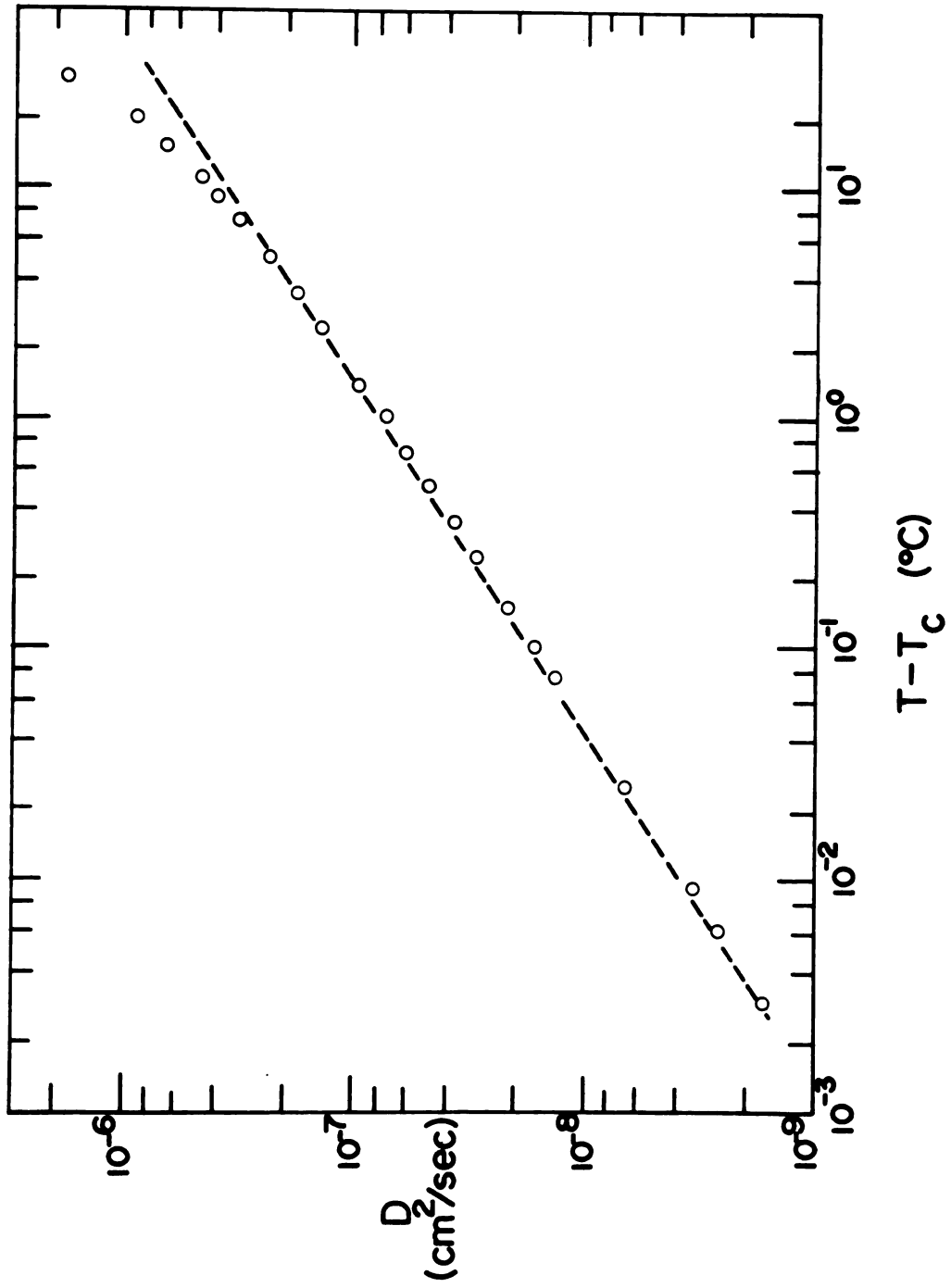


Figure 5.5.

Although experimental determination of the critical exponent λ does not provide the entire ϵ dependence of $f(\epsilon)$, the CE depicts the essential behavior sufficiently close to the CST. As Figure 5.6 shows, a negative CE characterizes a diverging function while a positive CE represents a vanishing function as $\epsilon \rightarrow 0$. The larger $|\lambda|$ is, the further away from T_c the anomalous behavior appears. The use of the word "anomalous" in reference to the ϵ -functionality of a property in the critical region indicates a deviation from the behavior predicted by extrapolation of the T -dependent behavior exhibited far from the CST.

Some of the more common thermostatic properties which exhibit anomalous critical behavior have been experimentally characterized quite well and have specific symbols reserved for their critical exponents. Thus

$$(x_2'' - x_2') \sim |\epsilon|^\beta \quad (\text{constant } P) \quad (5.8)$$

defines β ,

$$(\partial\mu_1/\partial x_1)_{T,P} \sim |\epsilon|^{\gamma_+} \quad (\text{constant } P; X_{2c}) \quad (5.9)$$

defines γ_+ where $+$ indicates $\epsilon \rightarrow 0$ from the positive side, and

Figure 5.6. Behavior of properties as functions of ϵ for various values of the critical exponent λ .

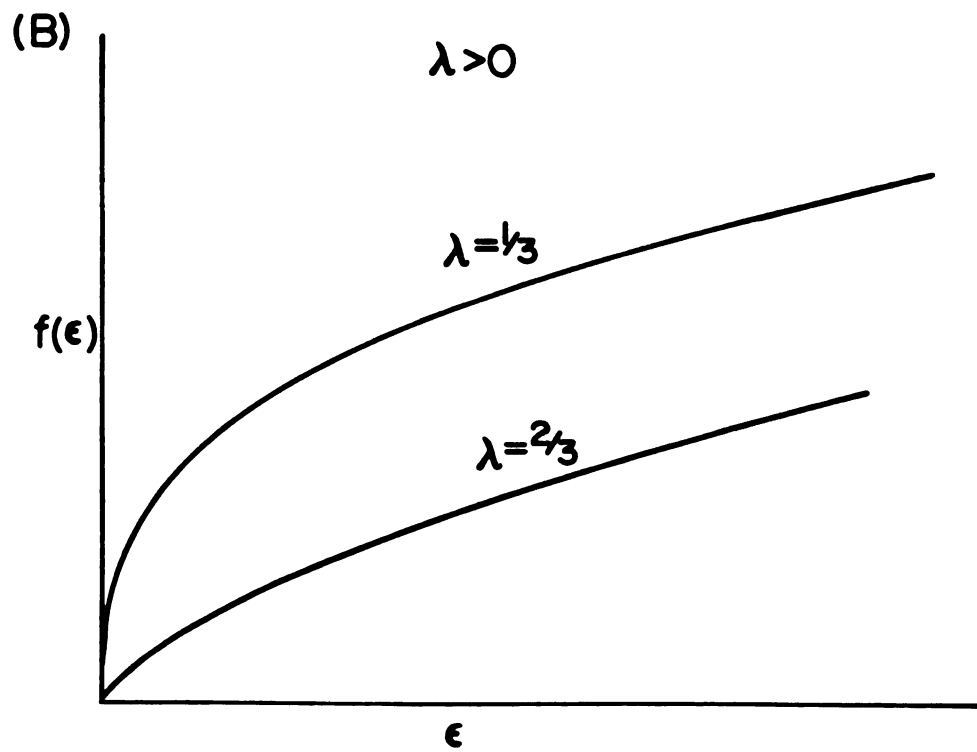
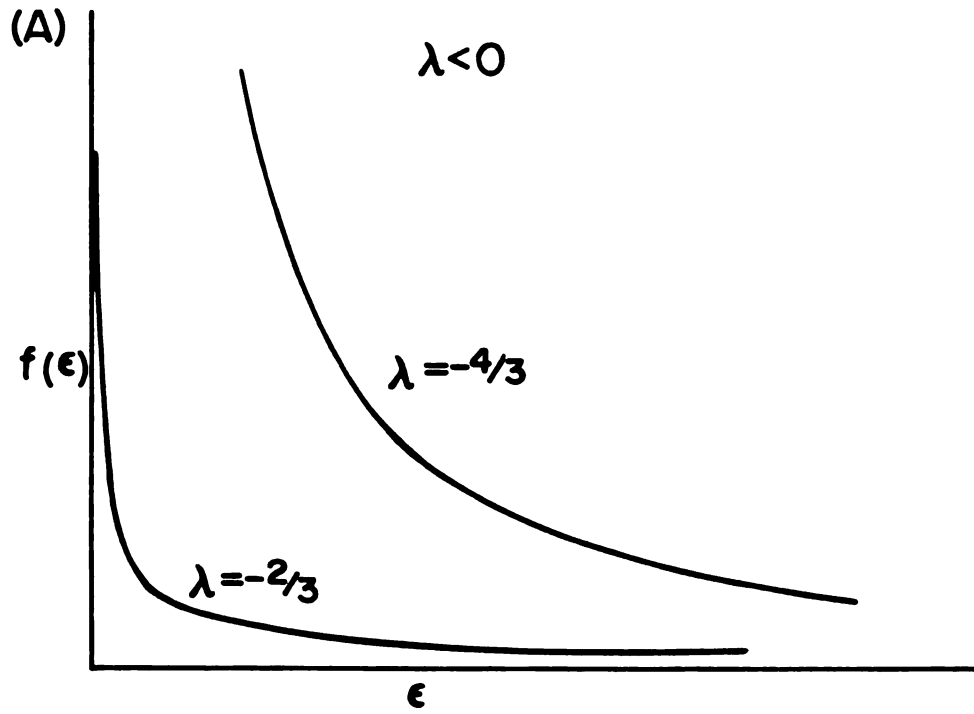


Figure 5.6

$$\tilde{C}_{P,x} \sim |\epsilon|^{-\alpha^+} \quad (\text{constant } P; X_{2c}) \quad (5.10)$$

defines α^+ . Table 5.1 lists some typical values for these thermostatic critical exponents as reviewed by Scott [1972].

In addition to anomalous behavior representation, critical exponents are themselves fundamentally important. Recent emphasis on experimental determination of CE's has had a two-fold incentive: (1) the value of a particular CE transcends the system under investigation (universality) and (2) equalities between several exponents allow prediction of unknown CE's from known ones (scaling).

2. Universality - The theory of universality states that when allowance is made for any extra variables and when the properly analogous quantities are compared, the CE's for different systems are identical. An illustrative example is the exponent β which characterizes the temperature behavior of the order parameter¹. Within experimental error, the order parameter for liquid-liquid systems ($x_1' - x_1''$), gas-liquid systems ($\rho_V - \rho_L$), and magnetic systems (magnetization M) all exhibit the same critical exponent $\beta = 0.33$.

¹An order parameter is the property that is nonzero for $T < T_c$ but zero for $T \geq T_c$. Equation (5.8) is an example.

Table 5.1. Critical exponents for some equilibrium thermodynamic properties. References are cited in Scott's [1972] review.

System	β	γ_+	α_+
$\text{CCl}_4 + \text{C}_7\text{F}_{14}$	0.33	1.2	
$\text{CH}_4 + \text{CF}_4$	0.35	1.3, 1.4	
$\underline{n}\text{-C}_6\text{H}_{14} + \underline{n}\text{-C}_6\text{F}_{14}$	0.34, 0.35	1.37	
$\underline{i}\text{-C}_3\text{H}_7\text{COOH} + \text{H}_2\text{O}$	0.33	1.24	0.12, 0.1
$\underline{n}\text{-C}_{10}\text{H}_{22} + (\beta\text{-ClC}_2\text{H}_4)_2\text{O}$	0.32	1.25	

3. Scaling - Scaling hypotheses predict relations among critical exponents on the assumption that the free energy is a generalized homogeneous function of the form

$$G(k^a x, k^b y) = kG(x, y). \quad (5.11)$$

Although the scaling parameters "a" and "b" are not specified, they can be identified by comparison with two known critical exponents. If two properties are derived by taking the appropriate partial derivatives of Equation (5.11), then the behavior of those properties in the critical region necessitates a relation between "a" and "b" and the properties' critical exponents. The two known CE's thereby fix the degree of homogeneity, scaling all other properties derivable from Equation (5.11). An equality involving the three CE's results. A typical example is $\alpha + 2\beta + \gamma = 2$, where the exponents α , β , and γ have their common definitions shown in Equations (5.8) - (5.10). Table 5.1 provides test data for the above equality.

C. Transport Properties in the Critical Region

As mentioned in the previous sections, the onset of phase separation as T approaches T_c may produce anomalous behavior in a given macroscopic property. The anomaly

is characterized by a nonzero critical exponent. The four transport phenomena of interest in binary nonelectrolyte liquid mixtures in the absence of pressure gradients are: (1) thermal conduction, (2) mutual diffusion, (3) thermal diffusion, and (4) the diffusion thermoeffect. Examination of anomalies in these properties near the CST is dedicated to understanding the microscopic contributions to the phenomena and to increasing predictive capabilities.

Toward the above goals, Table 5.2 shows the transport coefficients and their respective relationships to Onsager coefficients. In Table 5.2 and throughout this thesis, the following critical exponent symbols will be used: (1) λ_1 for Ω_{00} , (2) λ_2 for Ω_{11} , (3) λ_3 for Ω_{10} , and (4) λ_4 for Ω_{01} . Note that any anomalous behavior in the critical region can be ascribed to a kinetic effect (the Onsager coefficient), a thermodynamic effect $[\bar{\mu}_{1j}]$ where $\bar{\mu}_{1j} \equiv (\partial \bar{\mu}_1 / \partial w_j)_{T,P}$, or a combination of both. Phase coexistence is governed by equilibrium thermodynamic relations, and the purely equilibrium thermodynamic coefficient $\bar{\mu}_{1j}$ is known to vanish with a $+4/3$ exponent as the CST is approached. Thus, any anomalous contributions from Ω_{1j} 's should provide useful data for probing the microscopic or kinetic nature of the phenomenon. Of special interest, in this light, are κ and \bar{Q}_1^* , which have no direct dependence on the thermodynamic quantity $\bar{\mu}_{11}$.

Table 5.2. The behavior of transport coefficients in the critical region.

Property	Definition	Behavior Near CST	Exponents
κ	$\kappa = \Omega_{00}/T$	$\kappa \sim \Omega_{00}$	$\kappa \sim \epsilon^{\lambda_1}$ $\Omega_{00} \sim \epsilon^{\lambda_1}$
D	$D = \frac{\Omega_{11}\bar{\mu}_{11}}{\rho w_2}$	$D \sim \Omega_{11}\bar{\mu}_{11}$	$D \sim \epsilon^{\lambda_2+4/3}$ $\bar{\mu}_{11} \sim \epsilon^{4/3}$ $\Omega_{11} \sim \epsilon^{\lambda_2}$
D_T	$D_T = \Omega_{10}/\rho$	$D_T \sim \Omega_{10}$	$D_T \sim \epsilon^{\lambda_3}$
	$\alpha_1 = \frac{\Omega_{10}}{w_1 w_2 \rho D}$	$\alpha_1 \sim \frac{\Omega_{10}}{\Omega_{11}\bar{\mu}_{11}}$	$\alpha_1 \sim \epsilon^{\lambda_3-\lambda_2-4/3}$
	$K_T = \frac{\Omega_{10} w_2}{\Omega_{11}\bar{\mu}_{11}}$	$K_T \sim \frac{\Omega_{10}}{\Omega_{11}\bar{\mu}_{11}}$	$K_T \sim \epsilon^{\lambda_3-\lambda_2-4/3}$ $\Omega_{10} \sim \epsilon^{\lambda_3}$
\bar{Q}_1^*	$\bar{Q}_1^* = \frac{\Omega_{01}}{\Omega_{11}}$	$\bar{Q}_1^* \sim \frac{\Omega_{01}}{\Omega_{11}}$	$\bar{Q}_1^* \sim \epsilon^{\lambda_4-\lambda_2}$ $\Omega_{01} \sim \epsilon^{\lambda_4}$

Literature values of the CE's for the properties listed in Table 5.2 (with the exception of \bar{Q}_1^*) are discussed in the next sections. Chapter 6 presents original research and results on \bar{Q}_1^* for isobutyric acid-water mixtures in the critical solution region.

D. Predicted Liquid-Liquid Critical Exponents for Transport Phenomena

The utility and versatility of critical exponents have been firmly established by scaling hypotheses and universality theories. Extension of scaling procedures to nonequilibrium processes and development of mode-mode coupling theories constitute the most recent advances in transport CE prediction. Older mean-field theories implicitly or explicitly assume long range molecular interactions and are less accurate.

Mode-mode coupling arguments are based on nonlinearities in the hydrodynamic equations near the critical point. The nonlinearities are due to coupling among various energy dissipative modes. The best normal mode type solution of the nonlinear equations defines the corresponding transport coefficient. This coefficient may then contain an anomalous contribution in the critical region because of the included coupled dissipative term required for a normal mode solution. Fixman [1962] noted that near the CST, where long wavelength fluctuations become

intense, a velocity gradient, created by exerting shear forces at the boundaries, can easily induce nonhomogeneities in concentration. The return to uniform composition via diffusion dissipates some of the energy. Yet, from a macroscopic point of view, the total dissipation of energy through the coupled viscous and diffusive modes appears simply to be the result of an anomalously large viscosity.

Mode-mode coupling predictions are based on identification of the appropriate, coupled modes. An estimation (usually by scaling) of the contribution by the coupled or nonlinear terms to the coefficient in the normal mode solution yields a prediction for the expected anomaly. Values of the various CE's as theoretically predicted for binary liquid systems are shown in Table 5.3. When Table 5.3 is used, the necessary relationships between the thermal diffusion coefficient D_T , the thermal diffusion ratio K_T , and the thermal diffusion factor α_1 are readily obtained from Equations (2.15) and (2.16).

E. Experimental Liquid-Liquid Critical Exponents for Transport Parameters

1. Techniques - Measurement of transport phenomena near the CST commonly involve either (1) the system's response to a macroscopic gradient or (2) the time variation in the local fluctuations of thermodynamic variables

Table 5.3. Theoretical predictions for critical exponents of transport properties.

Reference (a)	D (b) & (c)	κ (b)	D_T & K_T (b) & (c)	Method (d)
Papoular [1974]			$K_T \sim \epsilon^{-4/3}$	S
Mistura [1975]			$K_T \sim \epsilon^{-\nu}$	MM
Kawasaki [1969]	$D \sim \epsilon^{1/2} \ell^{-1}$	$\kappa \sim \epsilon^{-1/2} \ell^{-1}$	$D_T \sim \epsilon^{-1/2} \ell^{-1}$	MM
Deutch [1967], Mountain [1968], and Kadanoff [1969]	$D \sim \epsilon^{1/2}$			M
Kadanoff [1969] and Swift [1968]	$D \sim \epsilon^\nu$	$\kappa \sim \epsilon^0$ (finite)	D_T at most weakly divergent	MM &S
Kawasaki [1970]	$D \sim \epsilon^\nu$			MM&S
Ferrell [1970]	$D \sim \epsilon^\nu$			MM&S
Kawasaki [1966]		Finite		M

(a) only first author is listed.

(b) ℓ = force range.(c) ν = critical exponent for correlation length $\xi \sim \epsilon^{-\nu}$ - usually taken as $\nu=2/3$.

(d) Prediction methods are: S-scaling, M-meanfield theories, and MM-mode-mode coupling.

in a system in macroscopic equilibrium. The former method constitutes a "thermodynamic" experiment, while the latter usually involves light scattering techniques. Although macroscopic gradients lead to experimental difficulties in systems near the consolute temperature, thermodynamic measurements are extremely important for understanding force-flux behavior in this region.

Determination of transport coefficients from non-equilibrium thermodynamics involves linear hydrodynamic equations; i.e., the coefficients are not gradient dependent. This is certainly valid for very small gradients. However, near the CST where the correlation length ξ diverges, coefficients may be nonconstant over distances on the order of ξ even for moderately small gradients. For this reason, several authors have suggested that nonlinearities are to be expected sufficiently close to the critical point (e.g., Fixman [1962], Kawasaki [1966], and Grossmann [1969]). Nevertheless, experiments have failed to show any gradient dependence in measured coefficients. To the contrary, Woermann and Sarholz [1965] and Tsai [1970] have shown the shear viscosity to be constant for a change in shear rate of 4 and 5 orders of magnitude respectively. Similarly, Michels and Sengers [1962] have shown the thermal conductivity near the gas-liquid critical point to be independent of ΔT . These results justify the assumption of linear

laws in the experimentally accessible neighborhood of the critical point - especially if gradient driving forces are kept small.

2. Thermal Conductivity - Thermal conductivity experiments (and pure thermal diffusion experiments) are plagued with convection problems. Convection is especially enhanced in the consolute region where thermal gradients can produce large density fluctuations. These difficulties have kept data scarce.

Gerts and Filippov [1956] and Filippov [1968] measured the thermal conductivity of nitrobenzene-n-hexane, nitrobenzene-n-heptane, methanol-n-hexane, and triethylamine-water mixtures as $T \rightarrow T_c$. The absence of convection was demonstrated by independence of results on ΔT (this also further justifies the linear flux-force laws). The results for two of the investigated systems as reported by Gerts and Filippov are shown in Figure 5.7. As is the case for the mixtures depicted in Figure 5.7, none of the four systems evidenced any anomaly.

Osipova [1957] did report an anomaly in the thermal conductivity of a phenol-water mixture. However, most reviewers (Sengers [1971]) suggest that the reported large scatter in data and large errors in measurement of ΔT are indicative of unreliable results.

Although further experiments are desirable, thermal

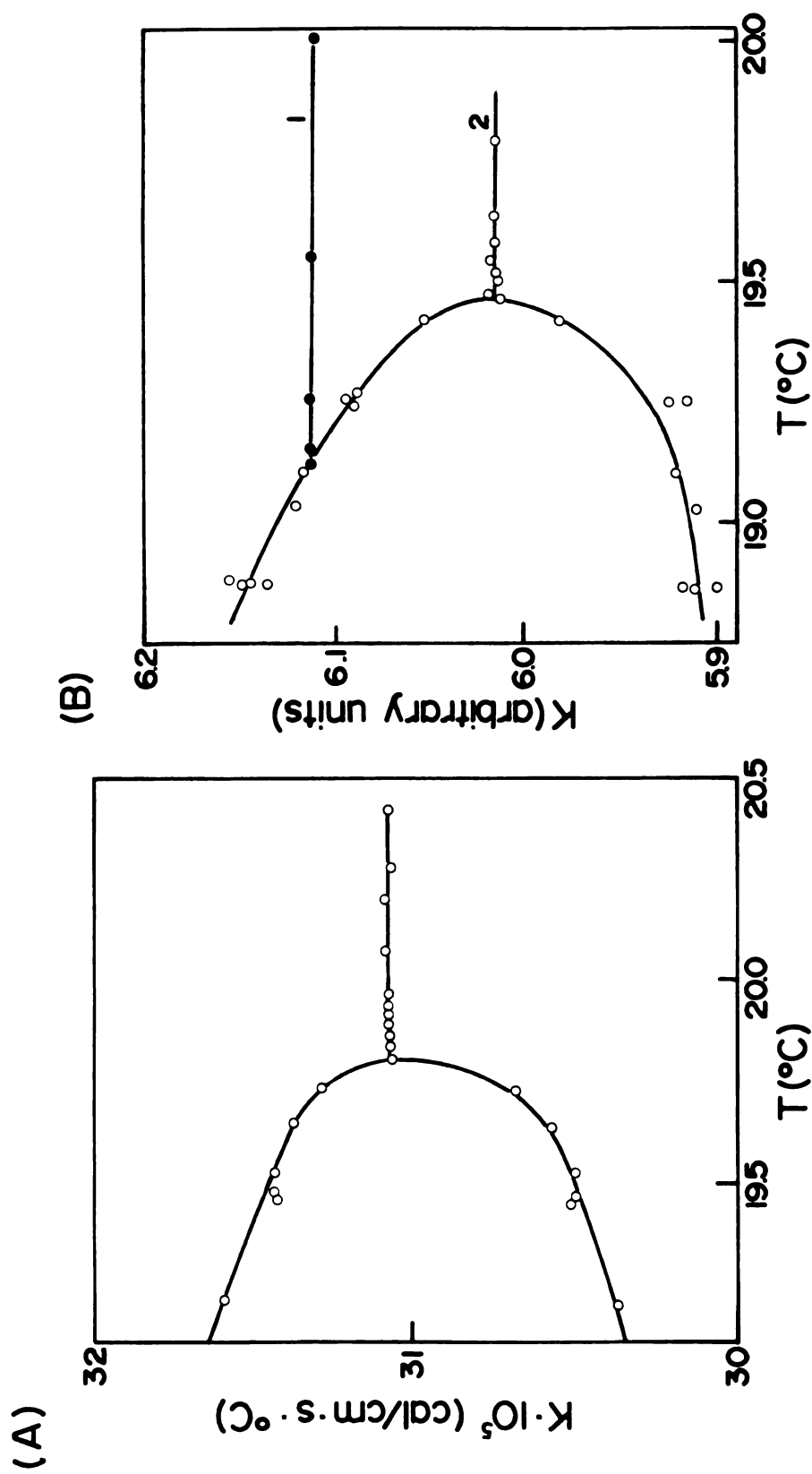


Figure 5.7. Thermal conductivity in the critical region as reported by Gerts and Filippov [1956]. (A) 63 wt. % *n*-hexane + 37 wt. % nitrobenzene. (B) System *n*-heptane-nitrobenzene with: 1. 62 wt. % nitrobenzene; 2. 52.3 wt. % nitrobenzene.

conductivity evidently remains finite as T_c is approached from the homogeneous fluid side. Thus, $\kappa = \Omega_{00}/T \sim \epsilon^0$.

3. Mutual Diffusivity - Thermodynamic measurements of mutual diffusion coefficients near the liquid-liquid critical point (Krichevskii et al. [1954], Claesson and Sundelöf [1957], Lorentzen and Hansen [1957] and [1958], Krichevskii et al. [1960], Haase and Siry [1968], and Balzarini [1974]) show unequivocally that D vanishes as $T \rightarrow T_c$. With the exception of Balzarini [1974], none of the above experimentalists report a critical exponent. The prominent feature of these more qualitative works is especially noticeable in Figure 5.8 where the representative results of Haase and Siry [1968], for the water-triethylamine system exhibiting a lower consolute temperature, and of Claesson and Sundelöf [1957], for the n-hexane-nitrobenzene system exhibiting an upper consolute temperature, clearly indicate that $(\partial D/\partial T)_{x_{1c}}$ becomes infinite as the CST is approached. Differentiating with respect to T the expression for D in Table 5.2 yields

$$(\partial D/\partial T)_{x_{1c}} \sim \epsilon^{\lambda_2+1/3}. \quad (5.12)$$

Recall from the discussion of critical exponents that in order for $(\partial D/\partial T)_{x_{1c}}$ to diverge as $\epsilon \rightarrow 0$, the critical exponent must be negative. With respect to Equation (5.12)

Figure 5.8. Mutual diffusion in the critical region. (A) Results of Haase and Siry [1968] for the water-triethylamine system exhibiting a lower consolute temperature at 91.26 mol % water and 18.3 °C. (B) Results of Claesson and Sundelöf [1957] for the n-hexane-nitrobenzene system at equal mole fractions.

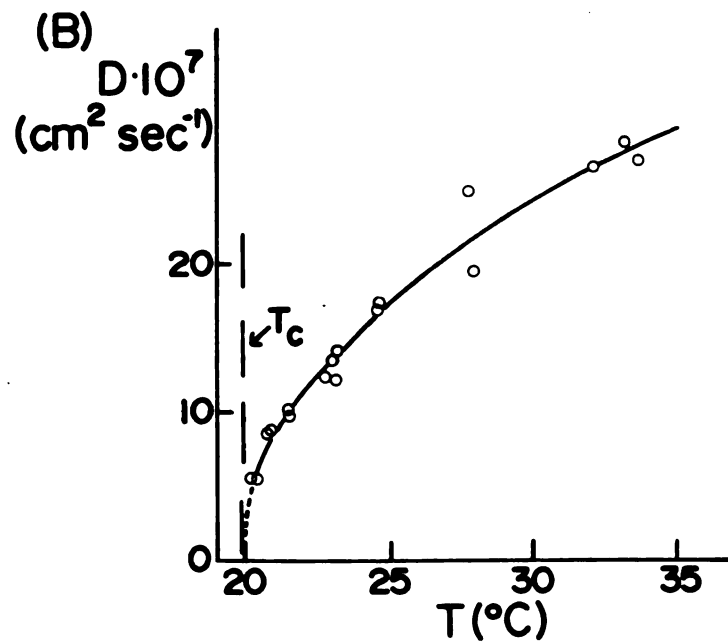
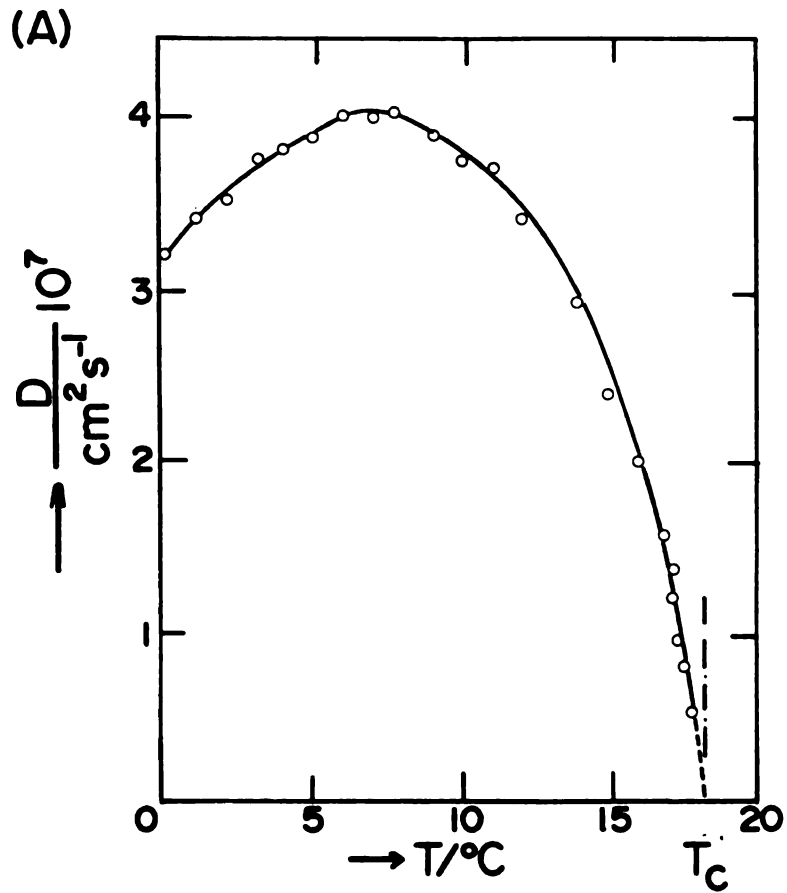


Figure 5.8

this means that $\lambda_2 < -1/3$. Reasoning along these lines constituted the first evidence that Ω_{11} diverged at the critical point; i.e., that the observed anomaly in D was not strictly dependent on the thermodynamic factor $\bar{\mu}_{11}$. Balzarini's more recent thermodynamic experiments yield 0.74 ± 0.08 for the CE of D .

Recently, values for λ_2 have been obtained much nearer the critical point by light scattering experiments. Light scattering measures the decay rate of concentration fluctuations and therefore eliminates the need for macroscopic gradients and system-perturbing response measurement devices (for example, the thermal lens effect associated with interferometry, Giglio and Vendramini [1974]). As Table 5.4 illustrates, the diffusion coefficient is unquestionably represented by $D \sim \epsilon^{\lambda'}$ with $\lambda' = \lambda_2 + 4/3 \approx 2/3$. This value (and the values in Table 5.4) compares favorably with the exponent for thermal diffusivity in gas-liquid systems, $\kappa/\rho C_p \sim \epsilon^{\lambda'}$ where $0.61 \leq \lambda' \leq 0.69$ (Sengers [1973]). As was mentioned earlier, universality requires that comparison of like modes in different systems yield identical exponents. Mutual diffusivity in liquid-liquid systems corresponds to the thermal diffusivity mode in gas-liquid one-component systems. The kinetic contribution Ω_{11} must therefore diverge as $\Omega_{11} \sim \epsilon^{\lambda_2}$ with $\lambda_2 \approx -2/3$ as $T \rightarrow T_c$.

Table 5.4. Light scattering results for the mutual diffusion critical exponent.

System	Exponent ^(a)	Reference ^(b)
Isobutyric acid-water	0.68±0.04 0.62±0.02 (c)	Chu [1968] Chu [1972]
n-hexane-nitrobenzene	0.66±0.02 0.63 (c)	Chen [1969] Chu [1972]
3-methylpentane-nitroethane	0.62 (c)	Chang [1972]
cyclohexane-aniline	0.61±0.01	Berge [1970]
perfluoromethylcyclohexane-carbon tetrachloride	0.66(5)±0.03 0.63±0.005 (c)	Chu [1968] Chu [1972]
lutidine-water	0.554±0.015	Gülyary [1972]
phenol-water	0.68±0.03	Goldburg [1972] and Bak [1969]
methane-tetrafluoromethane	0.67±0.02	Blagoi [1970]

(a) Exponent refers to λ' in $D \sim \epsilon^{\lambda'}$ where $\lambda' = \lambda_2 + 4/3$.

(b) Only first author is listed.

(c) Indicates renormalized values after taking into account the "regular part" and temperature dependence of the viscosity.

4. Thermal Diffusion - Much like thermal conductivity experiments, thermal diffusion measurements require substantial macroscopic temperature gradients which may induce convection. Furthermore, the consolute temperature cannot be approached very closely with temperature gradients present. For these reasons, early measurements of D_T in the liquid-liquid critical region yielded, at best, qualitative results (Thomaes [1956], Tichacek and Drickamer [1956], and Haase and Bienert [1967]). It is instructive to plot the data of Thomaes and those of Tichacek and Drickamer in a typical log-log plot of the thermal diffusion ratio K_T versus ϵ so as to obtain from the slope an effective value for the CE. This is done in Figure 5.9. Note the large scatter in data and more importantly the large discrepancy in the critical exponents or slopes obtained. The data of Haase and Bienert [1967] on the water-triethylamine system are not plotted here for two reasons: (1) the data are not given at the critical composition, and (2) the consolute temperature is not approached sufficiently closely for comparison purposes. Although all three sets of thermal diffusion data indicate that K_T diverges as $\epsilon \rightarrow 0$, Haase and Thomaes qualitatively argue that D_T also diverges while Tichacek indicates that D_T vanishes. That is, Thomaes's results indicate $D_T \sim \epsilon^{-1}$ while Tichacek and Drickamer's data yield $D_T \sim \epsilon^{+1/3}$.

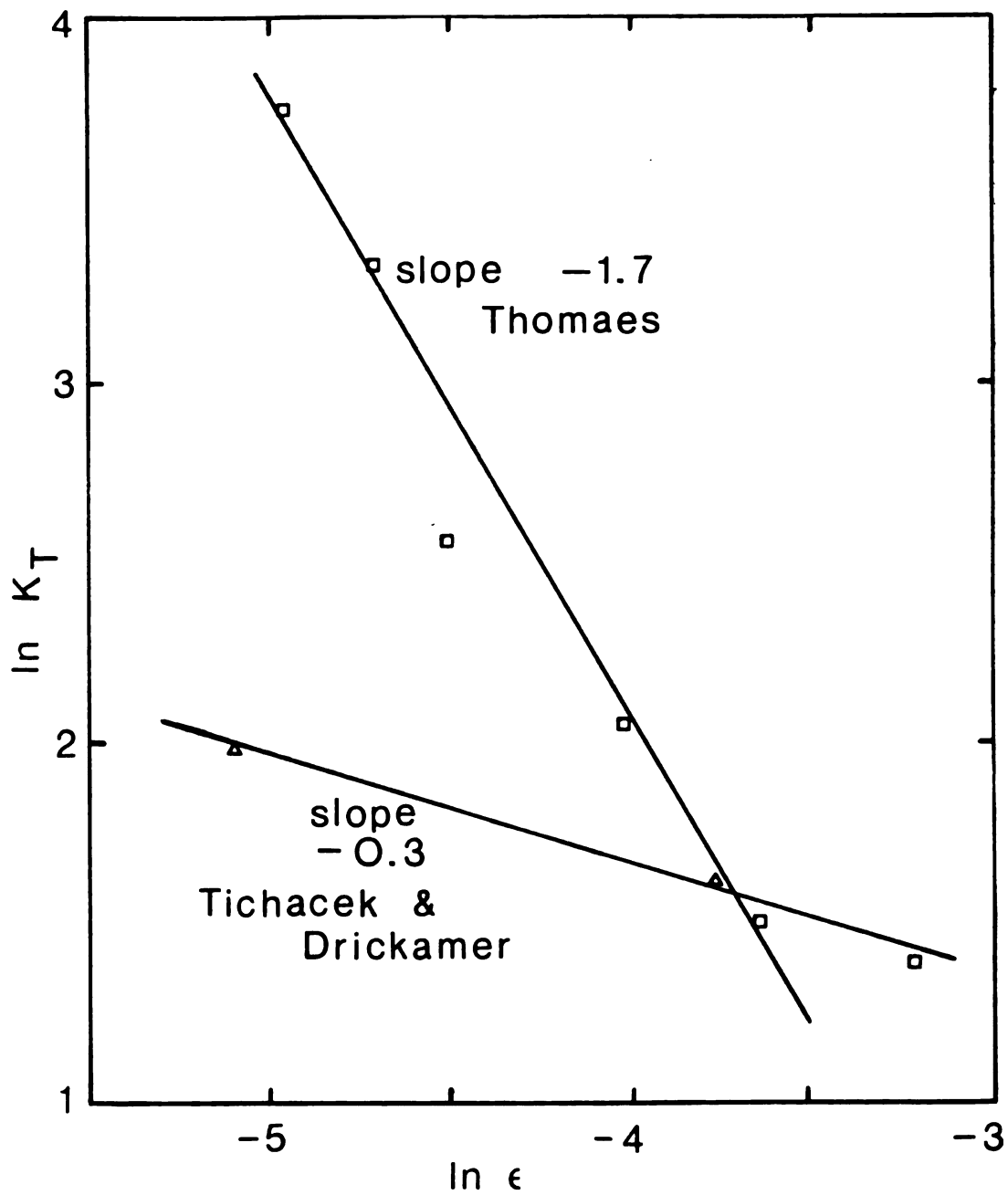


Figure 5.9. Log-log plot of the thermal diffusion data of Thomaes [1956] for the *n*-hexane-nitrobenzene system and of Tichacek and Drickamer [1956] for the perfluoro-*n*-heptane+2,2,4-trimethylpentane system.

Giglio and Vendramini [1975] claim the first "accurate measurements of the thermal diffusion ratio K_T in the neighborhood of the consolute critical point of the mixture aniline-cyclohexane." Their measurements were performed using a classical Soret cell and a steady-state beam-deflection technique. By evaluation of the time evolution of beam deflection, they also obtained the temperature dependence of the mutual diffusion coefficient. From these data, the behavior of D_T was obtained. Giglio and Vendramini's [1975] log-log plots of K_T , D , and D_T are shown in Figure 5.10. In this figure, the line through the diffusion data are the light scattering results of Berge et al. [1971]. Values for D_T are calculated from $D_T = K_T D$. The relatively good agreement for D with the light scattering experiments of Berge et al. [1971] seem indicative of reliable results. The "best-fit" CE value for K_T is $\lambda = -0.73 \pm 0.02$ in the expression $K_T \sim \epsilon^\lambda$. However, Giglio and Vendramini [1975] conclude that $K_T \sim D^{-1} \sim \epsilon^{-2/3}$ because calculation of D_T shows it to be temperature independent; i.e., $D_T \sim \epsilon^0$. The slightly larger exponent determined from the least squares fit of K_T is attributed to a deviation of the relation $K_T = A\epsilon^\lambda$ in the region where numerous data points are located. That is, K_T is expected to behave more like Equation (5.7) further away from the critical point. Inclusion of points in this region leads to an effective

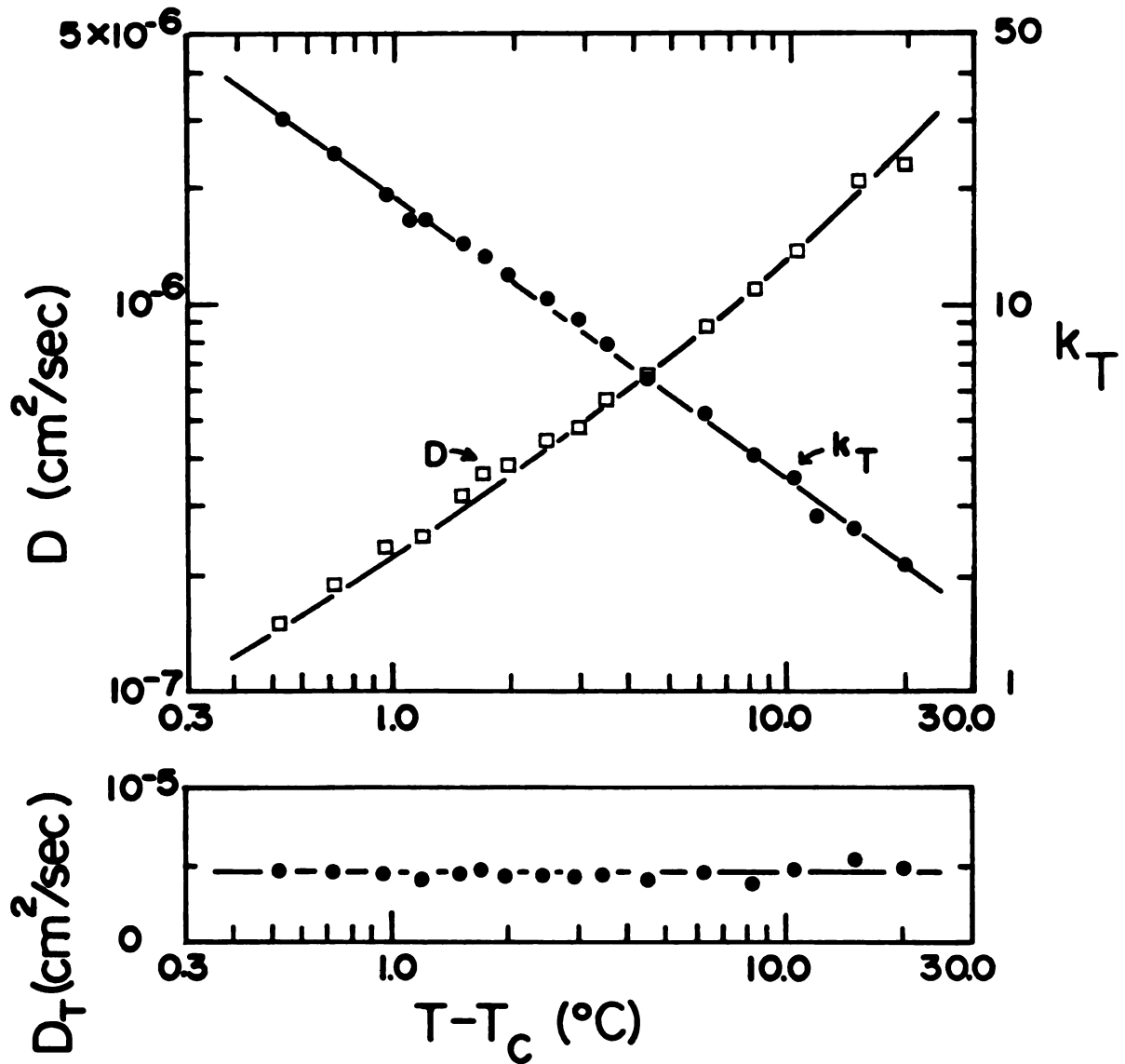


Figure 5.10. Thermal diffusion and mutual diffusion results of Giglio and Vendramini [1975] for the critical region of aniline-cyclohexane mixtures.

exponent of larger magnitude than the true exponent (cf. Figure 5.5).

5. Heat of Transport - The diffusion thermoeffect measurements discussed in Chapter 6 are believed to be the first direct evaluation of the temperature dependence for Q_1^* near the consolute point. Although Haase and Bienert [1967] calculated \tilde{Q}_1^* from Thomaes's [1956] thermal diffusion data, the values obtained were meaningless because (1) Thomaes's data are inconsistent with the more accurate work of Giglio and Vendramini [1975], and (2) no verification of the Onsager reciprocal relation in the critical region has ever been made. To indicate further the need for a direct study of the heat of transport, note that the critical exponent obtained for \bar{Q}_1^* on the basis of ORR is positive (+2/3) if the data of Giglio and Vendramini are used, positive (+1) if the data of Tichacek and Drickamer are used, but negative (-1/3) if Thomaes's data are used.

Table 5.5 summarizes the results of the preceding sections for the four transport properties of interest to the present discussion near the critical demixing point of a binary liquid mixture. The indicated ignorance of the temperature behavior of \bar{Q}_1^* as $T \rightarrow T_c$ gives impetus for the measurements described in the next chapter.

Table 5.5. Literature transport parameters and their critical exponents.

Property	Definition	Behavior Near CST	Critical Exponents
κ	$\kappa = \Omega_{00}/T$	$\kappa \sim \Omega_{00}$	$\kappa \sim \epsilon^0$ $\Omega_{00} \sim \epsilon^0$
D	$D = \frac{\Omega_{11}\bar{\mu}_{11}}{\rho w_2}$	$D \sim \Omega_{11}\bar{\mu}_{11}$	$D \sim \epsilon^{2/3}$ $\bar{\mu}_{11} \sim \epsilon^{4/3}$ $\Omega_{11} \sim \epsilon^{-2/3}$
D_T	$D_T = \frac{\Omega_{10}}{\rho}$	$D_T \sim \Omega_{10}$	$D_T \sim \epsilon^0$ (a)
	$\alpha_1 = \frac{-\Omega_{10}}{w_1 w_2 \rho D}$	$\alpha_1 \sim \frac{\Omega_{10}}{\Omega_{11}\bar{\mu}_{11}}$	$\alpha_1 \sim \epsilon^{-2/3}$ (a)
	$K_T = \frac{\Omega_{10} w_2}{\Omega_{11}\bar{\mu}_{11}}$	$K_T \sim \frac{\Omega_{10}}{\Omega_{11}\bar{\mu}_{11}}$	$K_T \sim \epsilon^{-2/3}$ (a) $\Omega_{10} \sim \epsilon^0$ (a)
\bar{Q}_1^*	$\bar{Q}_1^* = \frac{\Omega_{01}}{\Omega_{11}}$	$\bar{Q}_1^* \sim \frac{\Omega_{01}}{\Omega_{11}}$	$\bar{Q}_1^* \sim \epsilon^?$ $\Omega_{01} \sim \epsilon^?$

(a) Results of Giglio and Vendramini [1975] are used.

CHAPTER 6

THE HEAT OF TRANSPORT IN THE CRITICAL SOLUTION REGION OF ISOBUTYRIC ACID-WATER MIXTURES

A. Transport Equations

To evaluate the temperature dependence of the heat of transport Q_1^* as the CST is approached, the partial differential equations describing the diffusion thermoeffect must be solved and the solution fitted to the experimental points. Although this technique was introduced in Chapters 3 and 4 for the $\text{CCl}_4\text{-c-C}_6\text{H}_{12}$ system, each equation with its underlying assumptions must be checked for correctness in the critical region before use.

The starting partial differential equations of Chapter 2 can be written

$$(\partial\rho/\partial t) + (\partial\rho v/\partial z) = 0, \quad (6.1)$$

$$\rho(\partial w_1/\partial t) = \{\partial[\rho D(\partial w_1/\partial z)]/\partial z\} - \rho v(\partial w_1/\partial z), \quad (6.2)$$

and

$$\begin{aligned} \rho\bar{C}_p(\partial T/\partial t) &= \rho D[\partial(\bar{H}_1 - \bar{H}_2)/\partial z](\partial w_1/\partial z) - \rho\bar{C}_p v(\partial T/\partial z) \\ &+ \{\partial[\rho D\bar{Q}_1^*(\partial w_1/\partial z)]/\partial z\} + \{\partial[\kappa(\partial T/\partial z)]/\partial z\}. \end{aligned} \quad (6.3)$$

The assumptions made in obtaining Equations (6.1) - (6.3) are:

- (1) The linear hydrodynamic equations for conservation of mass and energy are valid.
- (2) The binary system is isotropic, nonreacting, and field free.
- (3) Local states are assumed; i.e., the equations of thermostatics apply for local regions.
- (4) Fluxes are linear combinations of those forces which appear in the entropy production equation and which have the same tensorial rank.
- (5) Pressure terms are negligible.
- (6) The bulk flow entropy source term is small.
- (7) The thermal diffusion portion of the mass flux is small compared to the diffusion portion.

Assumptions (2), (3), and (5) are obviously as correct near the CST as away from it. Assumptions (1) and (4) were discussed in Chapter 5. The demonstration that η , κ_{g-1} (thermal conductivity near the gas-liquid critical point), and κ_{l-1} (thermal conductivity near the liquid-liquid critical point) are independent of their respective driving forces is indicative of linearity in the critical region. Assumption (6) is also valid near the consolute point because the bulk flow entropy source term is proportional to the square of the barycentric velocity which is itself small (especially for the system to be

investigated here).

Assumption (7) must be dealt with somewhat more carefully. The mass flux, on the basis of the above assumptions, can be written

$$-j_1 = \rho D(\partial w_1/\partial z) - \rho D \alpha_1 w_1 w_2 T^{-1}(\partial T/\partial z). \quad (6.4)$$

The previous chapter (cf. Table 5.5) demonstrated that the most accurately determined temperature behaviors of D and α_1 in the critical region are $D \sim \epsilon^{2/3}$ and $\alpha_1 \sim \epsilon^{-2/3}$, respectively. Thus, while D vanishes in the critical region, α_1 becomes large at about the same rate. Although the first term in Equation (6.4) vanishes, $D\alpha_1$ in the second term remains finite. At first sight, it appears that the thermal diffusion term could be important sufficiently close to the CST. However, $(\partial w_1/\partial z)$ is always much larger than $(\partial T/\partial z)$. Away from the CST, Ingle and Horne [1973] estimate the maximum contribution of the thermal diffusion term to be 0.01%. With this estimate for temperatures away from the CST, calculations show that the critical point must be approached to within about 0.01°C before the decrease in D allows a 1% contribution to j_1 from the thermal diffusion term [at constant $(\partial T/\partial z)$ and $(\partial w_1/\partial z)$]. The experiments described herein show that $(\partial T/\partial z)$ also vanishes as the CST is approached while $(\partial w_1/\partial z)$ remains finite. Hence,

the thermal diffusion contribution to the mass flux will never reach 1% even for temperatures very near T_c and can be safely neglected. With all assumptions thus verified, Equations (6.1) - (6.3) can be used for critical mixtures.

The isobutyric acid-water system (IBW) is particularly convenient for measurement of Q_1^* in the critical region because of the very similar densities of the pure components ($\rho_{\text{IBA}}^{\circ}, 20^{\circ}\text{C} = 0.958 \text{ g/cm}^3$; $\rho_{\text{H}_2\text{O}}^{\circ}, 20^{\circ}\text{C} = 0.9989 \text{ g/cm}^3$). Regardless of the compositions in the initial layers, the density of the system will be essentially invariant with respect to position and time. Equation (6.1) then simplifies to

$$(\partial v / \partial z) = 0 \quad . \quad (6.5)$$

Integration of Equation (6.5) and application of the physically imposed boundary condition that the velocity vanish at the wall yields the trivial solution for the barycentric velocity

$$v \equiv 0 \quad . \quad (6.6)$$

Large concentration fluctuations characterize the liquid-liquid critical region. For systems in which the components have very dissimilar densities, density fluctuations result. The gravitational field will produce

density gradients in such a system (Mistura [1971]). Gravitationally induced density gradients have been measured for a few systems very near the CST where the sedimentation (pressure diffusion) coefficient diverges (Giglio and Vendramini [1975] and Greer et al. [1975]). As Morrison and Knobler [1976] indicate, the presence of a gravitational field poses no problems for this system because of the nearly equal pure component densities.

As was done in Chapter 2, Equations (6.2) and (6.3) can be transformed into equations involving molal parameters and mole fractions. This transformation with the use of Equation (6.6) yields analogous equations for both composition and temperature:

$$-D^{-1}(\partial x_1/\partial t) + (\partial^2 x_1/\partial z^2) + \{\partial[\ln(D/\tilde{V}\tilde{M})]/\partial z\}(\partial x_1/\partial z) = 0 \quad (6.7)$$

and

$$\begin{aligned} -\tilde{C}_p/\tilde{V}\kappa(\partial T/\partial t) + (\partial^2 T/\partial z^2) + (\partial \ln \kappa/\partial z)(\partial T/\partial z) \\ = \kappa^{-1}\{\partial[M_2 D \tilde{Q}_1^*(\partial x_1/\partial z)/\tilde{V}\tilde{M}]/\partial z\} \\ + D\kappa^{-1}\tilde{V}^{-1}(\partial^2 \tilde{H}^E/\partial x_1^2)(\partial x_1/\partial z)^2 . \end{aligned} \quad (6.8)$$

The initial and boundary conditions are the same as before

(cf. Chapter 2),

$$x_1(0.5 \leq z/a \leq 1, 0) = x_1^u; \quad x_1(0 \leq z/a \leq 0.5, 0) = x_1^L$$

$$T(z, 0) = \text{constant} \quad (6.9)$$

and

$$(\partial x_1 / \partial z)_{z/a=0, t} = 0 = (\partial x_1 / \partial z)_{z/a=1, t} \quad (6.10)$$

$$(\partial T / \partial z)_{z/a=0, t} = 0 = (\partial T / \partial z)_{z/a=1, t}$$

The solutions of Equations (6.7) and (6.8) subject to Equations (6.9) and (6.10) for a known set of parameters can now be numerically obtained using the previously described program based on the Crank-Nicholson finite difference scheme.

B. Experimental

1. Cell Considerations - Measurements of the diffusion thermoeffect near the consolute temperature cannot be performed in the "liquid gate" withdrawal cell described in Chapter 4 because there appears to be no liquid which is both (1) immiscible with both components and (2) of intermediate density. However, liquid phase

behavior in the critical demixing region allows design of a much simpler cell.

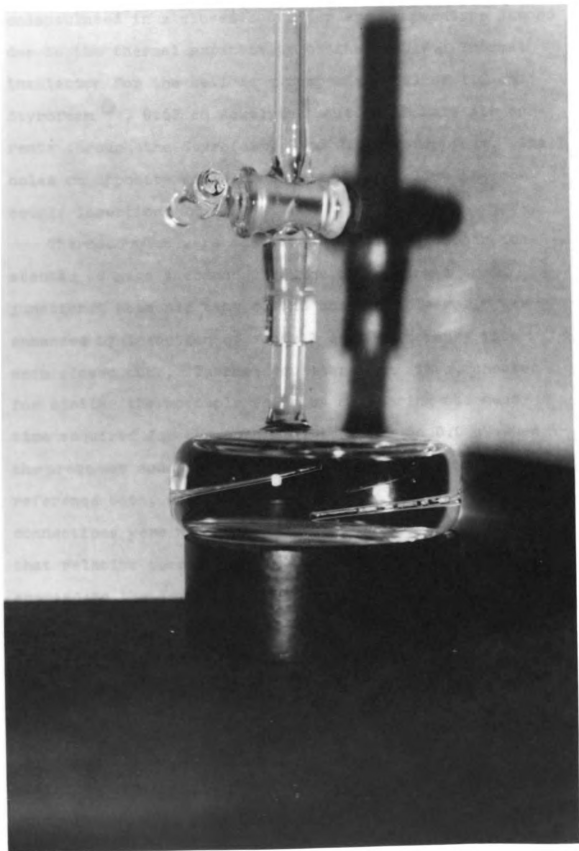
The "liquid gate" withdrawal cell used a third component to create the sharp diffusional interface. Systems that exhibit partial miscibility regions near room temperature are usually dissimilar enough that finding a third mutually insoluble component is virtually impossible. Even could such a liquid be found, it is undesirable to introduce a third component because of the large effect minute concentrations of impurities have on the absolute consolute temperature. The consolute temperature for IBW is known to be particularly sensitive to ionic impurities (Gammell and Angell [1974] and Greer [1976]) which tend to lower the CST dramatically. Although small amounts of impurities may affect the absolute T_c by several degrees, critical exponents and temperature dependencies of properties relative to the measured CST are not influenced by the presence of impurities (Sengers [1975], Hocken and Moldover [1976], Bak and Goldberg [1969], and Fisher and Seesney [1970]).

Instead of a mechanical (or fluid) technique to create the initially sharp interface, the natural, stationary, and unperturbed interface present in a binary mixture for $T < T_c$ can be utilized. With the binary mixture thermostatted at $T < T_c$, two phases characterized by $\mu_1' = \mu_1''$ are in equilibrium. If the temperature of the entire

diphasic fluid slab is suddenly jumped via microwave absorption such that $T > T_c$, then $\mu_1' \neq \mu_1''$ and diffusion accompanied by the diffusion thermoeffect must begin. Very gradual relaxation of T back toward T_c allows measurement of the difference in temperature ΔT , caused by the diffusion thermoeffect, between symmetrically placed thermocouples as a function of ϵ . Thermostatting of the mixture at $T < T_c$ allows reuse of the same mixture in subsequent runs (time must be allowed for phase equilibrium to occur).

The cell designed to perform the above experiment is shown in Figure 6.1. This cell, constructed of 2.0 mm thick glass, has an inside height of 1.2 cm and an inside diameter of 4.8 cm. The relatively large ratio of diameter to height minimizes wall effects. As shown in Figure 6.1, two tiny thin-walled glass, closed, conical tubes project into the radial center off the cell from opposite walls. These tubes, which serve as thermocouple wells, extend from the wall attachment site at half-height $[(z/a)=0.5]$ to positions $(z/a) = 0.80$ and $(z/a) = 0.20$ equidistant from the cell half-height (interface formation was at half-height). The average inside tube diameter is 0.4 mm. A small stopcock atop the cell prevents vapor loss (hence concentration changes) throughout the experiment but still allows pressure equilibration during the temperature jump. Large pressures result when liquid systems

Figure 6.1. Temperature jump cell for diffusion thermo-effect experiments in the critical region.



encapsulated in a closed container are temperature jumped due to the thermal expansivity of the liquid. Thermal insulation for the cell is a composite wall of 1.3 cm Styrofoam[®], 0.67 cm Acrolyte[®] (to eliminate air currents through the Styrofoam), and 2.0 cm Styrofoam. Small holes on opposite sides of this assembly allow thermocouple insertion.

Thermocouples were made from calibrated copper-constantan 40 gage thermocouple wire by welding a small junction. Response time of the thermocouple wells was enhanced by insertion of a small drop of mercury into each closed tube. Thermal equilibration times, checked for similar thermocouple wells by monitoring the mean time required for the potential to relax to 0.0 μV when the probe was suddenly introduced into the thermocouple reference bath, were about 2.5 seconds. Thermocouple connections were made to the potentiometer facility such that relative temperatures (the upper thermocouple referenced to the lower) could be directly measured in addition to absolute temperatures. This allowed relative temperatures or temperature differences to be measured to $\pm 0.1 \mu\text{V}$ (ca. 0.002°C).

2. Critical Temperature Measurements - Each experimental determination of the critical exponent for the heat of transport also involved measurement of the critical

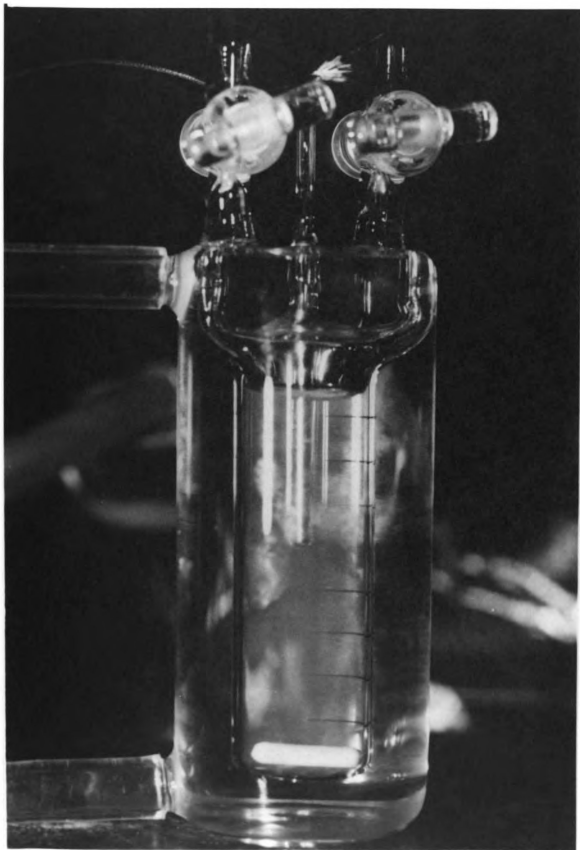
solution temperature. As previously mentioned, consolute temperatures vary significantly with small impurity concentrations. In order to obtain Q_1^* as a function of $T-T_c$, the CST determination was made on a portion of the same mixture immediately before and after the T-jump experiment. The literature value for the critical composition ($x_{1c} = 0.111 - 0.114$) was used without further verification.

The cell shown in Figure 6.2, constructed of 1.5 mm glass, was used for CST measurements. After filling with the homogeneous critical fluid ($x_1 = x_{1c}$, $T > T_c$), the cell was sealed against vapor loss with the small glass stopcocks shown. The consolute temperature drifted less than 0.03°C during a period of over a week, indicating essentially no change in concentration from vapor loss.

The outer water jacket depicted in Figure 6.2 controlled cell temperatures with circulating water from a Neslab Tamson T-9 (10 L capacity) constant temperature bath. Cooling water to the T-9 bath was from a Lab-Line Tempmobile (90 L capacity) while current to the heating element in the T-9 was maintained by a model 2156 Versa-Therm Proportional Electronic Temperature Controller.

Determination of T_c was visual. The onsets of both phase separation and phase disappearance were ascertained by careful temperature adjustment. Phase separation

Figure 6.2. Critical solution temperature cell.



temperatures agreed with phase disappearance temperatures to within 0.010°C . The visual technique of determining T_c is illustrated in Figure 5.4. Photographs (d) and (e) show that with T slightly above T_c , critical opalescence deepens from a light white fog to a dense white cloud. The onset (or disappearance) of a turbid cloud in the stirred opalescent mixture marks the phase separation (or disappearance) point. Figure 5.4 (e) depicts the turbid dense cloud observed for temperatures just below T_c . Transition between states depicted by photographs (d) and (e) is rapid with respect to temperature change, allowing determination of T_c to about $\pm 0.005^{\circ}\text{C}$. Maintenance of constant temperature without stirring for several minutes to observe meniscus formation was periodically used as a check on the stirred visual technique of CST determination. Figure 5.4 (f) illustrates meniscus formation for $T < T_c$. All temperatures were measured with copper-constantan thermocouples similar to those used in the diffusion thermoeffect cell as described in the preceding section. The thermocouple well visible in Figure 6.2 was a small mercury-filled glass capillary tube into which the welded junction was inserted. The length of this well positioned the welded thermocouple junction at cell half height.

3. Experimental Procedure - Fisher Certified Reagent Grade isobutyric acid was used without further purification. However, Karl Fischer analysis of water content in the isobutyric acid yielded 0.070 wt. % water. This was accounted for in preparing the mixtures at the critical composition. Distilled, deionized water was used for the second component.

Mixtures were prepared by additive weighing of pure components in separate two-armed 50 mL bottles equipped with stopcocks on each arm to prevent vapor loss. Excess vapor space was minimized, and no vapor loss with time could be noticed gravimetrically. The two pure component weighing bottles were then connected with a short piece of tygon tubing and thermostatted above T_c . Subsequent transfer of the pure components (through the connected sidearms) back and forth between the two weighing bottles served to mix the components while maintaining a sealed environment. With the mixture prepared and located entirely in one of the two bottles, the side arm stopcock was closed and the second bottle was removed.

Transfer of the homogeneous mixture through the top arm of the filling bottle fitted with a short piece of narrow tygon tubing, into the T-jump cell of Figure 6.1, was completed quickly with $T \gtrsim T_c$. To exclude any vapor space, the cell was filled above the stopcock region and the stopcock was then closed. The cell of Figure 6.2

used for CST determinations was immediately thereafter filled in an analogous manner except that a small vapor space was left. All glassware was thoroughly washed, rinsed in deionized water, oven dried for several hours, and filled immediately upon cooling before each use to eliminate adsorbed water and ionic impurities. Phase equilibrium was established with the cell sitting unperturbed. Occasionally it was necessary to rotate the cell carefully to dislodge "droplets" of discontinuous phase from cell walls. A few days were assumed sufficient for equilibrium to be established.

Actual experimental runs were made in the following manner.

- (1) Filling and stirring of the ice point thermocouple reference bath with distilled water and finely ground ice.

- (2) Observation of the initial temperatures of both thermocouples and any difference in reading between them.

- (3) Removal of the thermocouples (microwaves were absorbed by the coatings and insulation on the wires).

- (4) Simultaneous activation of the Litton industrial microwave oven and the digital, 0.1 second readout timer.

- (5) Disengagement of the microwave temperature jump after a 1.0 to 2.2 second heating pulse.

- (6) Careful insertion of thermocouple leads into appropriate wells. Temperature readings as a function of

time were begun.

(7) Acquisition of temperature data. Temperature difference readings were obtained at 20 to 40 second intervals and absolute readings were taken about every 100 seconds. Absolute readings of the two thermocouples were taken within about 10 seconds of each other.

(8) Reestablishment of phase equilibrium after the temperature had relaxed below T_c . The cell was set aside for future runs.

(9) Measurement of T_c in the critical solution temperature cell. This was done both immediately before and immediately after each run. Values obtained for phase separation and phase disappearance were averaged.

4. Data Analysis - Any one run consisted of absolute temperatures at each thermocouple as a function of time, temperature differences between the thermocouples as a function of time, the consolute temperature T_c , and the initial temperature of the cell. The required data to fit $\tilde{Q}_1^* = A\epsilon^{\lambda_4}$ are ΔT vs. $(T_{\text{cell}} - T_c)$ and the initial phase compositions. Data reduction thus involved:

(1) Fit of absolute cell temperatures to a polynomial in time. Program "MULTREG" (Anderson [1968]) yielded a cubic equation for each thermocouple. These were averaged to give the instantaneous interfacial temperature. From the measured T_c , $(T_{\text{cell}} - T_c)$ was

available at any time.

(2) Determination of the upper and lower phase concentrations x_1^u and x_1^L , respectively. The concentrations were calculated from knowledge of the initial temperature. Figure 6.3 shows the coexistence curve (temperature-composition relation) for IBW determined by Woermann and Sarholz [1965]. A more accurate method of obtaining phase concentrations for a given temperature uses the known critical exponent β for the order parameter; i.e., $x_1' - x_1'' = C(T_c - T)^{1/3}$. A plot of $(T_c - T)^{1/3}$ vs. x_1 containing the data of Woermann and Sarholz [1965] and Chu et al. [1968] is shown in Figure 6.4. A least squares fit of the data yielded

$$x_1' = x_{1c} + (T_c - T)^{1/3} / 14.518 \quad (6.11)$$

$$x_1'' = x_{1c} - (T_c - T)^{1/3} / 25.680$$

for the isobutyric acid rich (upper) layer and the water rich (lower) layer, respectively. These equations are the solid lines in Figure 6.4. Initial phase compositions were thereby readily calculable from the initial temperature.

(3) Provision of ΔT vs. $(T_{\text{cell}} - T_c)$ data from directly determined ΔT vs. time data and from fit $(T_{\text{cell}} - T_c)$ vs. time data. From these, coupled with the initial phase

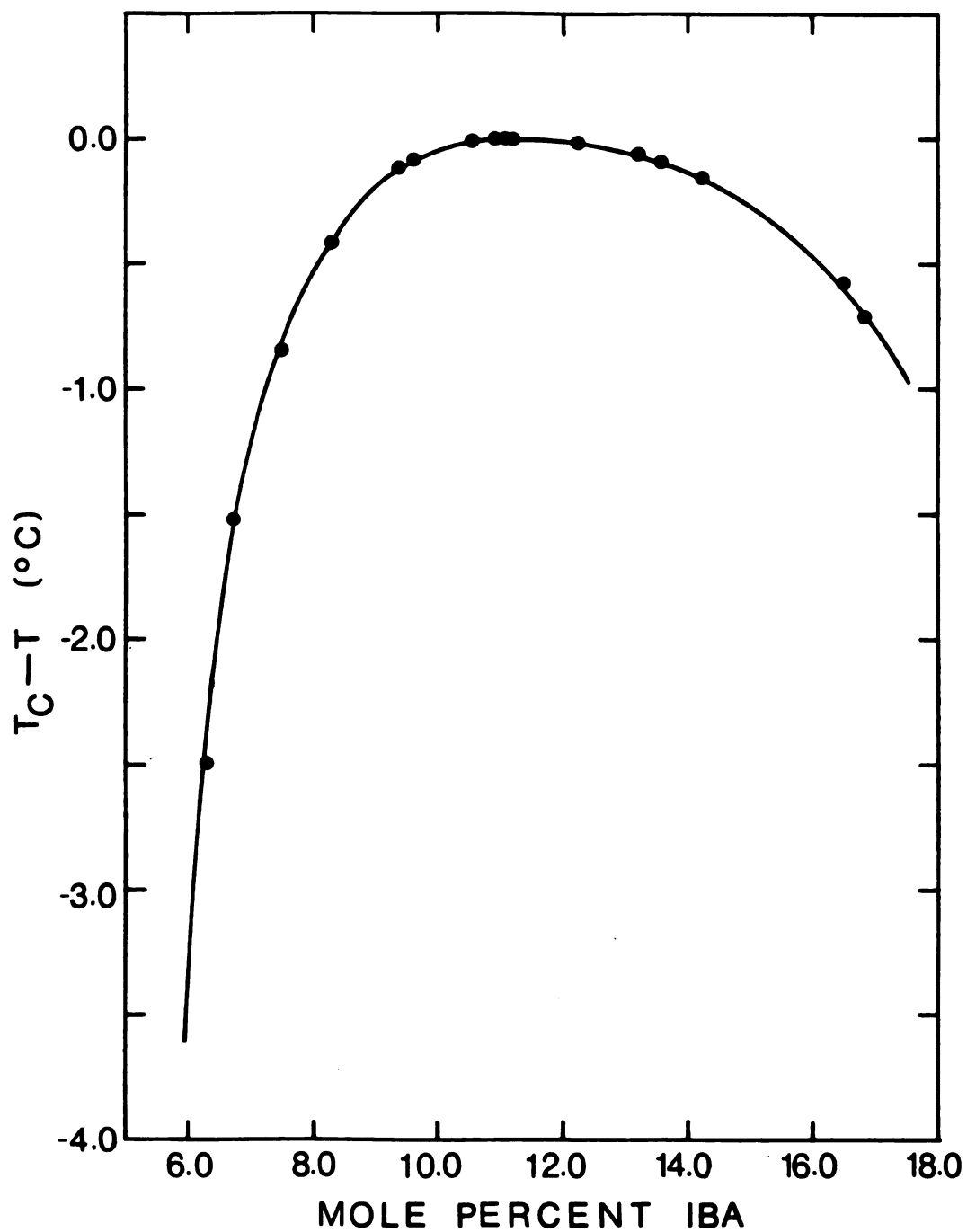


Figure 6.3. Coexistence curve for IBW as determined by Woermann and Sarholz [1965].

Figure 6.4. The function $(T_c - T)^{1/3}$ vs. mole fraction of isobutyric acid. \square , data of Woermann and Sarholz [1965]; \bullet , data of Chu et al. [1968]; —, least squares fit.

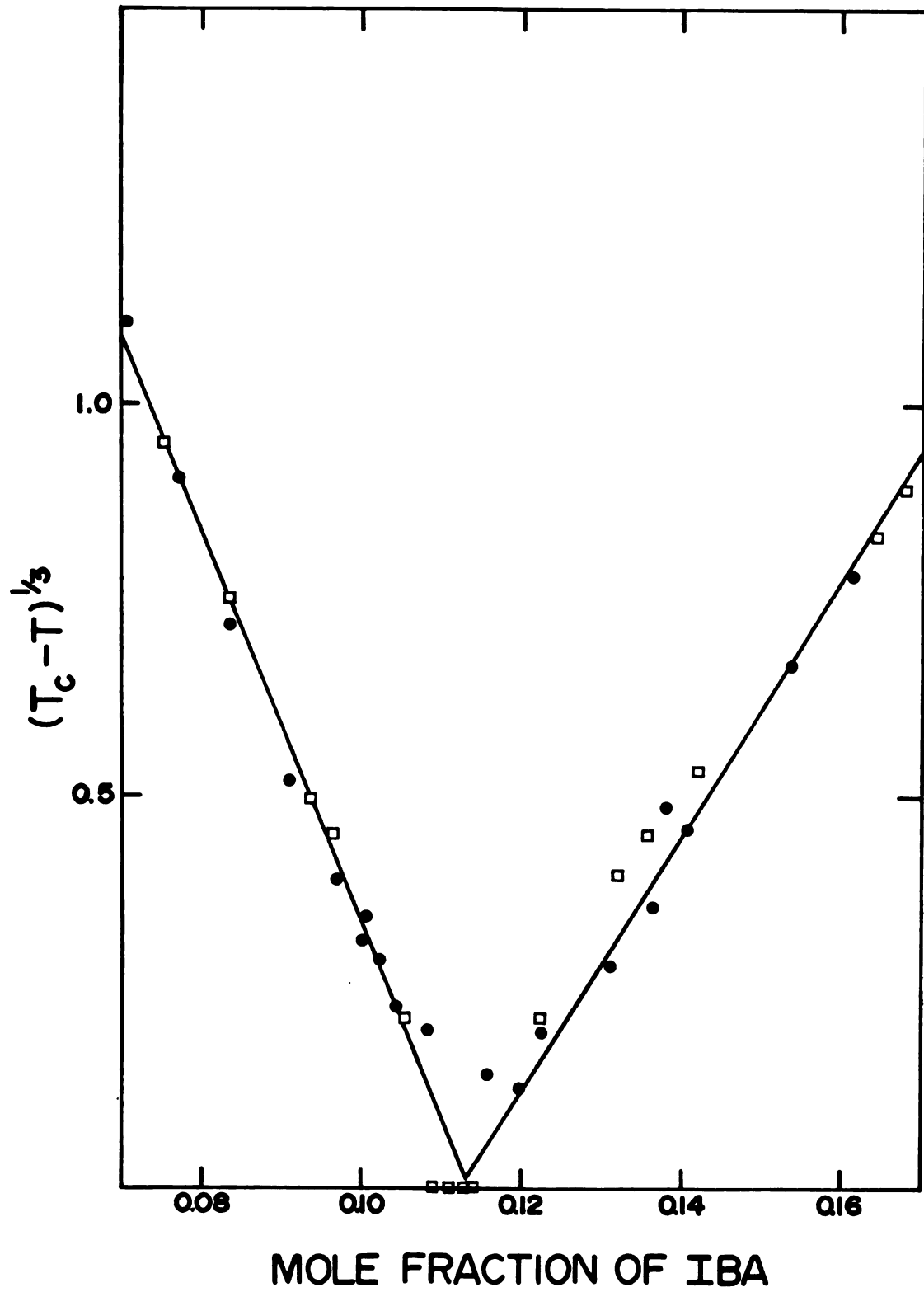


Figure 6.4

compositions, $\tilde{Q}_1^* = A\epsilon^{\lambda_4}$ was numerically fit by weighted, nonlinear least squares regression of ΔT as calculated from Equations (6.7) - (6.10). As before, program "KINFIT4" was used ("KINFIT4" is the 1977 version of the original "KINFIT" published by Dye and Nicely [1971]) intermeshed with the numerical integration routine.

C. The Temperature Jump Technique

The advantages of the temperature jump technique are apparent:

(1) The natural, stable interface between the two coexisting phases is undisturbed by the shearing action associated with mechanical formation techniques. Impurities are not introduced as they would be with a liquid extraction technique.

(2) There are no moving parts susceptible to leakage and vapor loss.

(3) There is no ambiguity in mixture preparation. Half-cell techniques require two phases of different composition which, when completely mixed, are at the critical composition. Use of the T-jump cell allows filling of the cell at the critical composition. For temperatures moderately below T_c , the difference in composition between the coexisting phases Δx_1 is not large, and a distinct interface with no preferential wetting of the walls (no

curvature in the meniscus) is formed.

(4) No special thermostating is required to maintain separate phases at a prescribed temperature ($T > T_c$) during interface formation.

It is desirable to make the temperature jumps as short-lived as possible. Temperature jumps of long duration obscure the initial time t_0 . As an example, consider a very long duration heating input, say by conduction. Even before the cell temperature reaches T_c , the concentrations of the two phases begin to change via diffusion. Although the two phases are not yet completely miscible, they are no longer at their equilibrium concentrations and some diffusion will occur. Such behavior cannot be described by the previous equations. This problem was avoided by use of a commercial Litton Industries microwave oven which supplied a short duration, moderate intensity heating pulse. Moreover, the pulse supplied uniform bulk heating rather than surface conduction heating. Heating constants for the previously described T-jump cell filled with the critical mixture were about $7^\circ\text{C}/\text{S}$. Total heating time was between 1.5 and 2.2 seconds. Despite bulk heating by the microwave oven, some nonuniformities are to be expected because of geometrical asymmetries with respect to the microwave source within the oven. Shortly after heating, it was found that the upper thermocouple often read 0.6°C higher than the lower thermocouple.

Although these temperature nonuniformities are not predictable, the time behavior of the cell temperature distribution after they have been measured is calculable using the diffusion thermoeffect program developed in Chapter 3. Fortunately, temperature nonuniformities relax via thermal conduction to the correct Dufour-effect-caused ΔT within 500 to 800 seconds. This is because the temperature gradients diminish by conduction until conduction just balances the heat transported by diffusion. Figure 6.5 illustrates this behavior for various initial temperature nonuniformities. All curves in Figure 6.5 were obtained by computer simulation for nonuniformities symmetric about $(z/a) = 0.5$. Although all curves refer to a mean cell temperature 4°C above the critical point, each individual curve corresponds to a different initial temperature nonuniformity. Curve "a" corresponds to the normal ΔT induced by the diffusion thermoeffect from initially isothermal conditions. Curves "b" and "c" correspond to the ΔT induced when initially the top (b) or bottom (c) 5% of the fluid is 2°C warmer than the bulk liquid while the bottom (b) or top (c) 5% is 2°C colder. This might physically correspond to a surface effect in the temperature jump. Curve "d" directly corresponds to two different initial temperature nonuniformities: (1) the initial temperature distribution in the cell varies continuously and linearly from the upper surface to the

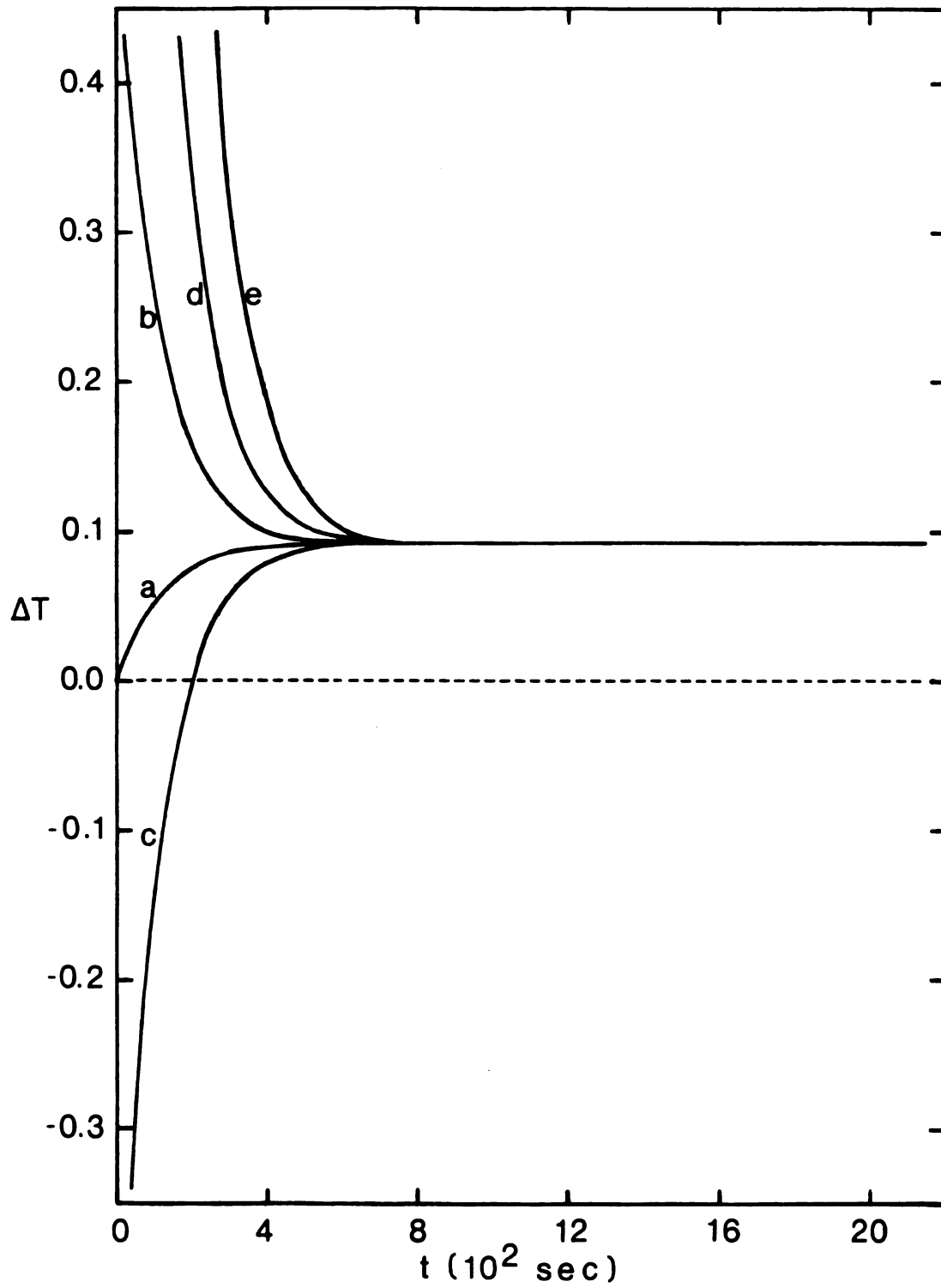


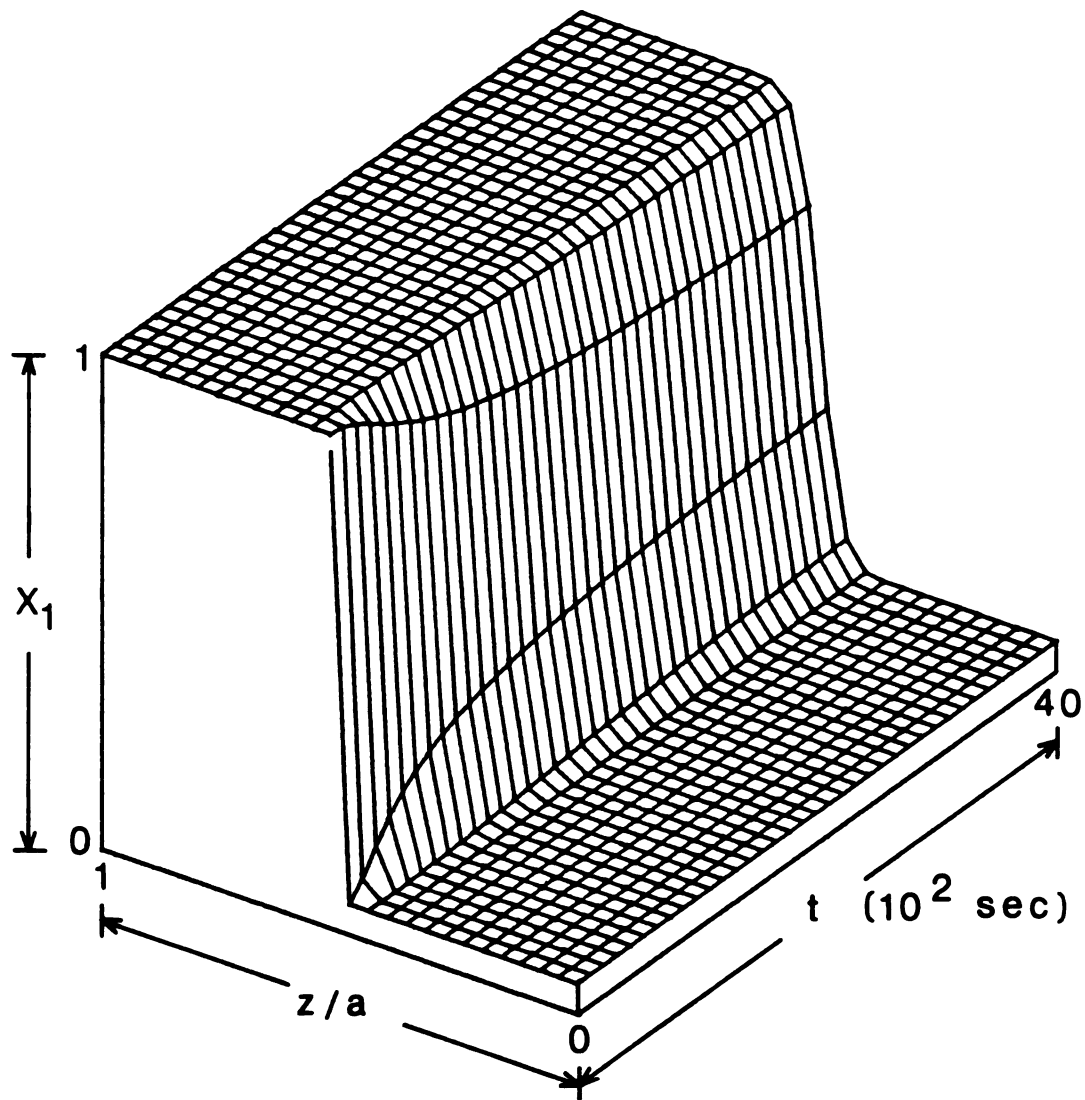
Figure 6.5. Predicted decay of initial temperature nonuniformities in a temperature jump diffusion thermoeffect experiment.

4°C colder lower surface, and (2) the entire upper phase is initially 2°C warmer than the entire lower phase. This latter nonuniformity might occur for preferential absorption of microwaves by one of the components. Curve "e" corresponds to an initial linear and continuous gradient of 8°C from top to bottom. The point of Figure 6.5 is the coalescence of ΔT for all these nonuniform initial temperature conditions into the identical ΔT produced by the diffusion thermoeffect with isothermal initial conditions. This occurs in each case within 500 to 800 seconds. Thus, in spite of moderate initial temperature distributions produced by the T-jump technique, the ΔT measured after 800 seconds is dependent upon only the heat of transport, not the initial conditions. For moderate T-jumps, ΔT values obtained at times longer than 800 seconds can therefore be used without knowledge of the actual T-distribution immediately following the heating pulse. Since relaxation to the mean temperature is quickest near the interface where diffusion occurs, no ambiguities in the composition distribution produced by heating nonuniformities are expected even though D has a significant temperature dependence in this region. No experimental data for times shorter than 1050 seconds were used in the calculation of \tilde{Q}_1^* . To verify further these computer simulations, pure water was T-jumped with the microwave oven. With T-jumps comparable to those

used for IBW, similar initial temperature nonuniformities were noticed shortly after perturbation. However, the measured ΔT vanished completely after about 500 seconds in the case of pure water. Obviously, the ΔT measured for the binary IBW system, persistent throughout our measurement region ($1050 \text{ seconds} \leq t \leq 5000 \text{ seconds}$) depends solely on the diffusion thermoeffect.

The T-jump technique is useful near the CST basically because the diffusion coefficient diminishes in this region while the thermal conductivity coefficient remains finite. This changes the diffusion thermoeffect from a transient phenomenon (Figure 4.4) to essentially a steady state phenomenon for times on the order of these experiments.

To see how this happens, compare the composition surfaces shown in Figures 6.6 and 3.5. Note that Figure 6.6 shows that the gradient of composition, the main driving force for the diffusional process, remains almost constant throughout the experiment except for an initial blurring of the sharp step function at the interface. The mass flux $j_1 = -\rho D(\partial w_1/\partial z)$ therefore remains practically constant in time for a given temperature. Heat conduction down the produced temperature gradient opposes the heat carried by the mass flux and will reach a point where it counter balances production of the gradient by the heat of transport. The transient phenomenon observed



COMPOSITION SURFACE AS T APPROACHES TCRIT

Figure 6.6. Predicted composition surface for IBW in a temperature jump diffusion thermoeffect experiment 4°C above T_c .

away from the CST is due to the constantly diminishing mass flux.

To quantify this point, the equation

$$q_{\text{net}} = q_{\text{HT}} - q_{\text{cond}} = j_1 \bar{Q}_1^* - \kappa \Delta T \quad (6.12)$$

(analogous to Equation 2.20) where q_{HT} is the heat flux due to the heat of transport and q_{cond} is that due to thermal conduction, shows that in the steady state $q_{\text{net}} = 0$ and $j_1 \bar{Q}_1^* / \kappa = \Delta T$. Because in the critical region at any given temperature $j_1 \bar{Q}_1^* / \kappa$ changes only very slowly, ΔT remains essentially constant.

In terms of the actual experiment, the effect of this steady state is that perturbations from the ΔT produced by the diffusion thermoeffect, will relax back to the correct value. The establishment of the steady state is rapid since thermal conduction remains large and finite in the critical region while diffusion diminishes.

Because near the critical point a steady state is established between thermal conduction and the heat of transport term, the cell temperature may be allowed to relax gradually toward T_c . The assumption is that the steady state is established more quickly than the finite drop in cell temperature. That is, the measured ΔT at any instant is the appropriate steady state ΔT produced

by \tilde{Q}_1^* based on the instantaneous cell temperature; i.e., $\tilde{Q}_1^* = A[(T_{\text{cell}} - T_c)/T_c]^{\lambda_4}$. This implies that measured ΔT values are essentially uncorrelated. They depend only on the composition profile and the immediate deviation of the cell temperature from the critical temperature and not directly on any past history of ΔT or T_{cell} . The measured ΔT as T_{cell} changes is always the appropriate ΔT relative to the instantaneous cell temperature because in the critical region the thermal conductivity is always much larger than the diffusion coefficient thereby rapidly establishing the steady state for slow changes in absolute cell temperature.

Verification of this assumption was checked numerically by comparing simulated ΔT 's for two kinds of systems. In system 1 T_{cell} decreases to T_c at a rate of about 10^{-3} °C/s (comparable to the experimental situation). System 2, following the T-jump, remains at a fixed mean temperature.¹ A comparison of the induced ΔT in system 1, when the decreasing cell temperature corresponded to that of system 2, to the induced ΔT in system 2 was made after correcting for small composition differences due to the temperature dependent diffusion coefficient. The results of this comparison are shown in Figure 6.7. In each case, the ΔT expected in system 1 as $T_{\text{cell}} \rightarrow T_c$

¹For these simulations, Q_1^* values from Table 6.3 were used.

Figure 6.7. Computer verification of steady state maintenance for diffusion thermo-effect as $T_{\text{cell}} \rightarrow T_c$. —, predicted ΔT in system 1; ----, ΔT in iso-thermal systems 2; ■, predicted ΔT in system 1 when T_{cell} is identical to that of system 2.

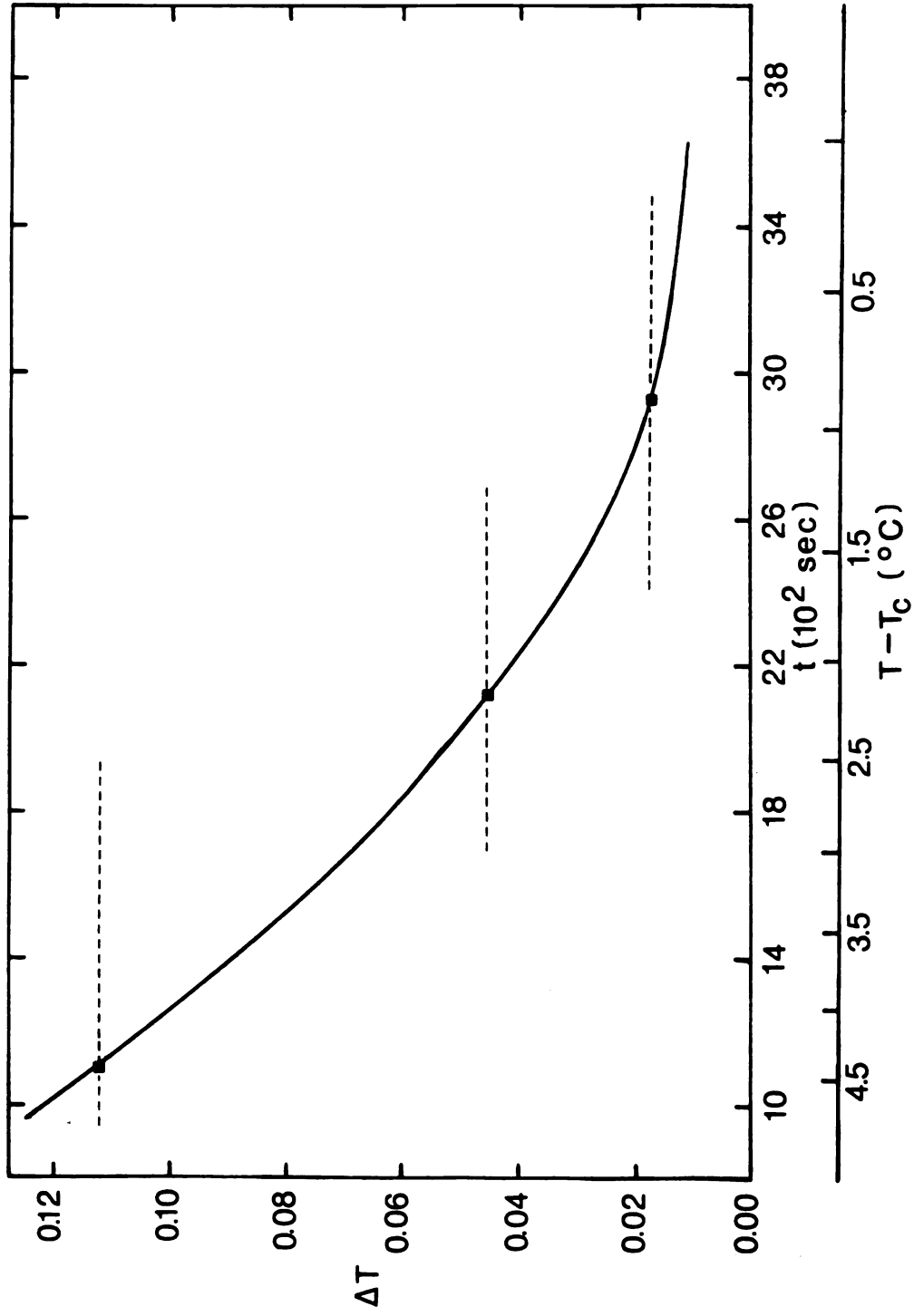


Figure 6.7

is identical to that predicted for system 2 when compared at the same mean cell temperature. In Figure 6.7, the dashed lines represent steady state ΔT values for systems 2, the solid line represents system 1 ΔT values, and the black squares are system 1 ΔT values at each of the system 2 cell temperatures. Note that when T_{cell} of system 1 reaches T_{cell} of each system 2 as indicated by the black squares, the expected ΔT values are indeed identical.

Experimental evidence that measured ΔT values are the appropriate steady state values at the instantaneous temperature was obtained by performing a similar T-jump experiment on a pure component - water. After the T-jump, no difference in temperature was measured between symmetric thermocouples ($\Delta T = 0$) throughout the time region of the measurements ($500 \text{ seconds} \leq t \leq 5000 \text{ seconds}$) during which the cell temperature dropped 4°C . No effects on the measured ΔT were due to the small heat losses through the walls required to allow the decrease in T_{cell} . Measured ΔT values for mixtures are therefore due entirely to the diffusion thermoeffect.

An obvious advantage of allowing T_{cell} to approach T_c is that each experiment contains the entire ϵ -behavior of \tilde{Q}_1^* from which the CE λ_4 can be obtained. Notice also that ΔT becomes very small as the consolute temperature is approached, allowing measurements very near T_c . How close measurements can be made to T_c is limited by the

cell temperature distribution. No meaning can be attached to any result for which $T < T_c$ in a portion of the cell. However, ΔT decreases as $\epsilon \rightarrow 0$, allowing closer and closer approach to the consolute temperature. A few measurements were obtained within 0.010°C of the consolute temperature.

D. Literature Parameters for IBW

Fitting \tilde{Q}_1^* and its temperature dependence from measured temperature differences requires fitting of the values calculated using the previously described numerical scheme. Literature values of the equilibrium and transport properties of the IBW system were used in this process. Composition dependencies of the parameters were included as polynomial expansions in mole fraction by fitting literature data using "MULTREG" (Anderson [1968]). The temperature dependence was included via critical exponents where known and applicable, and by polynomial fitting for properties with no anomaly in the critical region. Table 6.1 summarizes the actual expressions used for properties discussed below.

(1) Critical properties - The reported values of the critical mole fraction vary from 0.110 to 0.115. (Greer [1976], Woermann and Sarholz [1965], Chu et al. [1968], Allegra et al. [1971], and Friedländer [1901]). Because the consolute temperature is lowered by

Table 6.1. Expressions used for IBM transport and thermodynamic parameters in analysis of diffusion thermoeffect experiments in the critical region.

Property	Computational Relation	Values of Constants	r.m.s. deviation (a)
molecular weight	$\bar{M} = x_1 M_1 + x_2 M_2$	$M_1 = 0.08811 \text{ kg}\cdot\text{mol}^{-1}$ $M_2 = 0.01802 \text{ kg}\cdot\text{mol}^{-1}$	
mole fraction	$x_1 = x_{1c} + (T_c - T)^{1/3} / A$	$A = 14.518^\circ\text{K}^{1/3} \quad (x_1 > x_{1c})$ $A = -25.680^\circ\text{K}^{1/3} \quad (x_1 < x_{1c})$ $x_{1c} = 0.1125$	$\sigma_x = 0.0040$
molar volume	$\bar{V} = \bar{M} / \rho$ $\rho = A - Bw_1 - Cw_1^3 - (D + Ew_1)(T - 298.15)$	$A = 1.0032 \times 10^3 \text{ kg}\cdot\text{m}^{-3}$ $B = 16.48 \text{ kg}\cdot\text{m}^{-3}$ $C = 36.45 \text{ kg}\cdot\text{m}^{-3}$ $D = 0.366 \text{ kg}\cdot\text{m}^{-3}\text{K}^{-1}$ $E = 0.659 \text{ kg}\cdot\text{m}^{-3}\text{K}^{-1}$	$\sigma_\rho = 0.9 \text{ kg}\cdot\text{m}^{-3}$
heat capacity	$\bar{C}_p = \bar{M} [Akn(T - T_c) + B + C(T - T_c)]$	$A = -0.0137 \text{ kJ}\cdot\text{kg}^{-1}\text{K}^{-1}$ $B = 3.559 \text{ kJ}\cdot\text{kg}^{-1}\text{K}^{-1}$ $C = 2.67 \times 10^{-3} \text{ kJ}\cdot\text{kg}^{-1}\text{K}^{-1}$	$\sigma_{C_p} = 0.005 \text{ kJ}\cdot\text{kg}^{-1}\text{K}^{-1}$
diffusivity	$D = D_\epsilon \epsilon^{\lambda_2 + 10^{-9} x}$ $D_x = A + B(x_1 - x_{1c}) + C(x_1 - x_{1c})^2$	$D_\epsilon = 3.86 \times 10^{-10} \text{ m}^2\text{s}^{-1}$ $\lambda_2 = 0.67$ $A = 6.089 \times 10^{-4} \text{ m}^2\text{s}^{-1} \quad (x_1 > x_{1c})$ $A = 2.787 \times 10^{-4} \text{ m}^2\text{s}^{-1} \quad (x_1 < x_{1c})$ $B = 0.0663 \text{ m}^2\text{s}^{-1} \quad (x_1 > x_{1c})$ $B = -0.0163 \text{ m}^2\text{s}^{-1} \quad (x_1 < x_{1c})$ $C = 3.435 \text{ m}^2\text{s}^{-1} \quad (x_1 > x_{1c})$ $C = -0.925 \text{ m}^2\text{s}^{-1} \quad (x_1 < x_{1c})$ $D_x = 0 \text{ for } x_1 = x_{1c}$	$\sigma_{D_\epsilon} = 1.58 \times 10^{-11} \text{ m}^2\text{s}^{-1}$
thermal conductivity	$\kappa = \kappa_1^0 w_1 + \kappa_2^0 w_2 - C \kappa_2^0 - \kappa_1^0 (1 - \sqrt{w_2}) w_2$ $\kappa_1^0 = A_1 + B_1 (T - 298.15)$ $\kappa_2^0 = A_2 + B_2 (T - 298.15) + E_2 (T - 298.15)^2$	$C = 1.0$ $A_1 = 0.1421 \text{ W}\cdot\text{m}^{-1}\text{K}^{-1}$ $A_2 = 0.6078 \text{ W}\cdot\text{m}^{-1}\text{K}^{-1}$ $B_1 = -4.2 \times 10^{-5} \text{ W}\cdot\text{m}^{-1}\text{K}^{-2}$ $B_2 = 1.611 \times 10^{-3} \text{ W}\cdot\text{m}^{-1}\text{K}^{-2}$ $E_2 = -8.235 \times 10^{-6} \text{ W}\cdot\text{m}^{-1}\text{K}^{-3}$	$\sigma_{\kappa_2^0} = 0.0030 \text{ W}\cdot\text{m}^{-1}\text{K}^{-1}$

(a) root mean square deviation of calculated and experimental values.

impurities (especially ionic impurities), values tend to vary somewhat from laboratory to laboratory. Most recent experiments indicate the critical temperature to be between 25.988°C and 26.385°C (Greer [1976], Woermann and Sarholz [1965], Gammell and Angell [1974], and Allegra et al. [1971]). The apparatus previously described allowed measurement of relative temperatures in this laboratory to 0.002°C. Because only relative departures from T_c were needed for analysis, no elaborate calibration was made in an attempt to obtain absolute temperatures. However, the measured T_c appeared to be slightly higher than the best literature values. Only relative temperatures were used in data analysis. The small value of dT_c/dP ($-0.055^\circ\text{K}\cdot\text{atm}^{-1}$ reported by Morrison and Knobler [1976]) indicates that T_c is essentially independent of barometric pressure.

(2) Density and molar volume - Woermann and Sarholz [1965] and Greer [1976] report very accurately measured densities in the critical region as a function of composition and temperature. The best "MULTREG" fit of their data is shown in Table 6.1 for $|T-298.15| \leq 15^\circ\text{K}$. This equation fits the reported values to within 0.1% for all values of w_1 . The polynomial expression for ρ fits well very near T_c because thermal expansivity has such a small CE - Morrison and Knobler [1976] report it as 0.08 - 0.14 with an uncertainty of 0.1. Molar volumes were obtained

from $\tilde{V} = \tilde{M}/\rho$.

(3) Heat capacity - The temperature dependence of the specific heat at the critical composition can be well represented very near the critical point with a logarithmic singularity (Klein and Woermann [1975]). Klein and Woermann found that correction terms to the logarithmic singularity could not be neglected for deviations from T_c larger than 0.5°K . The fit of their data for $0^\circ\text{K} \leq T - T_c \leq 3.5^\circ\text{K}$ is shown in Table 6.1. This logarithmic singularity is in agreement with the very small critical exponents reported by investigators of other systems. For example, Pelger et al. [1977] report $\alpha = 0.55$ [see Equation (5.10) and Table 5.1 for the definition of α], Voronel and Ovodova [1969] and Cope et al. [1972] report $\alpha \approx 0.0$; and Gambhir et al. [1971] and Viswanathan et al. [1973] report $0 \leq \alpha \leq 0.1$. Although the results of Klein and Woermann were obtained only at $x_1 = x_{1c}$, the data of Davies [1935] and, to a lesser extent, those of Kresheck and Benjamin [1964] indicate that \bar{C}_p is relatively composition independent for the relevant range of interest for the experiments reported herein.

(4) Diffusion coefficient - Light scattering measurements of the diffusion coefficient for this system have been performed by Chu and coworkers [1968], [1969], and [1973]. The best "MULTREG" (Anderson [1968]) fit of their data is also given in Table 6.1. Data used in the fit

included the self diffusion coefficient of water for the point $x_1 = 0.0$ in addition to the concentrations reported by Chu et al. The values for D were measured by Chu et al. at only two compositions in addition to the critical composition.

(5) Thermal conductivity - No data exist for the thermal conductivity of IBW mixtures. Fortunately, the critical exponent of κ is well defined at the critical composition. As shown in Chapter 5, $\lambda_1 = 0$ and the thermal conductivity shows no anomaly; i.e., κ exhibits the same temperature behavior near the consolute temperature as it does further away from the CST. Consequently, the NEL equation (Jamieson [1975] and Chapter 4 of this thesis) was used for the composition dependence. The temperature dependence was included via the temperature dependencies of the pure component thermal conductivities. A linear interpolation of data reviewed by Jamieson [1975] defined the temperature dependence of κ_1^0 . The temperature behavior of κ_2^0 was obtained from a "MULTREG" fit of the data reviewed by McLaughlin [1964]. The NEL equation shown in Equation (4.2) was used with Jamieson's recommended value of $C = 1.0$ for the adjustable parameter C.

(6) Excess enthalpy - As discussed in Chapter 4, the heat of mixing effect is symmetric about the interface even for very nonideal mixtures. The excess enthalpy is therefore not required for determinations of \tilde{Q}_1^* based on

ΔT data taken at symmetric positions with respect to the interface. No data have been reported for \tilde{H}^E in the IBW critical region although Daoust and Lajoie [1976] have reported some heats of dilution.

(7) Heats of transport - The experimental results presented here are the first determinations of the critical exponent for the heat of transport in liquid mixtures in the critical region.

From the preceding discussion, it is apparent that the composition dependence of most of the parameters is not well known. Actual values of \tilde{Q}_1^* calculated from measured ΔT data would reflect this uncertainty and would certainly be no more accurate than the total uncertainty of the properties used. However, in determining the critical exponent of \tilde{Q}_1^* , composition changes very little in time. This is illustrated well by Figure 6.6. Therefore, the composition contribution to the value of any property remains the same when the consolute temperature is approached. That is to say, all of the compositional dependencies and uncertainties in the input properties contribute a constant amount to \tilde{Q}_1^* regardless of ϵ and are thus grouped together into the pre- ϵ factor A in the expression $\tilde{Q}_1^* = A\epsilon^{\lambda_4}$. Since the temperature dependence of all the input properties was well known, the critical exponent λ_4 can be calculated with good certainty. A fit of experimental data yields the true value of the CE

of the heat of transport λ_4 . The pre- ϵ factor A, however, will be an effective value for each run.

E. Experimental Results

Best estimates for $\tilde{Q}_1^* = A\epsilon^{\lambda_4}$ were obtained from the experimental ΔT data using nonlinear least squares and Gauss-Markov regression. The values of various properties used in the calculations are listed in Table 6.1. Table 6.2 contains the initial conditions for the seven runs that were performed on two independently prepared mixtures. Further experimental conditions are available from Table C.1 of Appendix C. The overall mole fraction of isobutyric acid at which the mixtures were prepared is denoted by $\langle x_1 \rangle$ in Table 6.2. $T_1 - T_c$ represents the initial temperature from which initial phase compositions x_1^u and x_1^l were calculated using Equations (6.11). The initial difference in composition between the upper and lower phases is given in the column labeled Δx_1 . $T_{\max} - T_i$ represents the temperature jump range.

The results obtained for the critical exponent λ_4 are shown in Table 6.3. Also listed in this table are values obtained for the pre- ϵ factor A. Negative values for \tilde{Q}_1^* indicate that the temperature of the phase rich in isobutyric acid increases while it decreases in the water rich phase. As mentioned above, the composition

Table 6.2. Experimental conditions for the diffusion thermoeffect experiments performed on IBW in the critical region.

Run	$\langle x_1 \rangle$	$-(T_1 - T_c)/^\circ K$	$(T_{\max} - T_c)/^\circ K$	x_1^u	x_1^L	Δx_1
I	0.1125	6.402	8.036	0.2404	0.0402	0.2002
II	0.1125	5.618	6.362	0.2349	0.0433	0.1916
III	0.1125	6.804	6.511	0.2430	0.0387	0.2043
IV	0.1125	6.607	7.013	0.2417	0.0394	0.2023
V	0.1130	5.720	11.384	0.2362	0.0434	0.1928
VI	0.1130	5.394	9.414	0.2338	0.0447	0.1891
VII	0.1130	5.687	4.291	0.2359	0.0435	0.1924

Table 6.3. Results of diffusion thermoeffect experiments in the IBW critical region.

Run	$\langle x_1 \rangle$	$-A/10^4 \text{kJ} \cdot \text{mol}^{-1}$	$\sigma_A/10^4 \text{kJ} \cdot \text{mol}^{-1}(\text{a})$	λ_4	σ_λ (a)
I	0.1125	1.2	0.1	0.72	0.02
II	0.1125	1.1	0.1	0.65	0.02
III	0.1125	0.5	0.1	0.56	0.03
IV	0.1125	0.6	0.1	0.55	0.02
V	0.1130	0.8	0.2	0.73	0.04
VI	0.1130	0.4	0.1	0.56	0.02
VII	0.1130	2.8	0.3	0.80	0.02
				MEAN:	0.65
					0.04 (b)

(a) Standard deviation as calculated by the least squares fitting program.

(b) Standard deviation of the mean.

dependence of the necessary input properties are not well known. This is because investigators of critical systems have been primarily interested in critical exponents at constant (critical) composition. Because the composition distribution remains essentially unchanged during the experimental time period (cf. Figure 6.6), the compositional contribution of all the properties in cell regions where $x_1 \neq x_{1c}$ also remains unchanged as $T \rightarrow T_c$. Therefore, the critical exponent λ_4 can be determined quite well, but the absolute value of \dot{Q}_1^* at a given temperature cannot be determined with any degree of certainty. The value of the pre- ε factor A contains the various compositional contributions of all the input properties and is therefore an effective value dependent upon the individual run conditions. Like that of previous workers, the goal of this dissertation has been the determination of a critical exponent - the CE for the heat of transport in this case. The lack of information about the composition dependence of properties in this region has not been detrimental to the fulfillment of this goal. Nevertheless, new measurements at various compositions are certainly in order for the input properties of Table 6.1. Once such measurements have been made, it is expected that the large uncertainties in A shown in Table 6.3 will be diminished and absolute values of the heat of transport will then be calculable.

Standard deviations for individual runs are listed in Table 6.3 as they were calculated by the least squares fitting program "KINFIT4". The mean critical exponent is shown at the bottom of this table with its calculated standard deviation. The most important result in Table 6.3 is $\lambda_4 = 0.65$ or $\lambda_4 \approx 2/3$, which indicates that \tilde{Q}_1^* vanishes as the critical point is approached.

Figures 6.8 - 6.14 show the fit data for each run. As this is a two parameter regression, one parameter (A) essentially determines the magnitude of ΔT while the other parameter (λ_4) determines the shape of the curve. Although all the ΔT data used are tabulated in Tables C.2 - C.7 of Appendix C, Figures 6.8 - 6.14 are included here to illustrate the shape of each curve. As mentioned, this is important since λ_4 principally determines the shape. A comparison of these seven figures readily indicates the validity of the simple power law $\tilde{Q}_1^* = A\epsilon^{\lambda_4}$ over the temperature regions depicted therein. Notice, however, that the first six runs (Figures 6.8 - 6.13) show points which begin to deviate from the simple power law at temperatures 4°C to 5°C above T_c . This is in agreement with the results of Chu et al [1973] depicted for the diffusion coefficient in Figure 5.5. No points for $T - T_c > 5.0^\circ\text{C}$ were included in the data analysis. Inclusion of data outside this range would yield an effective critical exponent rather than the true value corresponding to the definition of Equation 5.3.

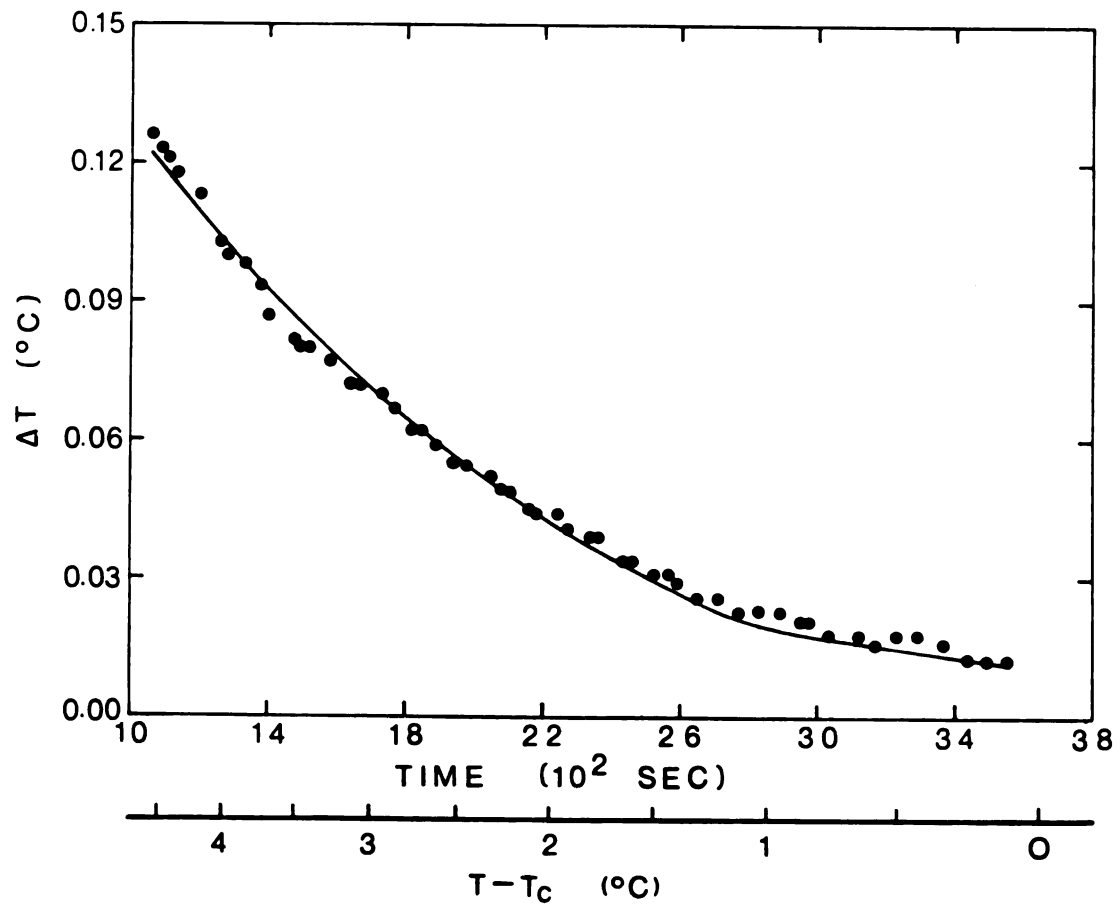


Figure 6.8. Run I. Experimental results for $\tilde{Q}_1^* = A\epsilon^{\lambda_4}$ with A and λ_4 as adjustable parameters.

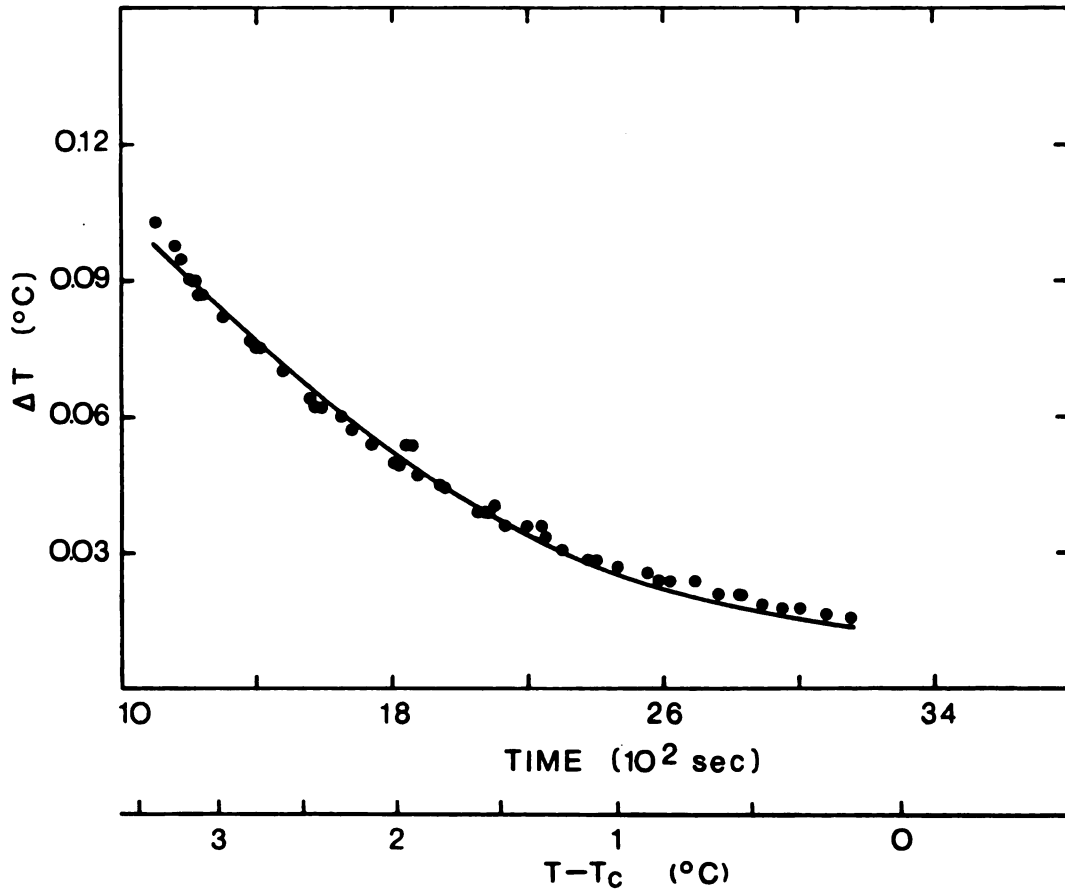


Figure 6.9. Run II. Experimental results for $\tilde{Q}_1^* = A\epsilon^{\lambda_4}$ with A and λ_4 as adjustable parameters.

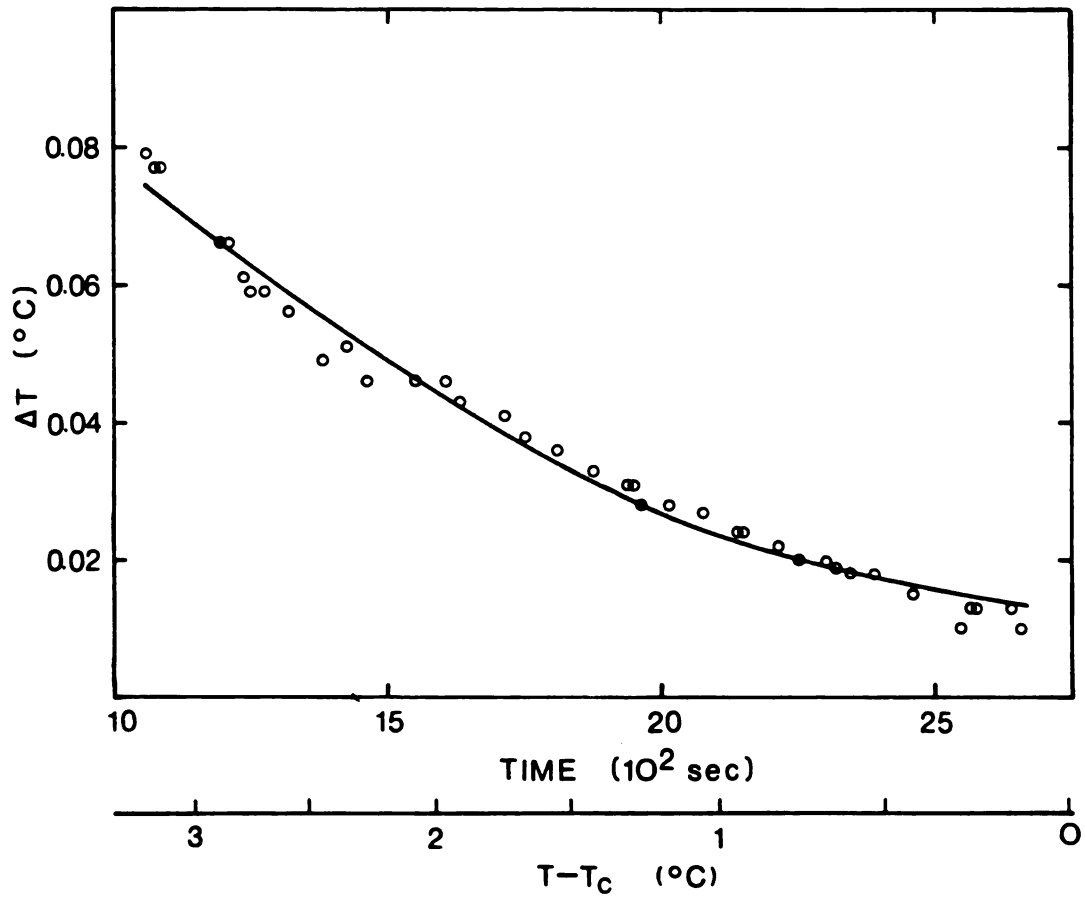


Figure 6.10. Run III. Experimental results for \tilde{Q}_1^*
 $= A\epsilon^{\lambda_4}$ with A and λ_4 as adjustable parameters.

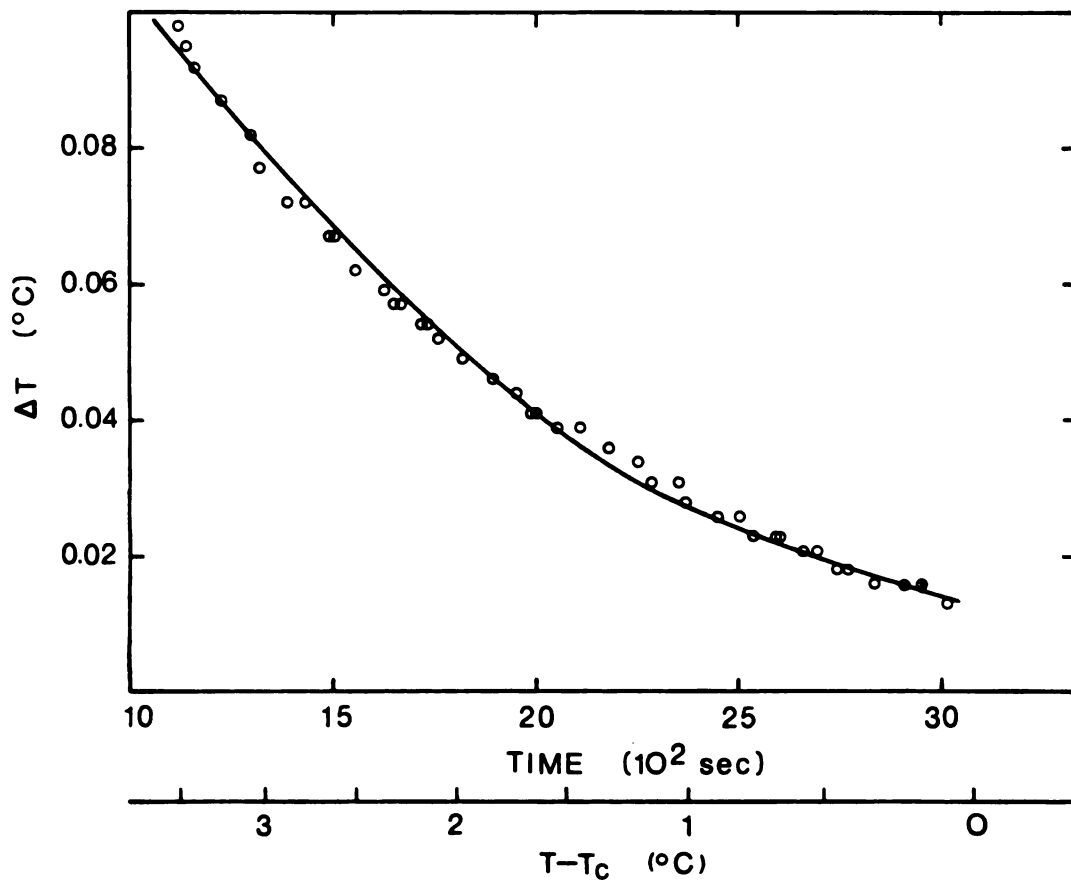


Figure 6.11. Run IV. Experimental results for $\tilde{Q}_1^* = A\epsilon^{\lambda_4}$ with A and λ_4 as adjustable parameters.

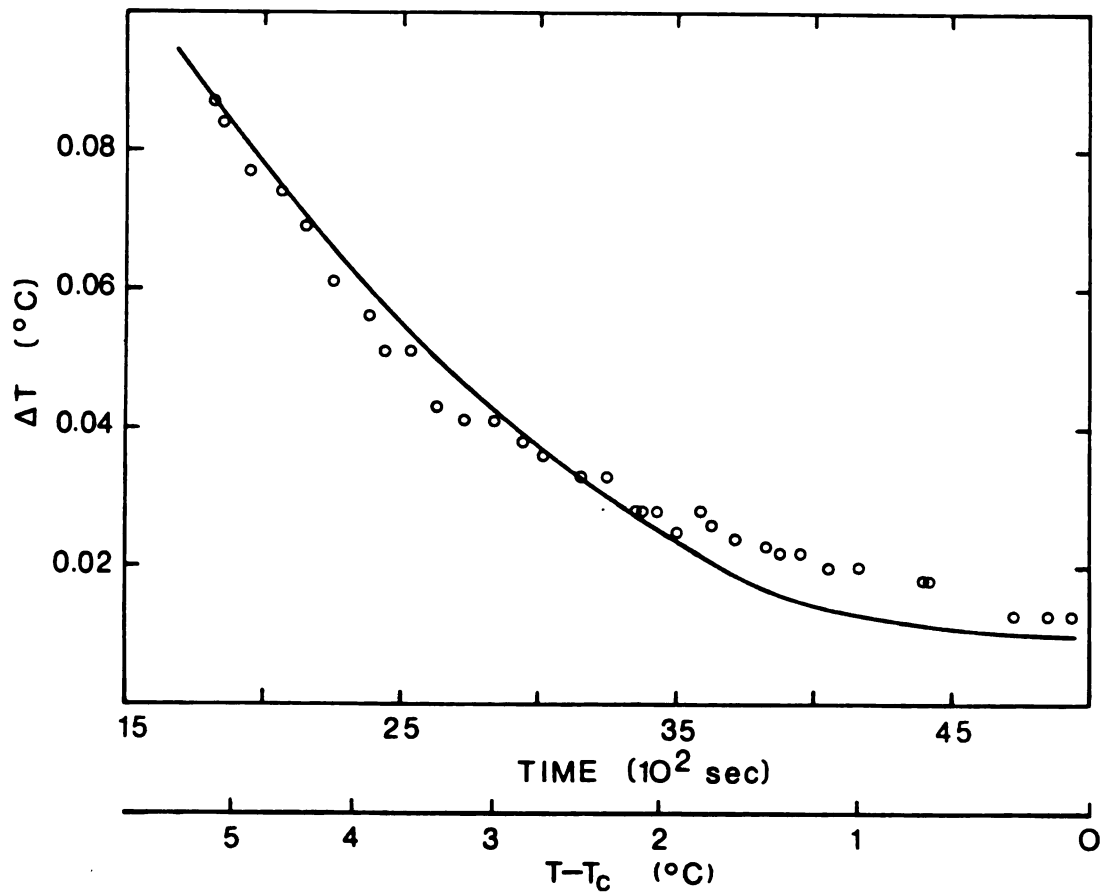


Figure 6.12. Run V. Experimental results for $\tilde{Q}_1^* = A\epsilon^{\lambda_4}$ with A and λ_4 as adjustable parameters.

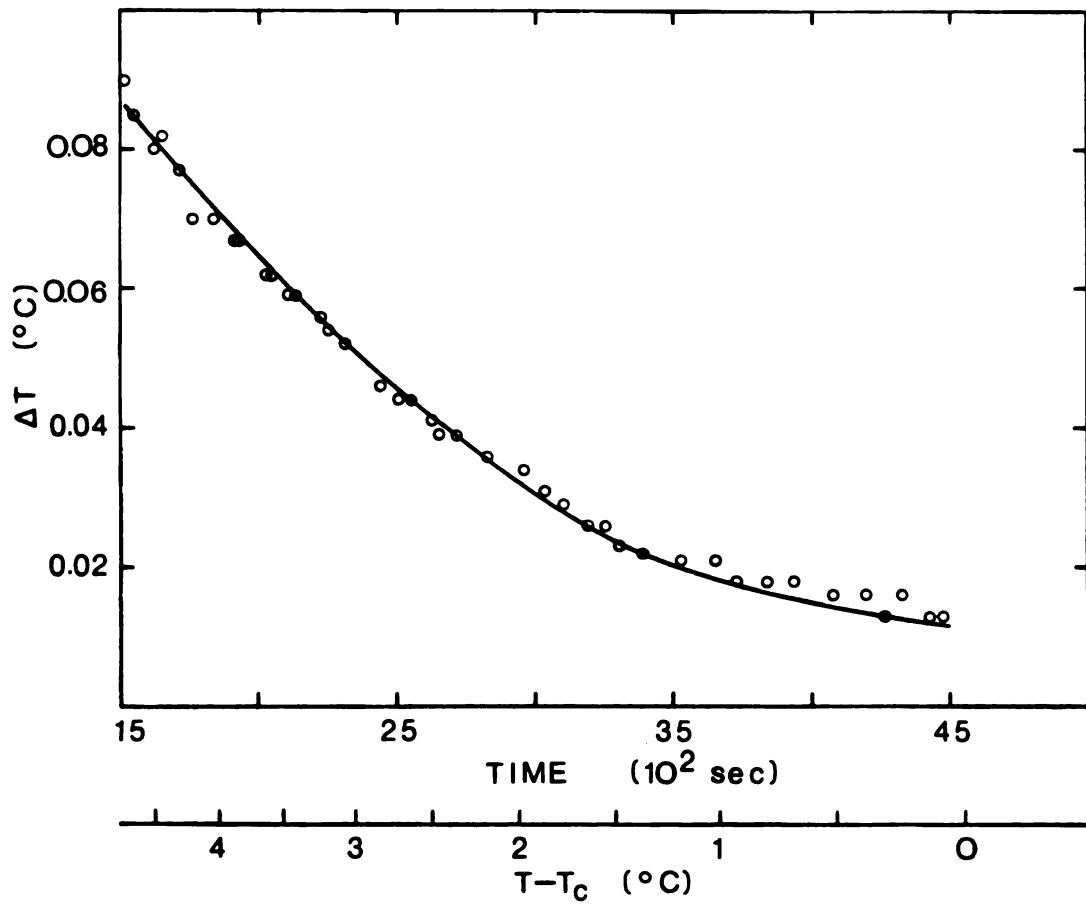


Figure 6.13. Run VI. Experimental results for $\tilde{Q}_1^* = A\epsilon^{\lambda_4}$ with A and λ_4 as adjustable parameters.

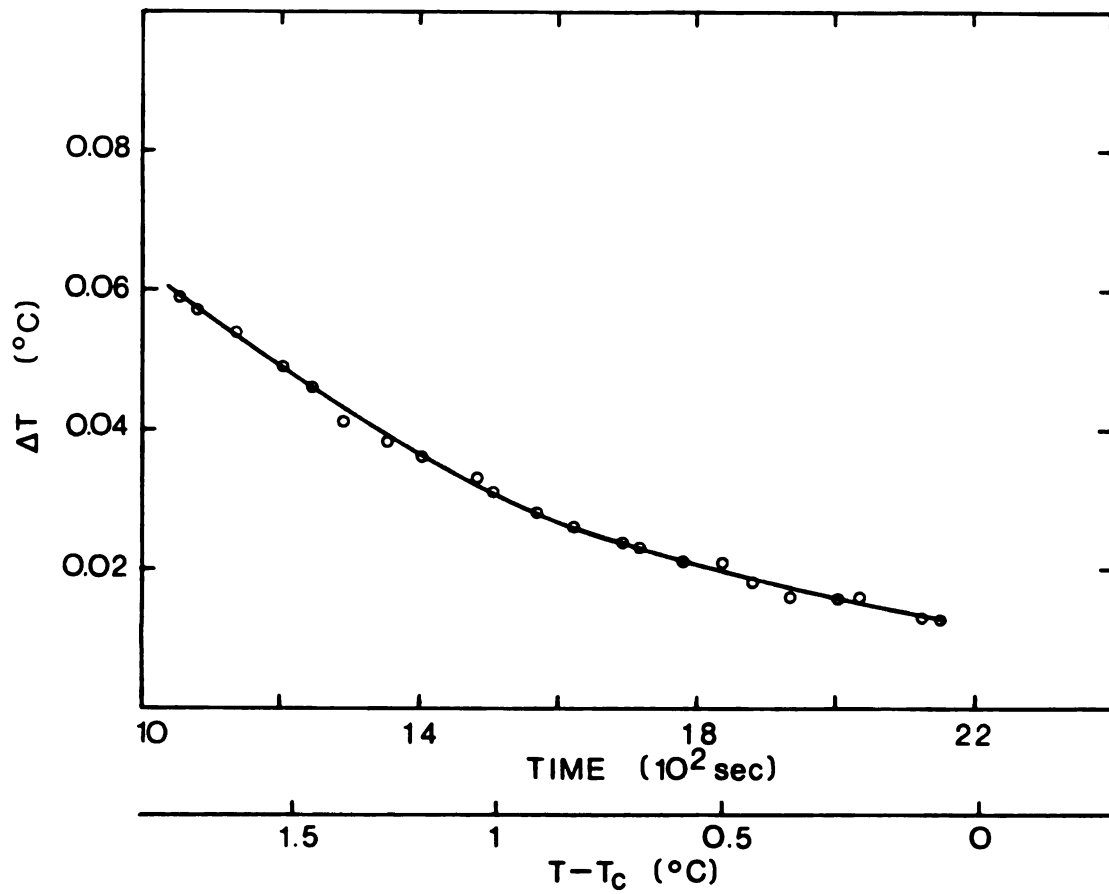


Figure 6.14. Run VII. Experimental results for \tilde{Q}_1^*
 $= A\epsilon^{\lambda_4}$ with A and λ_4 as adjustable parameters.

From Figures 6.8 - 6.14 note that even when T approaches T_c , the measured ΔT does not identically vanish. There also appear to be larger discrepancies between experiment and calculation in this region. These effects are primarily attributable to the composition dependence of \tilde{DQ}_1^* . As T approaches T_c , \tilde{DQ}_1^* becomes small near the interface where $x_1 = x_{1c}$. However, on either side of the interface, the composition differs from x_{1c} and the phase separation temperatures for those compositions are considerably lower than T_c . In these regions ($x_1 \neq x_{1c}$), \tilde{Q}_1^* and D are still finite even when $T = T_c$ because of the lower phase separation temperature at these compositions. The measured ΔT is related to \tilde{DQ}_1^* and will therefore be nonzero when $T = T_c$ because of the contribution from diffusion occurring in regions slightly removed from the interface. This contribution should also vanish if the cell temperature is lowered to the local phase separation temperature. Experimentally, ΔT did vanish at temperatures below T_c when diffusion entirely ceased.

As previously mentioned, this compositional contribution from various properties will be essentially constant as $T \rightarrow T_c$ and will not affect the determination of λ_4 except very near the CST when the main contribution from diffusion at the interface vanishes. To include the composition dependence in the predictive treatment, an empirical correction for ΔT as a function of ϵ was included

in the numerical integration program for the very near CST region. This empirical relation was obtained from a fit of Run I. This same relation was then applied equally to the other six runs which, as can be seen from Figures 6.9 - 6.14, gave good results in each case. This empirical fitting procedure affected the fit of experimental to predicted values only in the region of the last few data points. Furthermore, because all known composition dependencies were already included in the equations, the empirical correction was at most 0.008°C . Fits obtained with and without the data points of this region, where the empirical composition correction was used, yielded λ_4 values which agreed within 2%.

Table 6.4 is a reproduction of Table 5.5 with the now known critical exponent for the heat of transport included. Notice that \bar{Q}_1^* vanishes with a $+2/3$ exponent. Also notice that \bar{Q}_1^* is identical to Ω_{01}/Ω_{11} . Since no thermodynamic properties (such as $\bar{\mu}_{11}$) are involved in the behavior of \bar{Q}_1^* , the entire observed anomaly is due to the behavior of the Onsager coefficients. There is no ambiguity in attributing anomalous behavior to the kinetic or Onsager effects in the case of the heat of transport.

Since recent light scattering investigations of D in the critical region reveal that mutual diffusion vanishes with a $+2/3$ exponent and since $\bar{\mu}_{11} \sim \epsilon^{+4/3}$, Ω_{11} must diverge with a $-2/3$ exponent. Insertion of this value

Table 6.4. Transport parameters and their critical exponents.

Property	Definition	Behavior Near CST	Critical Exponents
κ	$\kappa = \Omega_{00}/T$	$\kappa \sim \Omega_{00}$	$\kappa \sim \epsilon^0$
D	$D = \frac{\Omega_{11}\bar{\mu}_{11}}{\rho w_2}$	$D \sim \Omega_{11}\bar{\mu}_{11}$	$\Omega_{00} \sim \epsilon^0$ $D \sim \epsilon^{2/3}$ $\bar{\mu}_{11} \sim \epsilon^{4/3}$ $\Omega_{11} \sim \epsilon^{-2/3}$
D_T	$D_T = \frac{\Omega_{10}}{\rho}$	$D_T \sim \Omega_{10}$	$D_T \sim \epsilon^0$ (a)
	$\alpha_1 = \frac{-\Omega_{10}}{w_1 w_2 \rho D}$	$\alpha_1 \sim \frac{\Omega_{10}}{\Omega_{11}\bar{\mu}_{11}}$	$\alpha_1 \sim \epsilon^{-2/3}$ (a)
	$K_T = \frac{\Omega_{10} w_2}{\Omega_{11}\bar{\mu}_{11}}$	$K_T \sim \frac{\Omega_{10}}{\Omega_{11}\bar{\mu}_{11}}$	$K_T \sim \epsilon^{-2/3}$ (a)
			$\Omega_{10} \sim \epsilon^0$ (a)
\bar{Q}_1^*	$\bar{Q}_1^* = \frac{\Omega_{01}}{\Omega_{11}}$	$\bar{Q}_1^* \sim \frac{\Omega_{01}}{\Omega_{11}}$	$\bar{Q}_1^* \sim \epsilon^{2/3}$ (b) $\Omega_{01} \sim \epsilon^0$ (b)

(a) Results of Giglio and Vendramini [1975] are used.

(b) Results of this work.

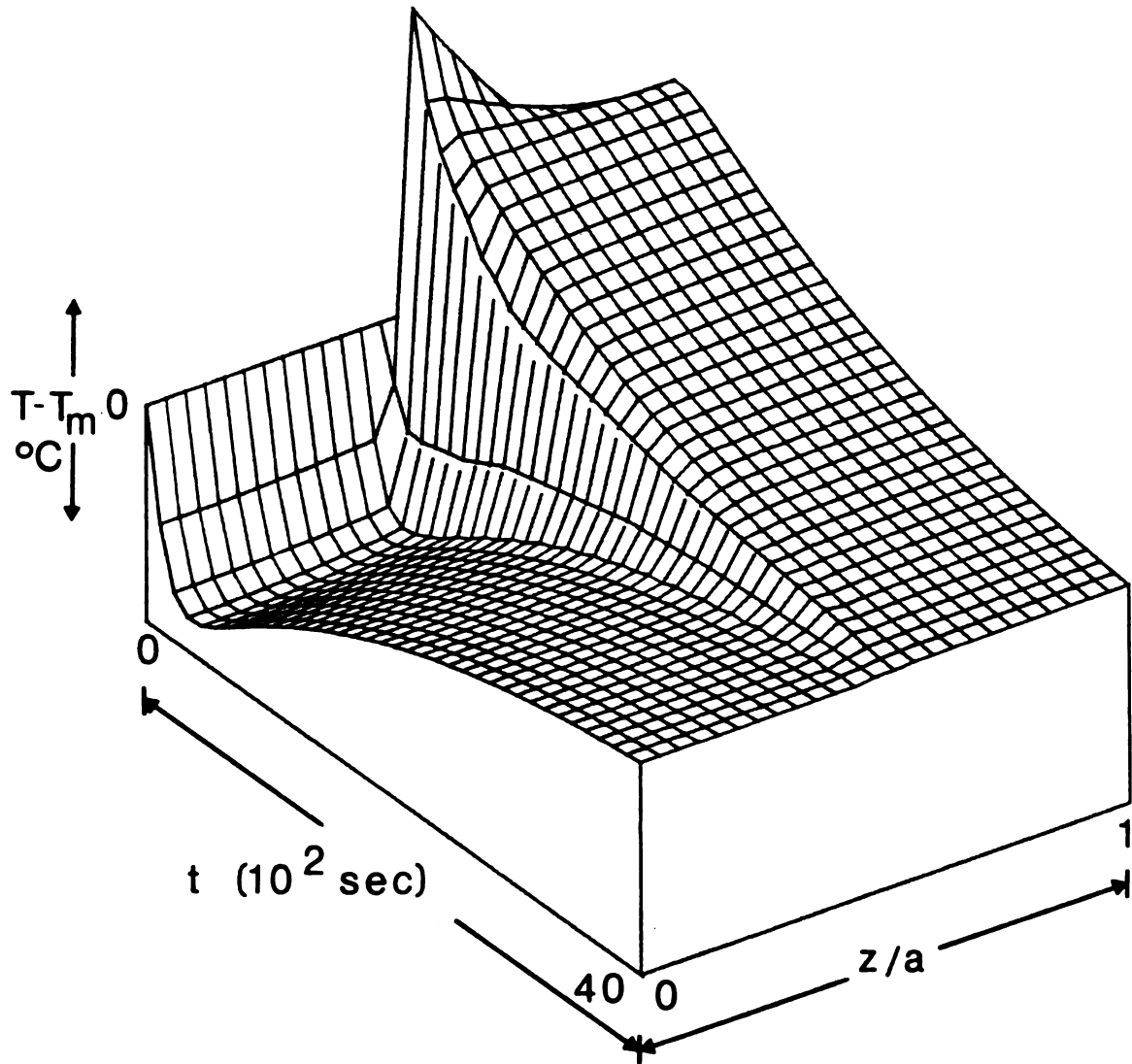
into the definition of \bar{Q}_1^* indicates that $\Omega_{01} \sim \epsilon^0$. It is interesting to note from Table 6.4 that Ω_{11} is therefore the only Onsager coefficient for a binary liquid mixture (without pressure gradients and external fields) with a nonzero critical exponent. This fact is, however, consistent with the general criterion for the direction of an irreversible process as derived by Haase [1969]:

$$\begin{vmatrix} \Omega_{00} & \Omega_{01} \\ \Omega_{10} & \Omega_{11} \end{vmatrix} > 0 . \quad (6.12)$$

Equation (6.12) implies $\Omega_{00}\Omega_{11} - \Omega_{01}\Omega_{10} > 0$. Since this expression is true away from the critical region and only Ω_{11} diverges (while the other coefficients remain finite), the relation is certainly still valid in the critical region.

Note that in qualitative support of Onsager reciprocity in the critical region $\Omega_{01} \sim \epsilon^0 \sim \Omega_{10}$. That is, the reciprocal effects have equal critical exponents. Actual verification of an identity between Ω_{01} and Ω_{10} must wait until composition dependencies of the various transport properties and thermodynamic properties have been accurately determined.

Figure 6.15 shows dramatically the manner in which the measured ΔT vanishes as the consolute temperature is approached. Since ΔT is related to DQ_1^* , where D



TEMPERATURE RELATIVE TO CELL MEAN TEMPERATURE.

Figure 6.15. Simulated temperatures relative to the mean cell temperature in temperature jump diffusion thermoeffect experiments as T approaches T_c .

vanishes as $T \rightarrow T_c$, the qualitative behavior of Figure 6.15 is to be expected. The feature unexpected a priori is that ΔT vanishes more quickly than D ; i.e., that Q_1^* (the heat "carried" by a diffusing molecule) itself vanishes. There is a critical decrease in Q_1^* as well as in D . This observed behavior obviously contains information relevant to the microscopic mechanism of the diffusion thermoeffect and is discussed in Chapter 7 as it pertains to current theories and molecular interpretations of the heat of transport.

CHAPTER 7

CONCLUSIONS

A. Interpretations of the Heat of Transport

Although the work described in this dissertation was the first quantitative measurement of the heat of transport in binary liquid mixtures, numerous papers on the theory of thermal diffusion and the heat of transport have been published during the last 50 years. Two main approaches can be identified, (1) the kinetic approach and (2) the statistical mechanical approach.

The kinetic interpretation of the heat of transport has developed from a model for diffusion akin to Eyring's significant structure theory. The basic reasoning follows that proposed by Wirtz [1939], Wirtz and Hiby [1943], Denbigh [1952], and Prigogine et al. [1950]. Some extensions have been made by Dougherty and Drickamer [1955] and Rutherford and Drickamer [1954]. If a particle is to leave its position on the quasi-crystalline liquid lattice and move to a new location, the activation energy can be divided into two parts: (1) q_H , the "Hemmungsenergie" required to break free from the attraction of the neighboring molecules, and (2) q_L , the "Lochbildungsenergie" required to form the hole into which the diffusing molecule passes. Thus the activation energy is

$$E_a = q_H + q_L \quad (7.1)$$

The diffusion coefficient and the mass flux can then be written in a typical Arrhenius fashion with the above activation energy. Consideration of a nonisothermal system in which a molecule passes from a temperature T_a to a temperature T_b requires q_H at T_a and q_L at T_b . Opposing rates for the flux can be written which when balanced for the case of the thermal diffusion steady state yields

$$-\left(\frac{d \ln C}{dT}\right)_{\text{S.S.}} = \frac{q_H - q_L}{RT^2} \quad (7.2)$$

where C is molarity. The definition can then be made

$$k_{Q_1}^* \equiv q_{H,1} - q_{L,1} \quad (7.3)$$

where $k_{Q_1}^*$ is the heat of transport based on the kinetic model. This is different from the phenomenological definition of Equation (2.19).

Denbigh's presentation is slightly different. He defines the "two energy terms involved in this process (the jumping of a molecule from one site to the next): (a) the energy of detaching the molecule from its neighbors; (b) the energy of creation or filling of the hole." With W_H and W_L representing these two energies respectively, the energy associated with the transfer of a

molecule of component 1 is $W_{H,1} - W_L$, which prompts the definition

$$k_{Q1}^* \equiv W_{H,1} - W_L \quad (7.4)$$

Consideration of the regular solution theory facilitates a representation of W_H and W_L in terms of configuration or interchange energies for the case in which molecules of both components are about equal in size. The excess molar free energy \tilde{G}^E in regular solution theory is

$$\tilde{G}^E = N_A w x_1 x_2 = w' x_1 x_2 \quad (7.5)$$

in which N_A is the Avogadro number, w is the interchange energy, and $w' = N_A w$. Because the two components of the mixture are perfectly randomly arranged, the excess entropy of mixing is zero - the entropy of mixing corresponds to that of an ideal mixture. The interchange energy can be thought of as the change in potential energy when z dissimilar 1-2 molecular pairs are formed from $z/2$ 1-1 and $z/2$ 2-2 molecular pairs. The interchange energy is related to the pair potential energies relative to infinite separation w_{ij} by

$$w = z[w_{12} - \frac{1}{2}(w_{11} + w_{22})] \quad (7.6)$$

where z is the coordination number (Prausnitz [1969]).

In terms of w_{ij} , Denbigh found

$$k_{Q_1}^* = -zN_A f x_2 / 2 [x_1 (w_{11} - w_{12}) - x_2 (w_{22} - w_{12})] \quad (7.7)$$

where f is a numerical factor less than unity which physically corresponds to the fraction of nearest neighbor "bonds" broken during the jump.

Dougherty and Drickamer [1955] have made some comparisons of experimental values for Q_1^* , obtained from thermal diffusion experiments on the assumption of Onsager reciprocity for Ω_{01} and Ω_{10} , with values calculated from Equation (7.7). In this comparison, the w_{ij} were related to physical properties such as latent heats of vaporization. Good qualitative agreement was found in the comparison but the quantitative agreement was poor.

As Tyrrell [1961] indicates, $k_{Q_1}^*$ and Q_1^* are not necessarily the same. The heat of transport depends on the reference plane. Denbigh's work assumes a volume fixed reference frame while the phenomenological definition of Equation (2.19) is for a barycentric or center of mass reference system. Although related, the two heats of transport are subtly different. Of course the heat of transport obtained from the kinetic theory is different from the excess enthalpy, which for a regular solution is

$$\tilde{H}^E = N_A z x_1 x_2 / 2 (2w_{12} - w_{11} - w_{22}). \quad (7.8)$$

The heat of transport must be due to the very mechanism of diffusion itself.

The statistical mechanical approach removes the restrictive assumptions about the structure of the liquid and the mechanism of diffusion. In so doing, the equations are difficult to evaluate for real systems because they contain integrals over pair correlation functions. Based on Kirkwood's Brownian motion method, Bearman, Kirkwood, and Fixman [1958] developed an expression for the heat of transport for a system in which: (1) particles react with central forces only, (2) intermolecular potentials can be written as sums of pair potentials; and (3) both components possess only translational energy. The heat of transport for such a system in the absence of external forces can be split into two terms

$$Q_1^* = Q_{11}^* + Q_{12}^* \quad (7.9)$$

where Q_1^* is the heat of transport defined by Equation (2.19), Q_{11}^* is a term involving averages over equilibrium ensembles, and Q_{12}^* involves perturbations of the equilibrium distribution due to the flow of heat and matter. Bearman et al. derived a general form for Q_{11}^* and Q_{12}^* . In the case of regular solutions they are

$$Q_{11}^* = \frac{1}{2} \left(\frac{m_1 x_1}{M_2} + x_2 \right) \frac{\bar{v}_1 \bar{v}_2}{v} \left(\frac{\bar{L}_2}{\bar{v}_2} - \frac{\bar{L}_1}{\bar{v}_1} \right) \quad (7.10)$$

$$Q_{12}^* = \frac{1}{2v} \frac{D_2 - D_1}{D_2 + D_1} \left(\frac{m_1 x_1}{M_2} + x_2 \right) \left\{ v_1 v_2 \left(\frac{\bar{L}_1}{\bar{v}_1} + \frac{\bar{L}_2}{\bar{v}_2} \right) + 2x_1 (\bar{L}_1 \bar{v}_1 - L_1 v_1) \right. \\ \left. + 2x_2 (\bar{L}_2 \bar{v}_2 - L_2 v_2) - \frac{2}{3} \int r \left(\frac{d\psi_{21}}{dr} - 1 \right) V'_{21} g_{21}^{(2,0)} d^3 \underline{r} \right\} \quad (7.11)$$

where v is the mean molecular volume, \bar{v}_1 and \bar{v}_2 are the partial molecular volumes of components 1 and 2 respectively, v_1 and v_2 are the molecular volumes of the pure components, \bar{L}_1 and \bar{L}_2 are the negatives of the latent heats of vaporization of components 1 and 2, respectively, from the solution to the ideal gas state, L_1 and L_2 are the negatives of the latent heats of vaporization of the pure component to the ideal gas state, m_1 and m_2 are molecular masses of components 1 and 2, D_1 and D_2 are self diffusion coefficients for each species in the mixture, and r and \underline{r} are the magnitude and vector distances between two molecules, respectively. The integral term in Equation (7.11) cannot yet be evaluated for real systems because it contains the radial distribution function $g_{12}^{(2,0)}$, the intermolecular potential V'_{21} and a term involving ψ_{21} which is related to the nonequilibrium radial distribution function. The above functions are unknown for real liquids. Notice that the equations from the kinetic theory

are analogous to Equation (7.10), but neglect completely the nonequilibrium portion Q_{12}^* of the phenomenon.

Bearman and Horne [1965] have compared experimental thermal diffusion factors with (1) thermal diffusion factors calculated from Equations (7.10) and (7.11) on the assumption of ORR, and (2) thermal diffusion factors calculated from similar statistical mechanical equations derived directly for thermal diffusion in terms of molecular properties. The integral terms involving radial distribution functions were left out. This corresponded to a hard-sphere assumption. Because these integrals were left out, the thermal diffusion factors calculated from the thermal diffusion theory were somewhat lower than those obtained from the heat of transport theory. The values obtained from the heat of transport theory for the thermal diffusion factors in carbon tetrachloride-cyclohexane mixtures agreed quite well with the experimental results. An important result of their calculations, was that the Q_{12}^* term contributed over 50% of the absolute value of Q_1^* . Thus, the nonequilibrium term in the Bearman-Kirkwood-Fixman theory, which the kinetic theory completely neglects, is in fact the predominant term.

Story [1967] and Story and Turner [1969] have examined experimental thermal diffusion factors for carbon tetrachloride-benzene and cyclohexane-benzene mixtures with respect to both the kinetic theory and the statistical

mechanical theory. They find that the kinetic theory is not only in error with respect to magnitude, but often yields the wrong sign. They found similar difficulties in magnitude and sign using the statistical mechanical theory with the integral of Equation (7.11) neglected.

B. A New Interpretation of the Heat of Transport

The kinetic approach results in an expression for the heat of transport obtained entirely from equilibrium properties of mixtures. The Bearman-Kirkwood-Fixman theory indicates that this cannot be done. In order for the heat of transport to be nonzero, the molar energy transported by diffusion must be different from the partial molar enthalpy contribution due to the mass flux. This is readily seen from Equations (2.4) and (2.19). It therefore seems likely that the heat of transport is not just a difference in potential energies experienced by the diffusing particle, but should depend on the kinetics of transport - the very mechanism of diffusion itself.

The results of Chapter 6 clearly indicate that Q_1^* vanishes as the consolute temperature is approached and does so with a $+2/3$ critical exponent. An implicit goal throughout the evaluation of the critical behavior of Q_1^* has been that the results would provide insight into the microscopic nature of heat and matter coupling and its relationship to the diverging correlation length

associated with critical mixtures. Clearly, any consistent model for Q_1^* must also explain the observed behavior $Q_1^* \sim \epsilon^{2/3}$ in the near critical region. The kinetic theory of Q_1^* appears to be inconsistent with these experimental findings. In the regular solution theory, the configuration energy w is at most a weak function of temperature, and therefore Equation (7.7) does not exhibit the required behavior in the critical region. Even the basic definition given in Equation (7.4), where regular solution theory has not been invoked, does not display the experimentally observed behavior. Note that Equation (7.4) is consistent with the observed decrease of the diffusion coefficient in the critical region if the increased correlation length is assumed to enhance the diffusional activation energy. The heat of transport defined in Equation (7.4) does not depend on the activation energy. It depends only on the difference in energy required to remove a molecule and the energy released when its hole is filled. It would seem that this difference would depend on relative potential energies rather than lengths of correlation and therefore this model does not adequately describe the critical behavior of Q_1^* .

To formulate a new kinetic theory for the heat of transport which is consistent with the experimental behavior in the critical region, the lattice model for liquid structure must be discarded in favor of the more

intuitive idea of randomness due to molecular thermal motions. Hildebrand [1977] has shown that "changes of viscosity and diffusivity with temperature can be accurately and more simply expressed in nonexponential formulas than by plotting their logarithms against reciprocal temperatures." "Activation energy" is therefore not a necessary construct. The mechanism of diffusion in this formulation is a succession of small displacements due to random molecular thermal motions rather than to actual "jumping" from one lattice site to the next. The temperature dependence of the diffusion coefficient is simply due to increased thermal motion, which decreases the time needed for a net transference of molecules from one location to another.

The thermal motions of each molecule vary but presumably obey a maxwellian or normal distribution. In fact, the mode or expectation value of this distribution of energies defines the thermodynamic temperature as kT , where k is Boltzmann's constant. Because of this distribution of energies, some molecules are more energetic than others at any given time. For convenience of discussion, define the "excess energy" of a particle or molecule as that amount of energy which it possesses at a given time in excess of the expectation or kT amount of energy. Thus, the further out in the leading wing of the distribution, the more "excess energy" the molecule

has relative to the average value. Now bring two isothermal subsystems (of different pure components for the moment) into contact and allow mutual diffusion to begin. Which molecules from the energy distribution for subsystem 1 will be more likely to be found in subsystem 2 shortly after initial contact of the phases has been made? The conclusion that the more energetic molecules diffuse more rapidly than their "average" energy counterparts is inescapable. Although collisions are energy randomizing events, molecules at any one time possessing "excess energy" move faster through the solution than their lower energy counterparts and for any given period of time will move further through the mixture. The heat of transport of component 1 is simply the "excess energy" transported by molecules which undergo diffusion.

From this picture of the heat of transport, several concepts, vague in the previous kinetic theory, become clear. Notice that the difference between the heat of transport and the heat of mixing is evident. The heat of mixing is a state function dependent only on the states of the initial pure components and the final mixture. The heat of transport cannot be separated from the diffusional mixing process. The heat of transport is thus dependent upon the nonequilibrium movement of molecules as in the Bearman-Kirkwood-Fixman theory and cannot be calculated merely from equilibrium properties and/or

equilibrium intermolecular potentials. The heat of transport is a property of the system because the distribution of energies is certainly dependent upon the components (mass, vibrational degrees of freedom, rotational degrees of freedom, etc.) and the relative amounts of each present. Q_1^* is specific to the mixture and retains its value even if two mixtures of equal chemical potential are brought into contact. For this case Q_1^* is nonzero, but no temperature change occurs in the system because a forward diffusional event is as likely to occur as a reverse event. The previous kinetic theory predicts $k_{Q_1^*} = 0$ in this case.

The temperature changes in a diffusion thermoeffect experiment are explicable from this model of the heat of transport. When a molecule of component 1 migrates from a particular region carrying with it "excess energy", the molecules behind are lowered in energy relative to the previous kT value by an amount equal to the "excess energy" transported. However, other high energy molecules are finding their way into that region carrying "excess energy" which tends to raise the distribution of energies. Because there is a competing effect between the net diffusion of component 1 in one direction (into the lower chemical potential region) and the net diffusion of component 2 in the other direction, the temperature change in a particular location is related to the difference between the two distributions of energies in

the initial phases. It is dependent upon the "book-keeping" of "excess energies" carried into and out of the region. The molecular distributions of energy for the two initial phases are themselves dependent upon the masses, intermolecular potentials, and complexity of the molecules.

The same statistical nature of molecular thermal motion gives rise to thermal diffusion. Consider a uniform, isothermal, binary liquid mixture between two parallel plates. Because the system is isothermal, both components have the same expectation value for their thermal energy distributions. However, the breadth of the distributions need not be the same and is dependent upon the properties of the components. If a temperature gradient is now imposed, the energy distributions of both components very near the hot wall are shifted up in energy while the distributions near the cold wall are shifted down. Because both components are more energetic near the hot wall, there is a net random migration of both components toward the cold wall (thermal expansion). However, the component with the broader distribution of energies will tend to move faster, i.e., its more energetic molecules, on the average, move through the fluid faster than those of the component with the narrower distribution. Unlike isothermal conditions where the faster migration of the component with the broader

distribution occurs equally in both directions, under the influence of a temperature gradient this statistical "excess migration" is predominately toward the cold wall since the distribution of energies was lowered in that region. There is a net accumulation of this component in the cold region (as thermal energy is now absorbed into the cold plate) hence a relative accumulation of the other component near the warm wall where heat is continuously supplied. Finally, a steady state is reached when the above accumulation process balances diffusion in the reverse direction caused by unequal populations.

The critical behavior of the heat of transport for this model is closely tied to the critical behavior of diffusion. Both are kinetic processes (as opposed to thermal processes such as thermal conduction). The Stokes-Einstein-Kawasaki equation (Kawasaki [1970])

$$D = kT/(6\pi\eta\xi) \sim \epsilon^{2/3}, \quad (7.12)$$

where η is shear viscosity, describes the critical decrease of the diffusion coefficient near the consolute point in terms of a rapidly diverging size effect as more and more particles become correlated. Thus, $D \sim \xi^{-1} \sim \epsilon^{2/3}$, and D vanishes as groups of molecules become correlated. It should be mentioned that the critical exponent for η

is still not known exactly, but appears to be zero or slightly negative (the small anomaly observed may be a logarithmic singularity).

For a related reason, Q_1^* in the proposed model must also vanish as correlation lengths increase. As the consolute temperature is approached, correlation lengths increase rapidly. As correlations increase, the Maxwellian distribution of energies must necessarily narrow. This can be viewed as an effect due to increased mass per diffusing particle or as a decrease in large magnitude fluctuations due to increased correlations. Since the heat of transport is viewed as the "excess energy" or energy above the expectation value carried by a diffusing molecule, Q_1^* must vanish as the distribution of energies narrows about the kT or expectation value. In the limit of perfect correlation between the molecules, each diffusing species has exactly kT of energy associated with it, Q_1^* is identically zero, and no change in local temperature is produced by the diffusional event. This can be viewed as the limiting case when $T \rightarrow T_c$. As T approaches T_c the diversity of energies associated with particles decreases and appears to do so inversely proportional to the correlation length ξ . Therefore

$$Q_1^* \sim \xi^{-1} \sim \epsilon^{2/3} \quad (7.13)$$

in agreement with the experimental measurements of Chapter 6.

C. Summary and Future Work Needed

As stated in the Introduction, the objectives of this work have been fourfold: (1) to measure quantitatively for the first time the diffusion thermoeffect in liquid mixtures, (2) to test experimentally the Onsager heat-mass reciprocal relation, (3) to study the behavior of the diffusion thermoeffect in the consolute region of a binary mixture in order to understand how it may relate to microscopic phenomena; and (4) to examine experimentally and compare the behavior of the Onsager heat-mass and mass-heat coefficients in the consolute region. It was felt that the accomplishment of these four goals would contribute to the overall objective of transport investigations: to understand the microscopic causes of observed macroscopic phenomena sufficiently enough to make accurate a priori predictions.

In fulfillment of the above objectives, a new cell was designed which enabled quantitative observation of the diffusion thermoeffect. This cell used a withdrawable third component to create an initially sharp diffusional interface. The equations of nonequilibrium thermodynamics and hydrodynamics were solved numerically for the conditions involved in the actual experiments, leaving $(\tilde{Q}_1^*/\tilde{M})$ as an adjustable parameter. Nonlinear least squares fitting of these solutions to the measured temperature differences between thermocouples placed

symmetrically about the interface led to the first direct determination of the heats of transport in carbon tetrachloride-cyclohexane mixtures. These values compared well with those obtained via thermal diffusion techniques, which led to the first experimental verification of the Onsager reciprocal relation for the heat-mass and mass-heat coefficients.

The temperature dependence of the heat of transport was determined for isobutyric acid-water mixtures as a function of distance from the critical temperature via the diffusion thermoeffect technique. A temperature jump cell was employed. The local temperature could be rapidly jumped (with a microwave oven) to temperatures above the consolute temperature. The difference in temperature between two points symmetric about the interface was monitored as a function of cell mean temperature. The cell temperature was allowed to slowly relax toward T_c permitting determination of the critical exponent for the heat of transport by nonlinear least squares fitting. It was found that \tilde{Q}_1^* vanishes rapidly as T_c is approached and can be represented by $\tilde{Q}_1^* \sim \epsilon^{2/3}$. From these results, the critical exponent for the Onsager coefficient Ω_{01} is 0. Very recent thermal diffusion experiments indicate $\Omega_{10} \sim \epsilon^0$. The reciprocal heat-mass and mass-heat Onsager coefficients therefore have identical critical behavior. Furthermore, existing kinetic theories

of Q_1^* do not explain its critical behavior. A new model based on the thermal motion picture for diffusion not only explains the critical behavior of Q_1^* , but also explains the basic features of the heat of transport left vague in existing models.

More research is needed to verify and quantify the model for Q_1^* . The mathematical formulation of the model is the next step. Of further interest would be diffusion thermoeffect experiments in multicomponent systems, especially near critical points of higher order. The more areas in which the heat of transport can be evaluated to give special criteria which must be met by any consistent theory, the better the model will become as well as our understanding of the processes involved.

With respect to the experiments themselves, it would be desirable to perform similar studies on other systems near their consolute temperature. Further studies on the composition dependencies of thermodynamic and transport properties in this region need to be performed so that absolute values of heats of transport can be calculated in this region. This would then establish a basis for examination of Ω_{01} and Ω_{10} to test Onsager reciprocity in the critical region.

Additional measurements of the temperature and pressure dependence of Q_1^* away from the critical temperature are desirable to facilitate empirical predictive capabilities

and to elucidate the microscopic coupling of heat and mass transport.

These first experiments on the diffusion thermo-effect in liquids have opened an area of investigation in the study of transport processes which for decades was discounted as unfeasible. Much information can be gained from study of this cross transport coefficient. It is hoped that other cross coefficients can also be tapped and used as tools in the study of transport phenomena.

APPENDICES

APPENDIX A

TRANSFORMATION RELATIONS AND IDENTITIES

The transformation of mass fraction-specific property Equations (2.25) - (2.27) to mole fraction-molar property Equations (2.33) - (2.35) involves the following definitions, identities, and procedures:

A.1. Mass fraction-mole fraction.

The relationship between mass fraction w_i and mole fraction x_i is

$$w_i = x_i M_i / \tilde{M} \quad (\text{A.1})$$

where M_i is the molecular weight of component i and $\tilde{M} \equiv x_1 M_1 + x_2 M_2$ is the mean molecular weight.

A.2. Specific property-molar property.

If \bar{J} is any specific property either of the mixture or of the pure component and \tilde{J} is the corresponding molar property, then

$$\bar{J} = \tilde{J} / \tilde{M} . \quad (\text{A.2})$$

A.3. Mass fraction derivatives-mole fraction derivatives.

The following identity is easily shown from the

chain rule:

$$(dw_1/d) = M_1 M_2 / \tilde{M}^2 (dx_1/d). \quad (\text{A.3})$$

A.4. Partial specific enthalpies.

The derivative of the difference in partial specific enthalpies contained in Equation (2.27) can be related to the excess molar enthalpy \tilde{H}^E . From the chain rule, Equation (A.2), and the Euler relation

$$x_1 d\tilde{H}_1 + x_2 d\tilde{H}_2 = 0 ,$$

the derivative of the difference in partial specific enthalpies can be written as

$$[\partial(\bar{H}_1 - \bar{H}_2)/\partial z] = (\tilde{M}/M_1 M_2 x_2) (\partial \tilde{H}_1 / \partial x_1)_{T,P} (\partial x_1 / \partial z).$$

The definition of partial molar enthalpy implies

$$[\partial(\bar{H}_1 - \bar{H}_2)/\partial z] = (\tilde{M}/M_1 M_2) (\partial^2 \tilde{H} / \partial x_1^2) (\partial x_1 / \partial z)$$

where the total molar enthalpy \tilde{H} is usually split into ideal and excess contributions

$$\tilde{H} = x_1 \tilde{H}_1^0 + x_2 \tilde{H}_2^0 + \tilde{H}^E$$

with \tilde{H}_1^0 and \tilde{H}_2^0 representing pure component molar enthalpies. These two equations combine to yield

$$[\partial(\bar{H}_1 - \bar{H}_2)/\partial z] = (\tilde{M}/M_1 M_2)(\partial^2 \tilde{H}^E / \partial x_1^2)_{T,P} (\partial x_1 / \partial z) \quad (\text{A.4})$$

which is the desired result identical to Equation (2.36).

A.5. Thermodynamic factor.

The transformation from heats of transport to thermal diffusion factors involves the thermodynamic factor $(1+\Gamma)$ defined as

$$(1+\Gamma) \equiv [1 + (\partial \ln \gamma_1 / \partial \ln x_1)_{T,P}] \quad (\text{A.5})$$

where γ_1 is the activity coefficient for component 1. The relationship between \tilde{Q}_1^* and α_1 is

$$\tilde{Q}_1^* = -\alpha_1 \tilde{M} (\partial \tilde{\mu}_1 / \partial \ln x_1)_{T,P} (M_1 M_2)^{-1}$$

as is easily shown from Equations (2.14), (2.15), and (2.16). The molar quantities \tilde{Q}_1^* and $\tilde{\mu}_1$ are related to their specific quantities by Equation (A.2) where \tilde{M} becomes M_1 . From thermostatics, the molar chemical potential is related to the activity coefficient γ_1 and the standard state chemical potential μ_1^θ of component 1 by

$$\tilde{\mu}_1 = \mu_1^\theta + RT \ln x_1 \gamma_1.$$

Obviously, γ_1 is the activity coefficient based on the same standard state chosen for μ_1^θ . Therefore,

$$(\partial \tilde{\mu}_1 / \partial \ln x_1)_{T,P} = RT(1 + \partial \ln \gamma_1 / \partial \ln x_1)_{T,P} = RT(1 + \Gamma)$$

and

$$\tilde{Q}_1^* = -\alpha_1 \tilde{M} RT(1 + \Gamma) / M_1 M_2 \quad (\text{A.6})$$

as required in Equation (4.1).

APPENDIX B

DIFFUSION THERMOEFFECT DATA FOR THE CARBON TETRACHLORIDE-CYCLOHEXANE SYSTEM

Using the withdrawable "liquid gate" cell described in Chapter 4, diffusion thermoeffect measurements were made on five mixtures of CCl_4 - \underline{c} - C_6H_{12} . The boundary conditions used were for adiabatic, impermeable walls at $(z/a) = 0$ and $(z/a) = 1$. Initial conditions for each run are listed in Table B.1 where x_1^u is the initial mole fraction of carbon tetrachloride in the upper phase and x_1^L is the initial mole fraction of carbon tetrachloride in the lower phase. The initial temperature distribution T_0 obtained from thermocouple readings just prior to interface creation is given by

$$T_0 = T_{00} - T_z(z/a - 0.5)$$

with T_{00} and T_z listed in Table B.1. Isothermal initial conditions correspond to $T_z = 0$.

Temperature differences between thermocouples located at $(z/a) = 0.4$ and $(z/a) = 0.6$ are listed as functions of time in Table B.2. The initial contact of the upper and lower phases established the diffusion interface and was assigned the time $t = 0$.

Table B.1. Initial Conditions.

Run #	x_1^u	x_1^L	$T_{00}/^\circ\text{K}$	T_z
I	0.0179	0.8044	296.160	0
II	0.0503	0.6436	295.355	0.068
III	0.0951	0.7638	295.131	0
IV	0.0750	0.8935	296.020	0
V	0.1934	0.9094	296.429	0.062

Table B.2. Temperature differences.

Datum #	Run I		Run II		Run III		Run IV		Run V	
	t/s	$\Delta T/^\circ K$	t/s	$\Delta T/^\circ K$	t/s	$\Delta T/^\circ K$	t/s	$\Delta T/^\circ K$	t/s	$\Delta T/^\circ K$
1	105	0.114	54	0.057	80	0.109	103	0.165	111	0.099
2	226	0.237	113	0.116	169	0.141	180	0.211	167	0.120
3	366	0.239	186	0.138	254	0.165	268	0.258	225	0.182
4	497	0.237	277	0.138	349	0.180	374	0.275	318	0.193
5	701	0.230	400	0.163	476	0.170	515	0.286	430	0.200
6	831	0.229	514	0.178	607	0.168	640	0.303	540	0.209
7	990	0.224	622	0.200	730	0.178	796	0.297	665	0.218
8	1186	0.217	733	0.209	861	0.196	928	0.274	791	0.219
9	1371	0.212	836	0.206	984	0.209	1086	0.251	908	0.219
10	1541	0.214	954	0.194	1120	0.198	1230	0.237	1028	0.219
11	1732	0.213	1066	0.190	1236	0.188	1371	0.246	1147	0.211
12	1904	0.202	1198	0.184	1351	0.179	1523	0.234	1280	0.209
13	2067	0.198	1346	0.176	1477	0.181	1690	0.239	1410	0.206
14	2230	0.180	1540	0.190	1588	0.177	1846	0.244	1543	0.206
15	2467	0.178	1674	0.188	1726	0.179	1998	0.241	1665	0.217
16	2626	0.178	1805	0.190	1850	0.170	2172	0.251	1785	0.219
17	2830	0.176	1934	0.183	2070	0.171	2329	0.253	1903	0.209
18	2987	0.173	2046	0.180	2214	0.163	2498	0.229	2032	0.207
19	3351	0.163	2181	0.179	2348	0.165	2735	0.212	2172	0.209
20	3527	0.165	2319	0.175	2484	0.168	2912	0.211	2390	0.204
21	3714	0.166	2450	0.160	2631	0.174	3067	0.224	2559	0.217
22	3936	0.158	2591	0.170	2779	0.169	3238	0.234	2709	0.199
23	4147	0.155	2720	0.171	2956	0.162	3413	0.222	2839	0.204
24			2855	0.171	3186	0.158	3570	0.207	2973	0.196
25			2967	0.179	3322	0.182	3733	0.187	3118	0.192
26			3078	0.163	3462	0.190	3857	0.199	3246	0.182
27			3193	0.146	3596	0.161	4010	0.202	3375	0.184

Table B.2. Continued.

Datum #	Run I		Run III		Run III		Run IV		Run V	
	t/s	$\Delta T/^\circ K$	t/s	$\Delta T/^\circ K$	t/s	$\Delta T/^\circ K$	t/s	$\Delta T/^\circ K$	t/s	$\Delta T/^\circ K$
28			3346	0.142	3745	0.163			3495	0.187
29			3467	0.145	3906	0.163			3643	0.182
30			3610	0.143	4063	0.163			3787	0.177
31			3726	0.136					3931	0.181
32			3914	0.132					4085	0.174
33			4053	0.135						

APPENDIX C

DIFFUSION THERMOEFFECT DATA FOR THE ISOBUTYRIC ACID-WATER SYSTEM IN THE CRITICAL REGION

Using the temperature jump cell described in Chapter 6, diffusion thermoeffect measurements were performed on two different mixtures of isobutyric acid and water prepared at the critical composition. The initial conditions of each run are listed in Table C.1 along with temperature jump data. After the temperature jump, the mean cell temperature relaxed toward the critical temperature as monitored by thermocouples located at $(z/a) = 0.2$ and $(z/a) = 0.8$. A polynomial fit of mean cell temperature as a function of time was obtained for each run. The polynomial equations of the form

$$T - T_c = T_0 + T_1 t + T_2 t^2 + T_3 t^3$$

fit the individual data smoothly where $T - T_c$ is the cell temperature minus the measured critical temperature. The coefficients T_0 , T_1 , T_2 , and T_3 are listed in Table C.1. Also listed in Table C.1 are the critical mole fractions of isobutyric acid at which mixtures were prepared x_{1c} , initial temperatures relative to consolute temperatures (just prior to the T-jump) $T_i - T_c$, and the duration of the heating pulse

t_H .

Temperature differences between the two thermocouples were measured directly and are listed adjacent to the time at which they were observed in Tables C.2-C.8. All times are relative to initiation of the heating pulse. As discussed in Chapter 6, data obtained for times less than 980 seconds are not included because of possible heating non-uniformities.

Table C.1. Initial conditions.

Run #	x_{1c}	$(T_i - T_c)/^\circ K$	t_H/s	$T_0/^\circ K$	$T_1/10^{-3}^\circ K \cdot s^{-1}$	$T_2/10^{-7}^\circ K \cdot s^{-2}$	$T_3/10^{-11}^\circ K \cdot s^{-3}$
I	0.1125	-6.402	1.8	8.036	-3.922	6.521	-4.971
II	0.1125	-5.618	1.7	6.362	-3.214	5.153	-3.798
III	0.1125	-6.804	2.0	6.511	-3.705	6.229	-5.029
IV	0.1125	-6.607	2.4	7.013	-3.782	6.531	-5.350
V	0.1130	-5.720	2.3	11.378	-4.413	6.261	-3.969
VI	0.1130	-5.394	2.0	9.414	-3.822	5.466	-3.553
VII	0.1130	-5.687	1.3	4.291	-2.815	4.788	-3.804

Table C.2. Run I.

No.	t/s	$\Delta T/^{\circ}K$	No.	t/s	$\Delta T/^{\circ}K$	No.	t/s	$\Delta T/^{\circ}K$
1	1060	0.126	21	1753	0.067	41	2566	0.031
2	1091	0.123	22	1766	0.067	42	2585	0.029
3	1112	0.121	23	1819	0.062	43	2648	0.026
4	1135	0.118	24	1845	0.062	44	2705	0.026
5	1200	0.113	25	1888	0.059	45	2769	0.023
6	1260	0.103	26	1937	0.055	46	2786	0.023
7	1279	0.100	27	1980	0.054	47	2830	0.023
8	1331	0.098	28	2049	0.052	48	2890	0.023
9	1383	0.093	29	2078	0.049	49	2957	0.021
10	1401	0.087	30	2096	0.049	50	2974	0.021
11	1414	0.087	31	2163	0.045	51	3035	0.018
12	1476	0.082	32	2183	0.044	52	3118	0.018
13	1495	0.080	33	2241	0.044	53	3169	0.016
14	1518	0.080	34	2269	0.041	54	3233	0.018
15	1535	0.080	35	2343	0.039	55	3296	0.018
16	1578	0.077	36	2360	0.039	56	3370	0.016
17	1642	0.072	37	2432	0.034	57	3382	0.016
18	1655	0.072	38	2448	0.034	58	3439	0.013
19	1670	0.072	39	2458	0.034	59	3489	0.013
20	1730	0.070	40	2518	0.031	60	3554	0.013

Table C.3. Run II.

No.	t/s	$\Delta T/^{\circ}K$	No.	t/s	$\Delta T/^{\circ}K$	No.	t/s	$\Delta T/^{\circ}K$
1	1104	0.103	18	1681	0.057	35	2294	0.031
2	1158	0.098	19	1734	0.054	36	2374	0.029
3	1176	0.095	20	1804	0.050	37	2398	0.029
4	1195	0.090	21	1823	0.049	38	2464	0.027
5	1207	0.090	22	1841	0.054	39	2552	0.026
6	1214	0.090	23	1857	0.054	40	2587	0.024
7	1225	0.087	24	1873	0.047	41	2623	0.024
8	1238	0.087	25	1933	0.045	42	2687	0.023
9	1294	0.082	26	1952	0.044	43	2761	0.021
10	1376	0.077	27	2051	0.039	44	2809	0.021
11	1394	0.075	28	2068	0.039	45	2832	0.021
12	1404	0.075	29	2080	0.039	46	2888	0.019
13	1475	0.070	30	2095	0.041	47	2946	0.018
14	1556	0.064	31	2115	0.036	48	3006	0.018
15	1571	0.062	32	2193	0.036	49	3078	0.017
16	1586	0.062	33	2216	0.036	50	3154	0.016
17	1648	0.060	34	2244	0.034	51	3198	0.016

Table C.4. Run III.

No	t/s	$\Delta T/^{\circ}K$	No.	t/s	$\Delta T/^{\circ}K$	No.	t/s	$\Delta T/^{\circ}K$
1	1059	0.079	14	1608	0.046	27	2215	0.023
2	1073	0.077	15	1638	0.043	28	2247	0.020
3	1085	0.077	16	1715	0.041	29	2299	0.020
4	1193	0.066	17	1753	0.038	30	2318	0.019
5	1210	0.066	18	1810	0.036	31	2341	0.018
6	1236	0.061	19	1875	0.033	32	2390	0.018
7	1249	0.059	20	1936	0.031	33	2459	0.015
8	1276	0.059	21	1949	0.031	34	2547	0.010
9	1320	0.056	22	1960	0.028	35	2566	0.013
10	1380	0.049	23	2016	0.028	36	2578	0.013
11	1425	0.051	24	2071	0.028	37	2635	0.013
12	1459	0.046	25	2136	0.025	38	2655	0.010
13	1553	0.046	26	2149	0.025	39	2713	0.010

Table C.5. Run IV.

No.	t/s	$\Delta T/^{\circ}K$	No.	t/s	$\Delta T/^{\circ}K$	No.	t/s	$\Delta T/^{\circ}K$
1	1060	0.105	16	1719	0.054	31	2373	0.028
2	1122	0.098	17	1731	0.054	32	2448	0.026
3	1140	0.095	18	1755	0.052	33	2502	0.026
4	1160	0.092	19	1814	0.049	34	2535	0.023
5	1224	0.087	20	1895	0.046	35	2592	0.023
6	1296	0.082	21	1954	0.044	36	2607	0.023
7	1322	0.077	22	1971	0.041	37	2659	0.021
8	1387	0.072	23	1980	0.041	38	2690	0.021
9	1429	0.072	24	2000	0.041	39	2741	0.018
10	1489	0.067	25	2051	0.039	40	2764	0.018
11	1505	0.067	26	2110	0.039	41	2824	0.016
12	1555	0.062	27	2180	0.036	42	2834	0.016
13	1622	0.059	28	2251	0.034	43	2910	0.016
14	1652	0.057	29	2285	0.031	44	2951	0.016
15	1667	0.057	30	2354	0.031	45	3014	0.013

Table C.6. Run V.

No.	t/s	$\Delta T/^{\circ}K$	No.	t/s	$\Delta T/^{\circ}K$	No.	t/s	$\Delta T/^{\circ}K$
1	1810	0.087	13	2934	0.038	25	3830	0.023
2	1848	0.084	14	3015	0.036	26	3877	0.022
3	1946	0.077	15	3151	0.033	27	3954	0.022
4	2065	0.074	16	3242	0.033	28	4047	0.020
5	2149	0.069	17	3349	0.028	29	4159	0.020
6	2245	0.061	18	3376	0.028	30	4290	0.020
7	2381	0.056	19	3431	0.028	31	4334	0.018
8	2442	0.051	20	3495	0.025	32	4393	0.018
9	2530	0.051	21	3589	0.028	33	4424	0.018
10	2619	0.043	22	3620	0.026	34	4731	0.013
11	2725	0.041	23	3713	0.024	35	4853	0.013
12	2833	0.041	24	3740	0.023	36	4937	0.013

Table C.7. Run VI.

No.	t/s	$\Delta T/^{\circ}K$	No.	t/s	$\Delta T/^{\circ}K$	No.	t/s	$\Delta T/^{\circ}K$
1	1446	0.093	18	2437	0.046	35	3527	0.021
2	1512	0.090	19	2507	0.044	36	3568	0.021
3	1550	0.085	20	2555	0.044	37	3655	0.021
4	1618	0.080	21	2624	0.041	38	3678	0.018
5	1648	0.082	22	2650	0.039	39	3727	0.018
6	1707	0.077	23	2714	0.039	40	3794	0.018
7	1762	0.070	24	2753	0.038	41	3836	0.018
8	1832	0.070	25	2825	0.036	42	3913	0.018
9	1913	0.067	26	2870	0.034	43	3933	0.018
10	1929	0.067	27	2958	0.034	44	3990	0.016
11	2027	0.062	28	3036	0.031	45	4076	0.016
12	2051	0.062	29	3102	0.029	46	4142	0.016
13	2106	0.059	30	3187	0.026	47	4196	0.015
14	2132	0.059	31	3246	0.026	48	4257	0.013
15	2224	0.056	32	3302	0.023	49	4330	0.016
16	2250	0.054	33	3392	0.022	50	4427	0.013
17	2317	0.052	34	3429	0.023	51	4485	0.013

Table C.8. Run VII.

No.	t/s	$\Delta T/^{\circ}K$	No.	t/s	$\Delta T/^{\circ}K$	No.	t/s	$\Delta T/^{\circ}K$
1	1053	0.059	9	1482	0.033	17	1879	0.018
2	1081	0.057	10	1506	0.031	18	1934	0.016
3	1137	0.054	11	1568	0.028	19	2003	0.016
4	1203	0.049	12	1623	0.026	20	2036	0.016
5	1244	0.046	13	1693	0.024	21	2125	0.013
6	1290	0.041	14	1718	0.023	22	2148	0.013
7	1353	0.039	15	1780	0.021	23	2208	0.013
8	1403	0.036	16	1838	0.021			

REFERENCES

REFERENCES

- Allegra, J. C., A. Stein, and G. F. Allen, *J. Chem. Phys.* 55, 1716 (1971).
- Anderson, T. G., Ph.D. Dissertation, Michigan State University, 1968.
- Anderson, T. G., and F. H. Horne, *J. Chem. Phys.* 53, 2332 (1970).
- Anderson, T. G., and F. H. Horne, *J. Chem. Phys.* 55, 2831 (1971).
- Bak, C. S., and W. I. Goldberg, *Phys. Rev. Lett.* 23, 1218 (1969).
- Balzarini, D. A., *Can. J. Phys.* 52, 499 (1974).
- Bearman, R. J., and F. H. Horne, *J. Chem. Phys.* 42, 2015 (1965).
- Bearman, R. J., J. G. Kirkwood, and M. Fixman, *Advances in Chemical Physics*, Vol. 1, 1 (1958).
- Berge, P., P. Calmettes, C. Lai, M. Toumarie, and B. Voloshine, *Phys. Rev. Lett.* 24, 1223 (1970).
- Blagoi, Yu. P., Doctoral Dissertation, Physico-tech. Inst. of Low Temp., Ukr. Acad. Sci., 1970.
- Boushehri, A., and S. Afrashtehfar, *Bull. Chem. Soc. Jap.* 48, 2372 (1975).
- Bryngdahl, O., *Acta Chem. Scand.* 12, 648 (1958).
- Chu, B., and F. J. Schoenes, *Phys. Rev. Lett.* 21, 6 (1968).
- Chu, B., F. J. Schoenes, and W. P. Kao, *J. Amer. Chem. Soc.* 90, 3042 (1968).
- Chu, B., and F. J. Schoenes, *Phys. Rev.* 185, 219 (1969).
- Chu, B., *Ber. Bunsenges. Phys. Chem.* 76, 202 (1972).
- Chu, B., D. Thiel, W. Tscharnuter, and D. V. Fenby, *J. Phys. Paris* 133, suppl. Nr. 2/3, C1-111 (1972).
- Chu, B., S. P. Lee, and W. Tscharnuter, *Phys. Rev. A* 7, 353 (1973).

- Chang, R. F., P. H. Keyes, J. V. Sengers, and C. O. Alley, Ber. Bunsenges. Phys. Chem. 76, 260 (1972).
- Chen, S. H., and P. Polonsky-Ostrovsky, Opt. Comm. 1, 64 (1969).
- Claesson, S., and L. O. Sundelöf, J. Chim. Phys. Physico. Chim. Biol. 54, 914 (1957).
- Cope, A. F. G., H. H. Reamer, and C. J. Pings, Ber. Bunsenges. Physik. Chem. 76, 318 (1972).
- Daoust, H., and A. Lajoie, Can. J. Chem. 54, 1853 (1976).
- Davies, D. G., J. Chem. Soc. London 1935, 1166 (1935).
- Denbigh, K. G., Trans. Faraday Soc. 48, 1 (1952).
- de Groot, S. R., and P. Mazur, Non-Equilibrium Thermodynamics (North-Holland Publishing Co., Amsterdam, 1969).
- Deutch, J. M., and R. Zwanzig, J. Chem. Phys. 46, 1612 (1967).
- Dougherty, E. L., and H. G. Drickamer, J. Chem. Phys. 23, 295 (1955).
- Dougherty, E. L., and H. G. Drickamer, J. Phys. Chem. 59, 443 (1955).
- Dufour, L., Poggend. Ann. Physik. 148, 490 (1873).
- Dye, J. L., and V. A. Nicely, J. Chem. Ed. 48, 443 (1971).
- Ewing, M. B., and K. N. Marsh, J. Chem. Thermodyn. 2, 351 (1970).
- Ferrell, R. A., Phys. Rev. Lett. 24, 1169 (1970).
- Filippov, L. P., Int. J. Heat Mass Transfer 11, 331 (1968).
- Fisher, M. E., and P. E. Seesney, Phys. Rev. A. 2, 825 (1970).
- Fitts, D., Nonequilibrium Thermodynamics (McGraw-Hill, New York, 1962).
- Fixman, M., J. Chem. Phys. 36, 310 (1962).
- Friedländer, J., Z. Phys. Chem. Leipzig 38, 385 (1901).

- Gambhir, R. D., B. Viswanathan, and E. S. R. Gopal, Indian J. Pure Appl. Phys. 9, 787 (1971).
- Gammell, P. M., and C. A. Angell, J. Chem. Phys. 60, 584 (1974).
- Gerts, L. G., and L. P. Filippov, Zh. Fiz. Khim. 30, 2424 (1956).
- Giglio, M., and A. Vendramini, Appl. Phys. Lett. 25, 556 (1974).
- Giglio, M., and A. Vendramini, Phys. Rev. Lett. 34, 561 (1975).
- Giglio, M., and A. Vendramini, Phys. Rev. Lett. 35, 168 (1975).
- Goldburg, W. I., and P. N. Pusey, Phys. Rev. A 3, 766 (1971).
- Greer, S. C., T. E. Block, and C. M. Knobler, Phys. Rev. Lett. 34, 250 (1975).
- Greer, S. C., Phys. Rev. A 14, 1770 (1976).
- Grossmann, S., Phys. Lett. A 30, 374 (1969).
- Gülarý, E., A. F. Collings, R. L. Schmidt, and C. J. Pings, J. Chem. Phys. 56, 6169 (1972).
- Haase, R., and B. K. Bienert, Ber. Bunsenges. Phys. Chem. 71, 392 (1967).
- Haase, R., and M. Siry, Z. Phys. Chem. Frankfurt 57, 56 (1968).
- Haase, R., Thermodynamics of Irreversible Processes (Addison-Wesley, Mass., 1969).
- Hildebrand, J. H., Viscosity and Diffusivity: A Predictive Treatment (John Wiley and Sons, New York, 1977).
- Hocken, R., and M. R. Moldover, Phys. Rev. Lett. 37, 29 (1976).
- Horne, F. H., Ph.D. Thesis, University of Kansas, 1962.
- Horne, F. H., J. Chem. Phys. 45, 3069 (1966).
- Horne, F. H., and R. J. Bearman, J. Chem. Phys. 46, 4128 (1967).

Ingle, S. E., and F. H. Horne, J. Chem. Phys. 59, 5882 (1973).

Jamieson, D. T., and E. H. Hastings, Thermal Conductivity, Proc. 8th Conf., C. Y. Ho and R. E. Taylor, Eds. (Plenum Press, New York, 1969).

Jamieson, D. T., J. B. Irving, and J. S. Tudhope, Eds., Liquid Thermal Conductivity, a data survey to 1973 (H.M.S., Edinburgh, 1975).

Kadanoff, L. P., and J. Swift, Phys. Rev. 166, 89 (1968).

Kadanoff, L. P., J. Phys. Soc. Jap., 26, suppl. 122 (1969).

Kawasaki, K., Phys. Rev. 150, 291 (1966).

Kawasaki, K., Progr. Theor. Phys. 41, 119 (1969).

Kawasaki, K., Ann. Phys. 61, 1 (1970).

Kawasaki, K., Phys. Rev. A 1, 1750 (1970).

Klein, H., and D. Woermann, Ber. Bunsenges. Phys. Chem. 79, 1180 (1975).

Kresheck, G. C., and L. Benjamin, J. Phys. Chem. 68, 2476 (1964).

Krichevskii, I. R., N. E. Khazanova, and L. R. Linshits, Dokl. Akad. Nauk. SSSR 99, 113 (1954).

Krichevskii, I. R., N. E. Khazanova, and I. V. Tsekhanskaia, Russ. J. Phys. Chem. 34, 598 (1960).

Lorentzen, H. L., and B. B. Hansen, Acta Chem. Scand. 11, 893 (1957).

Lorentzen, H. L., and B. B. Hansen, Acta Chem. Scand. 12, 139 (1958).

Mason, E. A., L. Miller, and T. H. Spurling, J. Chem. Phys. 47, 1669 (1967).

McLaughlin, E., Chem. Rev. 64, 389 (1964).

Michels, A., and J. V. Sengers, Physica 28, 1239 (1962).

Miller, L., Z. Naturforsch A 4, 262 (1949).

Miller, D. G., Chem. Rev. 60, 15 (1960).

- Miller, D. G., Found. Continuum Thermodyn. Proc. Int. Symp. 1973, J. J. D. Domingos, M. N. R. Nina, and J. H. Whitelaw, Eds., (Wiley, New York, 1975).
- Mistura, L., J. Chem. Phys. 55, 2375 (1971).
- Mistura, L., J. Chem. Phys. 62, 4571 (1975).
- Moore, W. J., Physical Chemistry (Prentice-Hall, New Jersey 1972).
- Morrison, G., and C. M. Knobler, J. Chem. Phys. 65, 5507 (1976).
- Mountain, R. D., and R. Zwanzig, J. Chem. Phys. 48, 1451 (1968).
- Onsager, L., Phys. Rev. 37, 405 (1931).
- Onsager, L., Phys. Rev. 38, 2265 (1931).
- Osipova, V. A., Dokl. Akad. Nauk. Azerb. SSR 13, 3 (1957).
- Papoular, M., J. Chem. Phys. 60, 86 (1974).
- Pelger, M., H. Klein, and D. Woermann, J. Chem. Phys. 67, 5362 (1977).
- Prausnitz, J. M., Molecular Thermodynamics of Fluid-Phase Equilibria (Prentice-Hall, New Jersey, 1969).
- Prigogine, I., L. deBrouckere, and R. Armand, Physica 16, 577 (1950).
- Prigogine, I., and R. Defay, Chemical Thermodynamics, D. H. Everett, trans. (Longmans Green and Co., London, 1954).
- Rastogi, R. P., and G. L. Madan, J. Chem. Phys. 43, 4179 (1965).
- Rastogi, R. P., and B. L. S. Yadava, J. Chem. Phys. 51, 2826 (1969).
- Rastogi, R. P., and B. L. S. Yadava, J. Chem. Phys. 52, 2791 (1970).
- Rosenberg, D. U., Methods for the Numerical Solution of Partial Differential Equations (American Elsevier, New York, 1969).

- Rowley, R. L., and F. H. Horne, J. Chem. Phys. 68, 325 (1978).
- Rutherford, W. M., and H. G. Drickamer, J. Chem. Phys. 22, 1157 (1954).
- Scott, R. L., Ber. Bunsenges. Phys. Chem. 76, 296 (1972).
- Sengers, J. V., Critical Phenomena, Proc. Intern. School "Enrico Fermi", Course LI, M. S. Green, Ed. (Academic Press, New York, 1971).
- Sengers, J. V., Transport Phenomena, 1973 A.I.P. Conf. Proc. No. 11, J. Kestin, Ed. (A.I.P., New York, 1973).
- Sengers, J. M., and H. L. Sengers, Experimental Thermodynamics of Non-reacting Fluids, Vol. II, Butterworths, London, 1975.
- Stanford, D. J., and A. Beyerlein, J. Chem. Phys. 58, 4338 (1973).
- Stanley, H. E., Introduction to Critical Phenomena (Oxford, New York, 1971).
- Story, M. J., Ph. D. Thesis (University of Cambridge, 1967).
- Story, M. J., and J. C. R. Turner, Trans. Faraday Soc. 65, 349 (1969).
- Sundelöf, L., Ark. Kemi 15, 317 (1960).
- Swift, J., Phys. Rev. 173, 257 (1968).
- Thomaes, G., J. Chem. Phys. 25, 32 (1956).
- Tichacek, L. J., and H. G. Drickamer, J. Phys. Chem. 60, 820 (1956).
- Tsai, R. C., Masters Thesis, University of Akron, 1970.
- Turner, J. C. R., B. D. butler, and M. J. Story, Trans. Faraday Soc. 63, 1906 (1967).
- Tyrrell, H. J. V., Diffusion and Heat Flow in Liquids (Butterworths, London, 1961).
- Venart, J. E. S., Thermophysical Properties, 4th Symp. (Univ. Delaware, Delaware, 1968).
- Viswanathan, B., K. Govindarajan, and E. S. R. Gopal, Indian J. Pure Appl. Phys. 11, 157 (1973).

- Rowley, R. L., and F. H. Horne, J. Chem. Phys. 68, 325 (1978).
- Rutherford, W. M., and H. G. Drickamer, J. Chem. Phys. 22, 1157 (1954).
- Scott, R. L., Ber. Bunsenges. Phys. Chem. 76, 296 (1972).
- Sengers, J. V., Critical Phenomena, Proc. Intern. School "Enrico Fermi", Course LI, M. S. Green, Ed. (Academic Press, New York, 1971).
- Sengers, J. V., Transport Phenomena, 1973 A.I.P. Conf. Proc. No. 11, J. Kestin, Ed. (A.I.P., New York, 1973).
- Sengers, J. M., and H. L. Sengers, Experimental Thermodynamics of Non-reacting Fluids, Vol. II, Butterworths, London, 1975.
- Stanford, D. J., and A. Beyerlein, J. Chem. Phys. 58, 4338 (1973).
- Stanley, H. E., Introduction to Critical Phenomena (Oxford, New York, 1971).
- Story, M. J., Ph. D. Thesis (University of Cambridge, 1967).
- Story, M. J., and J. C. R. Turner, Trans. Faraday Soc. 65, 349 (1969).
- Sundelöf, L., Ark. Kemi 15, 317 (1960).
- Swift, J., Phys. Rev. 173, 257 (1968).
- Thomaes, G., J. Chem. Phys. 25, 32 (1956).
- Tichacek, L. J., and H. G. Drickamer, J. Phys. Chem. 60, 820 (1956).
- Tsai, R. C., Masters Thesis, University of Akron, 1970.
- Turner, J. C. R., B. D. butler, and M. J. Story, Trans. Faraday Soc. 63, 1906 (1967).
- Tyrrell, H. J. V., Diffusion and Heat Flow in Liquids (Butterworths, London, 1961).
- Venart, J. E. S., Thermophysical Properties, 4th Symp. (Univ. Delaware, Delaware, 1968).
- Viswanathan, B., K. Govindarajan, and E. S. R. Gopal, Indian J. Pure Appl. Phys. 11, 157 (1973).

- Voronel, A. V., and T. Ovodova, Sov. Phys. JETP 9, 169 (1969).
- Waldmann, L., Z. Phys. 114, 53 (1939).
- Waldmann, L., Z. Phys. 121, 501 (1943).
- Waldmann, L., Z. Phys. 124, 2 (1947).
- Waldmann, L., Z. Phys. 124, 30 (1947).
- Waldmann, L., Z. Naturforsch. A 2, 358 (1947).
- Waldmann, L., Z. Naturforsch. A 4, 105 (1949).
- Weasts, R. C., Ed., Handbook of Chemistry and Physics, 51st Edition (The Chemical Rubber Co., Ohio, 1970).
- Wilhelm, V. E., M. Zettler, and H. Sackmann, Ber. Bunsenges. Phys. Chem. 78, 795 (1974).
- Wirtz, K., Ann. Physik., Leipzig, 36, 295 (1939).
- Wirtz, K., and J. W. Hiby, Physik. Z. Leipzig 44, 369 (1943).
- Woermann, D., and W. Sarholz, Ber. Bunsenges. Phys. Chem. 69, 319 (1965).
- Wood, S. E., and J. A. Gray III, J. Amer. Chem. Soc. 74, 3729 (1952).

MICHIGAN STATE UNIVERSITY LIBRARIES



3 1293 03168 9817